Aus der Klinik für Urologie
im Universitätsklinikum Düsseldorf
an der Heinrich-Heine-Universität Düsseldorf
Direktor: Prof. Dr. med. Peter Albers

Characterization of CDK12 as a Potential Therapeutic Target in Urothelial Carcinoma Cells

Dissertation

zur Erlangung des Grades eines Doktors der Medizin
der medizinischen Fakultät der Heinrich-Heine-Universität Düsseldorf

Vorgelegt von
Markus Fortmeyer
2026

Als Inauguraldissertation gedruckt mit Genehmigung der
Medizinischen Fakultät der Heinrich-Heine-Universität Düsseldorf.

gez.:
Dekan: Prof. Dr. med. Nikolaj Klöcker
Erstgutachterin: PD Dr. rer. nat. Michèle Hoffmann
Zweitgutachter: Prof. Dr. rer. nat. Gerhard Fritz

Zusammenfassung

Cisplatin zählt zu den zentralen therapeutischen Säulen in der Behandlung des muskelinvasiven Urothelkarzinoms. Trotz guter Ansprechraten entwickelt ein erheblicher Anteil der Patienten Resistenz gegenüber cisplatinhaltigen Therapien. Die zugrundeliegenden molekularen Mechanismen sind bislang unvollständig verstanden. Die Cyclin-abhängige Kinase 12 (CDK12) spielt eine Schlüsselrolle in der Regulation zahlreicher DNA-Reparaturgene und wurde in mehreren Tumorentitäten mit Chemoresistenz und Tumorprogression in Verbindung gebracht. Für das Urothelkarzinom lagen bisher jedoch kaum funktionelle Daten vor. Ziel dieser Arbeit war es, die Rolle von CDK12 im Kontext der Cisplatinantwort und -resistenz in Urothelkarzinomzelllinien systematisch zu untersuchen. Dabei wurden drei experimentelle Ansätze verfolgt: ein CDK12-Überexpressionsmodell zur Analyse eines möglichen „gain-of-function"-Effekts, ein siRNA-vermittelter Knockdown als „loss-of-function"-Modell sowie eine pharmakologische Inhibition mittels THZ531, einem selektiven CDK12/CDK13-Inhibitor. In allen Modellen wurden das Ausmaß der DNA-Schädigung, die Apoptoseinduktion und die Regulation zentraler DNA-Reparaturgene analysiert. Ergänzend wurden cisplatinresistente Sublinien (LTT) herangezogen, um klinisch relevante Therapiebedingungen nachzuahmen.

Die Ergebnisse zeigen, dass CDK12 in LTT-Zellen konsistent erhöht ist und mit einer verstärkten Aktivierung verschiedener DNA-Reparaturwege assoziiert sein kann. Es zeigte sich weder im Überexpressionsmodell ein verändertes Ansprechen auf den Inhibitor THZ531, noch beeinflusste ein siRNA-vermittelter Knockdown von CDK12 die Sensitivität der Zellen gegenüber Cisplatin. Die zelluläre Antwort auf DNA-Schäden, gemessen über γH2AX-Bildung und PARP-Spaltung, blieb in beiden Modellen weitgehend stabil und unabhängig vom CDK12-Level. Die Experimente zur CDK12-Modulation zeigten, dass eine Erhöhung oder Reduktion von CDK12 in mehreren Zelllinien die Expression verschiedener DNA-Reparaturgene veränderte.

Insgesamt zeigen die Daten, dass CDK12 im Urothelkarzinom die Transkription zentraler DNA-Reparaturgene beeinflusst, ohne jedoch das Ausmaß der durch Cisplatin induzierten DNA-Schädigung zu verändern. Cisplatinresistenz erweist sich weiterhin als multifaktorielles Phänomen, bei dem CDK12 eher eine unterstützende als eine steuernde Funktion einnimmt. Im Gegensatz dazu eröffnet die pharmakologische Inhibition von CDK12, insbesondere in Cisplatin resistenten Zellen potenziell neue therapeutische Perspektiven zur Überwindung refraktärer Therapiesituationen. Diese Arbeit liefert neue funktionelle Einblicke in die Rolle von CDK12 im Urothelkarzinom und hebt das Potenzial CDK12-gerichteter Ansätze für zukünftige Therapieoptionen hervor.

Abstract

Cisplatin remains a central therapeutic backbone in the treatment of muscle-invasive urothelial carcinoma. Despite initially favorable response rates, a substantial proportion of patients develop resistance to cisplatin-based therapies. The underlying molecular mechanisms of this acquired resistance are still only partially understood. Cyclin-dependent kinase 12 (CDK12) plays a key role in the regulation of numerous DNA repair genes and has been linked to chemoresistance and tumor progression in several cancer entities. However, functional data on its role in urothelial carcinoma have been largely lacking.

The aim of this study was to systematically investigate the role of CDK12 in the context of cisplatin response and resistance in urothelial carcinoma cell lines. To this end, three complementary experimental approaches were employed: a CDK12 overexpression model to assess potential gain-of-function effects, an siRNA-mediated knockdown model as a loss-of-function approach, and pharmacological inhibition using THZ531, a selective CDK12/CDK13 inhibitor. In all models, DNA damage induction, apoptotic response, and the regulation of key DNA repair genes were analyzed. Furthermore, cisplatin-resistant long-term treatment (LTT) models were included to mimic clinically relevant therapy conditions.

The results demonstrate that CDK12 levels are consistently elevated in LTT cells and may be associated with enhanced activation of several DNA repair pathways. Neither CDK12 overexpression altered the cellular response to THZ531, nor did siRNA-mediated CDK12 knockdown affect the sensitivity of cells to cisplatin. The cellular DNA damage response, assessed by γH2AX formation and PARP cleavage, remained largely stable and independent of CDK12 expression levels. Modulation of CDK12, however, impacted the expression of several DNA repair genes across multiple cell lines.

In summary, these findings indicate that CDK12 regulates the transcription of central DNA repair genes in urothelial carcinoma but does not modify the extent of cisplatin-induced DNA damage. Cisplatin resistance remains a multifactorial and cell line dependent phenomenon in which CDK12 appears to play a supportive rather than a decisive role. In contrast, pharmacological CDK12 inhibition, particularly in cisplatin-resistant cells, may offer promising therapeutic opportunities to overcome refractory disease. This work provides novel functional insights into the role of CDK12 in urothelial carcinoma and highlights the potential of CDK12-targeted approaches as an adjunct to future treatment strategies.

Abbreviations

APS	Ammonium Persulfate
BCA	Bicinchoninic Acid (Assay)
BCG	Bacillus Calmette-Guérin (Tuberculosis Vaccine)
BSA	Bovine Serum Albumin
CDK	Cyclin-Dependent Kinase
cDNA	Complementary DNA
DDR	DNA damage repair
DMEM	Dulbecco's Modified Eagle Medium
DMSO	Dimethyl Sulfoxide
DNA	Deoxyribonucleic Acid
EDTA	Ethylenediaminetetraacetic Acid
FCS	Fetal Calf Serum
Fwd	Forward (Primer)
GC	Gemcitabine, Cisplatin (Chemotherapy Regimen)
LTT	Long Term Treated
MTT	Methylthiazolyldiphenyl-tetrazolium Bromide (Assay)
MVAC	Methotrexate, Vinblastine, Adriamycin, Cisplatin (Chemotherapy Regimen)
PAA	Polyacrylamide
PBS	Phosphate-Buffered Saline
Rev	Reverse (Primer)
RIPA	Radioimmunoprecipitation Assay (Buffer)
RNA	Ribonucleic Acid
RT-qPCR	Real-Time Quantitative Polymerase Chain Reaction
SDS	Sodium Dodecyl Sulfate
siRNA	Small Interfering RNA
TBST	Tris-Buffered Saline with Tween
TEMED	Tetramethylethylenediamine
UCC	Urothelial carcinoma cells

Table of Content

1 Introduction 1
1.1 Urothelial Carcinoma 1
1.1.1 Epidemiological Data on Urothelial Carcincoma 1
1.1.2 Diagnosis and Treatment of Urothelial Carcinoma 1
1.1.3 Mechanisms of Cisplatin Resistance in Urothelial Carcinoma 3
1.2 Cellular DNA Repair Mechanisms 4
1.3 Cyclin-Dependent Kinase 12 (CDK12) 5
1.3.1 CDK12 Changes in Urothelial Carcinoma Patients 5
1.3.2 Role of CDK12 Inhibition in Cancer 6
1.4 Research Question and Objectives 7
2 Material und Methods 8
2.1 Material 8
2.1.1 Cell lines 8
2.1.2 Cell Culture 9
2.1.3 Pharmacological Substances 10
2.1.4 siRNA 10
2.1.5 RNA Isolation 11
2.1.6 cDNA Synthesis 11
2.1.7 RT-qPCR 11
2.1.8 Protein Extraction and Quantification 13
2.1.9 Western Blot 14
2.1.10 Cell Viability Measurement 16
2.1.11 Software 16
2.1.12 Equipment 17
2.2 Methods 18
2.2.1 Cell Culture 18
2.2.1.1 Cultivation of Urothelial Carcinoma Cells 18
2.2.2 Cultivation of Uroepithelial Cells 18
2.2.2.1 Cell Counting 18
2.2.2.2 Determination of IC50-Values 18
2.2.2.3 Treatment with Pharmaceuticals 19
2.2.2.4 Cell Viability Measurement 20
2.2.2.4.1 MTT Assay 20
2.2.2.4.2 CellTiterGlo® Luminescent Cell Viability Assay 20

2.2.2.5 siRNA Knockdown 21
2.2.2.6 Stable Overexpression 21
2.2.3 RNA Analysis 21
2.2.3.1 RNA Extraction 22
2.2.3.2 Reverse Transcription 22
2.2.3.3 RT-qPCR 22
2.2.4 Protein Analysis 23
2.2.4.1 Protein Extraction 23
2.2.4.2 Western Blot 23
2.2.4.3 Stripping 24
2.2.5 Statistics 24
3 Results 25
3.1 Molecular Response towards Short Term Treatment with Cisplatin 25
3.1.1 Changes in CDK12 Protein Levels 25
3.1.2 Gene Expression Changes of DNA Damage Repair Genes 26
3.2 Response of Urothelial Carcinoma Cells to the CDK12-Inhibitor THZ531 34
3.2.1 IC_{50}-Values for Urothelial Carcinoma Cells 34
3.2.2 Normal Cell Toxicity of THZ531 36
3.2.3 DNA Damage and Apoptosis Induction in LTTs 36
3.2.4 Changes in the Expression of DNA Damage Repair Genes Following THZ531 Treatment 37
3.3 Modulation of CDK12 and its Impact on Cisplatin Response 45
3.3.1 The Effects of CDK12 Overexpression 45
3.3.1.1 Validation of Overexpression 46
3.3.1.2 Response to the Inhibitor THZ531 47
3.3.1.3 Impact on DNA Damage and Apoptosis Induction 48
3.3.1.4 Changes in the Expression of DNA Damage Repair Genes Following Cisplatin Treatment 49
3.3.2 Effects of CDK12 Knockdown 53
3.3.2.1 Knockdown Validation 53
3.3.2.2 Response to Cisplatin 54
3.3.2.3 Impact on DNA Damage and Apoptosis Induction 55
3.3.2.4 Changes in the Expression of DNA Damage Repair Genes Following Cisplatin Treatment 56
3.3.3 Effects of Pharmacological CDK12 Inhibition Combined with Cisplatin 59
3.3.3.1 Impact on DNA Damage and Apoptosis Induction 59

3.3.3.2 Changes in the Expression of DNA Damage Repair Genes 60
3.4 Effectiveness of Combination Therapy with THZ531 and Cisplatin 62
3.5 Effectiveness of Combination Therapy with THZ531 and Talazoparib 65
3.5.1 Impact on Cell Viability 65
3.5.2 DNA Damage and Apoptosis Induction 68
4 Discussion 70
4.1 Correlation between Patient Data and In-vitro Findings 70
4.2 CDK12-dependent DNA Damage Response in LTTs 73
4.3 Mechanisms of CDK12 Modulation 74
4.3.1 CDK12 overexpression 74
4.3.1.1 Functional Consequences of CDK12 Overexpression 74
4.3.1.2 CDK12-dependent Stress Response under Cisplatin Exposure 74
4.3.1.3 Impact on Apoptosis and DNA Damage by Cisplatin 76
4.3.2 CDK12 Knockdown 76
4.3.2.1 Functional Consequences of CDK12 Knockdown 76
4.3.2.2 CDK12-dependent Stress Response under Cisplatin Exposure 76
4.3.2.3 Impact on Apoptosis and DNA Damage by Cisplatin 77
4.3.3 Pharmacological CDK12 Inhibition 78
4.4 Significance of CDK12 in Cisplatin Resistance of Urothelial Carcinoma 80
4.5 Mechanistic Effects of CDK12 Inhibitor THZ531 81
4.5.1 Effects on Cell Cycle and Apoptosis 82
4.5.2 Effects on DNA Damage Response 82
4.5.3 Tolerability and Side Effects 83
4.6 Therapeutic Potential of CDK12 Targeting by THZ531 84
4.6.1 THZ531 as a Monotherapy 84
4.6.2 THZ531 in Combination Therapy 85
4.6.2.1 THZ531 in Combination with Cisplatin 85
4.6.2.2 THZ531 in Combination with Talazoparib 85
4.6.3 Potential for Clinical Use and Implementation 86
4.7 Methodological Limitations 87
4.8 Outlook 88
5 References 89

1 Introduction

1.1 Urothelial Carcinoma

1.1.1 Epidemiological Data on Urothelial Carcincoma

The following discussion pertains to the epidemiological situation in Germany. Urothelial carcinoma is the fourth most common cancer in men and the ninth most common cancer in women in Germany. It is associated with an annual incidence of 30,000 new cases (in the year 2020). There is a gender-specific difference in incidence, with men being, on average, three times more likely to develop the disease than women [1]. The primary risk factor for the development of urothelial carcinoma is long-term nicotine abuse. Other risk factors include chronic cystitis and occupational exposure to substances such as aromatic amines, benzidine, or diesel exhaust [2]. Furthermore, there are iatrogenic risk factors, such as the administration of pioglitazone or cyclophosphamide [3, 4].

The majority of urothelial carcinomas are diagnosed in individuals over the age of 65, with the peak incidence occurring between 70 and 80 years of age [1].

Urothelial carcinomas are generally associated with a poor prognosis, as they are often diagnosed at advanced stages. The 5-year survival rate varies according to the depth of tumor infiltration and the presence of metastases at the time of diagnosis and during the course of the disease. Patients with metastatic disease typically succumb shortly after diagnosis, with a 5-year survival rate of less than 5 %. In contrast, patients with a localized tumor exhibit a 5-year survival rate of up to 70 % [5, 6].

1.1.2 Diagnosis and Treatment of Urothelial Carcinoma

Urothelial carcinoma can generally occur in all parts of the urinary tract lined with urothelium. The following explanations refer to bladder cancer, which accounts for approximately 90% of all urothelial carcinomas [5].

A common initial symptom is painless macroscopic hematuria, prompting patients to seek medical consultation. Urine cytology may reveal atypical cells. Cystoscopy is a key diagnostic tool for the inspection of the bladder and allows for tissue sampling to confirm the histopathological diagnosis. For the assessment of local invasion and staging, ultrasound, computed tomography (CT), and magnetic resonance imaging (MRI) are utilized [7].

Therapeutic options vary depending on the tumor stage, biological age, and patient preference. Tumors that do not invade the muscle can often be successfully removed by transurethral resection [7]. Intravesical chemotherapy has been established to reduce the risk of local

recurrence, with Mitomycin C or BCG being administered to patients [8, 9]. This approach preserves the bladder and is less invasive for the patient. In cases of local recurrence following adjuvant intravesical chemotherapy, radical cystectomy is considered if there is evidence of disease progression, such as the transition from pT1 high-grade to muscle-invasive disease, or in patients with high-risk features [7, 10].

Patients with muscle-invasive bladder carcinoma should undergo radical cystectomy with pelvic lymphadenectomy. To restore urinary continuity, urinary diversion using a segment of the small intestine or colon may be considered. Additionally, options such as neobladder construction or rectal urinary diversion via ureterosigmoidostomy are available [2, 7].

Systemic therapy is reserved for patients in advanced stages or with metastatic disease. Chemotherapy may be administered either neoadjuvantly or adjuvantly [7]. The standard regimen typically involves cisplatin, supplemented with gemcitabine (GC). Alternatively, the MVAC regimen (methotrexate, vinblastine, doxorubicin, cisplatin) may be employed. Due to its better tolerability and non-inferiority compared to MVAC, GC has been established as the primary therapeutic standard [11]. Poor general health or multiple comorbidities are frequently exclusion criteria for cisplatin therapy [7]. These patients may be considered for carboplatin therapy, although this has been associated with reduced overall survival in the past [12]. For patients unsuitable for either cisplatin or carboplatin, immune checkpoint inhibitors such as pembrolizumab or atezolizumab are available as first-line therapy [13, 14].

In second-line therapy, re-exposure to cisplatin, as well as the administration of additional cytostatic agents such as vinca alkaloids and taxanes, has been established; however, these have all shown suboptimal results regarding overall survival [15, 16]. The KEYNOTE study was the first to demonstrate the superiority of the checkpoint inhibitor pembrolizumab over second-line chemotherapy [17]. In the current german S3-guidelines, the use of nivolumab and atezolizumab in second-line therapy is assigned a weak recommendation [7].

Patients who experience disease progression while on checkpoint inhibition may be considered for additional chemotherapy [7]. Alternatively, antibody-drug conjugates, some of which have been approved by the EMA, are available [5]. Enfortumab vedotin is a member of this class of therapeutic agents and has been approved by the EMA. This antibody is directed against Nectin-4 and is conjugated to the cytotoxic agent monomethyl auristatin. Upon binding to Nectin-4 on tumor cells, the complex is internalized, allowing monomethyl auristatin to exert its targeted cytotoxic effect [5, 18].

1.1.3 Mechanisms of Cisplatin Resistance in Urothelial Carcinoma

A significant limitation in the therapeutic use of cisplatin is the development of resistance, which can manifest as either inherent resistance (indicated by non-response) or acquired resistance. This resistance contributes to disease progression and increased patient mortality [19]. To improve the treatment of this patient population in the future, extensive research has already been conducted on the mechanisms of cisplatin resistance. Numerous mechanisms have been identified and categorized by Galluzzi et al. The authors distinguish between pre-target, on-target, post-target, and off-target resistance [20].

Research has identified mechanisms in urothelial carcinoma cells that limit the effectiveness of cisplatin by reducing its intracellular presence (pre-target). In cisplatin-resistant cell lines (LTTs) that were generated by the working group, upregulation of *MRP2* transporters has been observed. These ion transporters can also expel cisplatin from the cell. Increased *MRP2* expression is associated with effective intracellular cisplatin elimination, thereby diminishing its efficacy [21].

Cisplatin-resistant cells also detoxify cisplatin through binding to metallothioneins. Upregulation of metallothioneins is found in RT-112-LTT cells [21].

Furthermore, cisplatin-resistant urothelial carcinoma cells mitigate the cytotoxicity of the drug by modulating DNA repair genes (on-target). Upregulation of *ERCC2* in T24-LTT cells allows the cells to compensate for cisplatin-induced damage through enhanced DNA repair. In cisplatin-resistant J82 cells, downregulation of mismatch repair genes has been observed. This downregulation is thought to prevent unnecessary repair cycles and potential induction of apoptosis [21].

Additionally, it has been demonstrated that LTT cells can bypass apoptosis induction through overexpression of survivin (post-target) [21].

Höhn et al. showed that in-vitro induced cisplatin resistance is associated with morphological changes comparable to epithelial-mesenchymal transition (off-target) [22].

Skowron et al. and Höhn et al. conclude that the resistance mechanisms in urothelial carcinoma cells are diverse and can differ significantly between various cell lines studied [21, 22].

1.2 Cellular DNA Repair Mechanisms

Cisplatin has established itself as a standard therapeutic agent in the systemic treatment of bladder cancer since decades (see 1.1.2). It induces DNA cross-linking, which can obstruct DNA replication and transcription, potentially leading to DNA double-strand breaks as secondary effects [23]. These double strand breaks lead to the phosphorylation of histone H2AX. Phosphorylated H2AX (γH2AX) is suitable for detecting DNA damage following cisplatin exposure [24].

Various protein complexes are involved in the detection and repair of DNA damage. For example, DNA damage is recognized by the kinases ATR and ATM. ATM functions as a specialized signaling molecule for DNA double-strand breaks (such as those induced by cisplatin) and can induce cell cycle arrest through the phosphorylation of p53. Additionally, ATM can phosphorylate the histone H2AX [25]. ATR can activate RAD51 through phosphorylation, thereby contributing to DNA repair [25].

To repair DNA double-strand breaks, cells rely mostly on homologous recombination. In this process, the break is recognized by the MRN complex and subsequently processed by nucleases. This results in the formation of single-stranded DNA with 3' overhangs. The single-stranded DNA is stabilized, and in the next step, RAD51 facilitates the search for the identical sequence on the homologous sister chromatid [26]. RAD51 enables the invasion of the single-stranded DNA into the homologous sister chromatid, forming a D-loop structure. In this structure, the intact DNA strand serves as a template for DNA synthesis, allowing the missing sequence to be copied [27]. During repair, Holliday junctions may form, leading to crossing-over events, where the double-strand break is resolved through the exchange of genetic material between sister chromatids [28]. Under the influence of BRCA2, complexes with RAD51 are formed, which collectively enable the accurate identification and repair of the damaged DNA [29].

Cells also utilize non-homologous end joining for the repair of double-strand breaks. In this process, the DNA ends are ligated in a sequence-independent manner. Prior to ligation, nucleotides are removed by nucleases. This repair pathway is associated with information loss in the DNA and is generally more error-prone compared to homologous recombination [30].

Polymerase θ (corresponding gene: *POLQ*) is involved in non-homologous end joining by utilizing microhomologies to ligate the broken DNA ends [31].

Polymerase η (corresponding gene: *POLH*) facilitates translesion synthesis, which refers to the synthesis across damaged DNA fragments, including DNA cross-links induced by cisplatin [32].

Additionally, other DNA repair mechanisms exist, such as base excision repair and nucleotide excision repair, which address erroneous base modifications and bulky DNA adducts, respectively. Mismatch repair, involving exonucleases, corrects base-pairing errors [33].

1.3 Cyclin-Dependent Kinase 12 (CDK12)

Cyclin-dependent kinases (CDKs) are a class of serine and threonine kinases. The binding of cyclins regulates the activity of these kinases and influences their substrate specificity. Various CDKs, such as CDK1, CDK2, CDK4, and CDK6, are involved in regulating cell cycle transitions and play an essential role in the control of cell division and growth [34]. Other CDKs are involved in DNA repair, gene expression, and partially in apoptosis [35].

CDK12, a member of the CDK family, is involved in transcriptional regulation. The kinase's activity is fully executed in the presence of Cyclin K, with CDK12 and Cyclin K forming a complex. CDK12 phosphorylates the C-terminal domain of RNA polymerase II, thereby exerting a significant influence on transcriptional elongation [36]. CDK12 has been described as having a regulatory effect on genes with complex transcription units, including those critical for homologous recombination. Regulatory effects on genes such as *ATR* and *BRCA1* have also been documented [37]. At the post-transcriptional level, CDK12 regulates the mRNA processing of DNA repair genes [38]. Due to its central role in DNA repair regulation, CDK12 is crucial for maintaining genomic stability [37].

Moreover, CDK12 is discussed in the literature as a potential tumor suppressor gene, as mutations in CDK12 lead to genomic instability, exemplified in breast cancer [39, 40].

Pharmacological inhibition of CDK12 is available in experimental settings using inhibitors such as THZ531 and SR-4835. For this study, THZ531 has been selected. THZ531 irreversibly inhibits CDK12 by covalently binding to a cysteine residue in the ATP-binding pocket of CDK12. This binding prevents ATP from binding and disrupts kinase activity, leading to the inhibition of RNA polymerase II phosphorylation and thereby affecting transcriptional elongation [36]. A search in ClinicalTrials.gov and PubMed (as of December 2025) did not reveal any registered clinical trials investigating selective CDK12/13 inhibitor THZ531 in human subjects.

1.3.1 CDK12 Changes in Urothelial Carcinoma Patients

When examining CDK12 alterations in urothelial carcinoma using databases, it is observed that CDK12 alterations occur in 9 % of the analyzed samples. In approximately half of these altered samples, a CDK12 amplification is present [41]. In comparison, CDK12 alterations are found

in only 2 % of prostate cancer cases. Most of these alterations are deletions and missense mutations [42].

Unpublished data from cooperation partners at Urology of University Hospital Essen also suggest a correlation between CDK12 and the chemotherapy response in urothelial carcinoma patients. Tissue microarray analyses have demonstrated that patients who received neoadjuvant cisplatin-based therapy exhibited an increase in CDK12 [43]. Furthermore, no correlation was observed between CDK12 levels and histopathological characteristics such as T-stage. However, in an untreated cohort, it was observed that patients with initially high CDK12 levels had prolonged overall survival compared to patients with low CDK12 expression. In contrast, patients who did not respond adequately to chemotherapy and had high CDK12 levels were associated with a poorer prognosis. Therefore, no correlation between the initial CDK12 level and the therapeutic response could be determined [43].

1.3.2 Role of CDK12 Inhibition in Cancer

The role of CDK12 inhibition has been documented for several tumor types in the literature. Inhibition of CDK12 represents a promising strategy to overcome resistance to PARP inhibitors (PARPi) in triple-negative breast cancer models (TNBC). This has been demonstrated in both BRCA wild-type and BRCA-mutant cells. In the referenced study, Dinaciclib was utilized as a pan-CDK inhibitor, targeting not only CDK12 but also other CDKs. Synergistic effects were observed when Dinaciclib was combined with PARP inhibitors. The authors describe CDK12 inhibition as a potential means to address both acquired and intrinsic PARPi resistance [44]. Furthermore, TNBC cells responded to the CDK12 inhibitor SR-4835. In studies, SR-4835 exhibited synergistic effects with DNA-damaging chemotherapies such as Irinotecan and Cisplatin, contributing to increased apoptosis and reduced tumor cell growth. It induced a BRCAness phenotype in BRCA wild-type cells, characterized by a similar DNA repair deficiency observed in BRCA-mutant cells [45, 46].

The effects of CDK12 inhibition have also been investigated outside gynecological tumor types. For instance, in hepatocellular carcinoma, CDK12 inhibition using THZ531 alone has demonstrated a growth-inhibitory effect. Synergistic effects were observed in combination with Sorafenib [47]. Additionally, in cholangiocarcinoma, Dinaciclib administration in vitro has been shown to induce growth inhibition through apoptosis and cell cycle arrest [48].

1.4 Research Question and Objectives

The role of CDK12 in tumorigenesis and tumor progression across various tumor types is an area of current research interest. Previous studies have demonstrated a correlation between CDK12 inhibition and response to DNA-damaging agents in breast cancer cells. Additionally, an increase in CDK12 levels has been observed in urothelial carcinoma during cisplatin-based chemotherapy, with CDK12 appearing to be amplified in a substantial number of urothelial carcinoma samples [41, 43].

The central research questions addressed in this study are: How does CDK12 influence the DNA damage response in urothelial carcinoma cells? What impact does CDK12 have on cisplatin sensitivity in both cisplatin-naive and cisplatin-resistant urothelial carcinoma cells?

To complement clinical data on CDK12 in urothelial carcinoma, this project will incorporate mechanistic in vitro analyses to investigate the role of CDK12 in acquired cisplatin resistance. This will involve examining the quantitative behavior of CDK12 in urothelial carcinoma cells and their cisplatin-resistant sublines, as well as assessing changes in CDK12 levels in response to cisplatin exposure. Mechanistic studies will include CDK12 modulation by evaluating urothelial carcinoma cells that overexpress CDK12 via a vector plasmid and comparing their DNA damage response before and after cisplatin treatment. Analogous investigations will be conducted in cells with CDK12 knockdown using siRNA. The aim is to determine the correlation between CDK12 levels and cisplatin response.

A significant focus of this study is the evaluation of the experimental pharmacological inhibitor THZ531. The effect of THZ531 on the DNA damage response in urothelial carcinoma cells will be analyzed. The study will explore the synergistic effects of CDK12 inhibition and DNA-damaging chemotherapy, as described in the literature, in the context of urothelial carcinoma.

It is hypothesized that CDK12 inhibition will impair the DNA repair capacity of urothelial carcinoma cells, thereby increasing their sensitivity to cisplatin. This study aims to characterize CDK12 as a potential future therapeutic target and prognostic biomarker.

2 Material und Methods

2.1 Material

2.1.1 Cell lines

Table 1: Description of the cell lines used. Additionally provided are the donor's sex and age, origin, and literature reference. All parental cell lines are commercially available. The designation LTT indicates sublines that have been generated by the research group and exhibit cisplatin resistance.

Cell line	Sex, age	Origin	Reference
RT-112	Female	Invasive urothelial carcinoma of the bladder	Masters 2000
RT-112 LTT	F	Invasive urothelial carcinoma of the bladder	
253J	M, 53	Lymph node metastasis	Elliott 1974, Masters 2000
253J LTT	M, 53	Lymph node metastasis	
T-24	F, 81		Williams 1980
T-24 LTT	F, 81		
J82	M		O'Toole 1978
J82 LTT	M		
UM-UC-3	M		Grossmann 1986
VM-CUB1	M		Williams 1980
HBLAK		Spontaneously immortalized urothelial cells (ureter)	Hoffmann 2016

Additionally, cell lines that overexpress CDK12 through a vector plasmid were used (RT-112, T-24, UM-UC-3)

2.1.2 Cell Culture

Table 2: Relevant materials for cell culture

Material	Manufacturer
DMEM	GIBCO
CnT Prime epithelial cell culture medium	CELLnTEC
PBS	Sigma-Aldrich
FCS	Biochrom/MERCK
Accutase	Sigma-Aldrich
Trypsin	GIBCO
DMSO	Sigma-Aldrich
Trypan Blue	Sigma-Aldrich
Hemocytometer	Bio-Rad
Cell culture flasks (T25, T75)	Greiner bio-one
Advanced cell culture flasks (T75) for HBLAK	Greiner bio-one
Cell culture dishes (10 cm diameter)	Sarstedt
Cell culture plates (96-well and 6-well)	Greiner bio-one
Eppendorf tubes	Eppendorf
Falcon tubes (15 ml, 50 ml)	Greiner bio-one
Micropipettes (1.5 µl, 10 µl, 20 µl, 100 µl, 1000 µl)	Eppendorf
Pipette tips	Sarstedt
Glass Pasteur pipettes	Brand
Multi-dispenser	Eppendorf
Pipettenaufsatz für Mehrfachdispenser (0.5 ml, 1 ml, 5 ml, 10 ml)	Eppendorf
Pipetting aid, Pipetus®	Hirschmann

2.1.3 Pharmacological Substances

Table 3: Pharmacological substances in cell culture

Substance	Solvent	Manufacturer
Cisplatin	Water	Hexal AG
THZ531	DMSO	Selleckchem
Talazoparib	DMSO	Cayman

2.1.4 siRNA

Table 4.1: Required materials for an siRNA knockdown

Material	Manufacturer
Optimem Medium	GIBCO
Lipofectamine	Invitrogen
20 µM SMARTpool siRNA	Dharmacon ™

Table 4.2: siRNA sequences targeting CDK12

	Sequence
ON-Target CDK12, J-004031-09	GUUCAAAGCGUUCGAAUGA
ON-Target CDK12, J-004031-10	CUACAGAGCGACUUCCUUA
ON-Target CDK12, J-004031-11	CCGAGAAGCAUCUUGUUAA
ON-Target CDK12, J-004031-12	UGAAUUGGCAGUGUUAUUA
ON-Target non targeting (4 Sequenzen)	UGGUUUACAUGUCGACUAA
	UGGUUUACAUGUUGUGUGA
	UGGUUUACAUGUUUUCUGA
	UGGUUUACAUGUUUUCCUA

2.1.5 RNA Isolation

Table 5: Materials for RNA precipitation and subsequent extraction procedures

Material	Manufacturer
TRIzol	Qiagen
Ethanol (100 %, 70 %)	VWR Chemicals
Cell scraper	Sarstedt
RNeasy Mini Kit	Qiagen
RNA Clean & Concentrator ™	ZYMO RESEARCH
Nanodrop 2000	Thermo Scientific

2.1.6 cDNA Synthesis

Table 6: Materials used for cDNA synthesis. Additionally, RNase-free water and previously isolated RNA were required.

Material	Catalog No.	Manufacturer
10 mM dNTP-Mix	R0192	Thermo Scientific
Oligo(dT) Primer (0,5 µg/µl)	S0132	Thermo Scientific
Random Hexamer Primer (0,2 µg/µl)	S0142	Thermo Scientific
5x RT-Buffer		Thermo Scientific
Maxima H Minus Reverse Transcriptase (200 U/µl)	EP0753	Thermo Scientific
RiboLock RNase Inhibitor (40 U/µl)	EO0382	Thermo Scientific

2.1.7 RT-qPCR

Table 7.1: Materials for quantitative Real-Time PCR

Material	Manufacturer Catalog No.
2x Luna Universal qPCR Mastermix	New England BioLabs #M3003G
Primer	Siehe Tabelle 7.2
96-well plate	Roche
Sealing film	Roche
LightCycler®	Roche

Table 7.2: Primer sequences for the analyzed genes. All primers have an annealing temperature of 60 °C.

Gene	Sequence
TBP	FWD: GAGCCAAGAGTGAAGAACAGTC REV: GCTCCCCACCATATTCTGAATCT
SDHA	FWD: TGGTTGTCTTTGGTCGGG REV: GCGTTTGGTTTAATTGGAGGG
CDK12	FWD: TTGTGGTACCGACCTCCAGAA REV: CCAGTTCCAGATTGGCTTGAA
BRCA1	FWD: AAAGGGCCTTCACAGTGTCC REV: CCTGTGTCAAGCTGAAAAGCA
BRCA2	FWD: GGAGCTGAGGTGGATCCTGA REV: CATGAGGAAATACAGTTTCAGATGCTT
RAD51	FWD: CAACCCATTTCACGGTTAGAGC REV: TTCTTTGGCGCATAGGCAACA
RAD51c	FWD: GCACCAGGTGTTGGAAAAAC REV: AAACTGCTTCACCTGCCACT
ATM	FWD: TGGATCCAGCTATTTGGTTTGA REV: CCAAGTATGTAACCAACAATAGAAGAAGTAG
ATR	FWD: CAGCTTTGTGCCATTTACTG REV: CTACCTCAATTCCAAGCACA
FANCD2	FWD: GGCCAAGTGGGGATAAAGAG REV: TGATCAGTTCTGGGACACCA
POLH	FWD: GCTAGGGGCCTCTGTCATTG REV: CCTCGGCACATGGCATATAG
POLQ	FWD: TTTTGCTGACCTGCAAAGAGC REV: TTGGCAACTTCTCCCATAAACA

2.1.8 Protein Extraction and Quantification

Table 8.1: Materials required for protein isolation

Material	Manufacturer Catalog No.
RIPA-Buffer	Cell Signaling #9806
Protease inhibitor	Sigma-Aldrich #P8340
Phosphatase inhibitor	Sigma-Aldrich #P0044
Cell scraper	Sarstedt

Table 8.2: Materials for protein concentration determination using BCA assay

Material	Manufacturer Catalog No.
BSA-dilution series	PAN-Biotech GmbH
Pierce BCA Protein Reagents A/B	Thermo Scientific
RIPA-Buffer	Cell Signaling #9806
96-well-plate	Greiner bio-one
Falcon tubes 50ml	Greiner bio-one
iMark Microplate Reader	Bio-Rad

2.1.9 Western Blot

Table 9.1: Electrophoresis and blotting

Material	Manufacturer Catalog No.
APS	Sigma-Aldrich
Glycin	Merck
Methanol	VWR Chemicals
SDS	Roth
Polyacrylamide	Roth
Hydrochloric acid	Merck
TEMED	Sigma-Aldrich
Tris	Merck
Tween 20	Sigma-Aldrich
Non fat dry milk powder	CARL ROTH GmbH CoKG
Roti-Load 4x	CARL ROTH GmbH CoKG
Protein ladder	Thermo Scientific #26625 #26616
Pre-cast gradient gels	Invitrogen
Mini Gel Tank	Thermo Scientific #A25977
Mini-PROTEAN Tetra Cell	Bio-Rad
PVDF membrane	Merck
Nitrocellulose membrane	Bio-Rad
Whatman Paper	GE Healthcare
Clarity Max Western ECL Substrate	Bio-Rad
Clarity Wester ECL Substrate	Bio-Rad
SuperSignal West Femto Maximum Sensitivity Substrate	Thermo Scientific

Table 9.3: Buffer solutions

Material	Manufacturer/Composition
10x Tris/Glycin Buffer	Bio-Rad
10x Tris/Glycin/SDS Buffer	Bio-Rad
10x TBS-Buffer	1.5 M NaCl, 0.1 M Tris pH adjusted to 7.6 with HCl
1x TBS-T-Buffer	1x TBS, 0.1% Tween

Table 9.4: Primary antibodies

Target	Species	Dilution	Blocking Medium	Manufacturer Catalog No.
CDK12	Rabbit	1:1000	5 % Milk	Sigma Aldrich HPA008038
Phospho-H2AX	Rabbit	1:1000	BSA	Cell Signaling 80312
Cleaved PARP	Rabbit	1:500	5 % Milk	Cell Signaling 9541S
Total PARP	Mouse	1:300	5 % Milk	Invitrogen 436400
ATM	Rabbit	1:1000	5 % Milk	Cell Signaling 2873S
ATR	Rabbit	1:1000	5 % Milk	Cell Signaling 2790S
Tubulin	Mouse	1:50000	1 % Milk	Sigma Aldrich T5168
Vinculin	Mouse	1:2000	5 % Milk	Merck Millipore 05-386

Table 9.5: Secondary Antibodies

Target	Species	Dilution	Blocking Medium	Manufacturer Catalog No.
Anti-rabbit	Goat	1:2000	5 % Milk	Dako P0448
Anti-mouse	Rabbit	1:1000	5 % Milk	Dako P0260

2.1.10 Cell Viability Measurement

Table 10: Materials and reagents for performing the MTT assay

Material	Manufacturer
DMSO	Sigma-Aldrich
MTT-reagent	Sigma-Aldrich
96-well plate	Greiner bio-one
iMark Microplate Reader	Bio-Rad
Cell Titer Glo Luminescent Assay	Promega

2.1.11 Software

Table 12: Software used

Software	Publisher
Bio-Rad CFX Maestro	BioRad
CompuSyn Version 1.0	CompuSyn, Inc.
EndNote X9	Clarivate Analytics
Light Cycler 96 Software	Roche
MACSQuantify Version 2.11	Miltenyi Biotec
Micosoft Word 2010	Microsoft
Microsoft Excel 2010	Microsoft
MPM6	BioRad
NanoDrop 2000/2000c	Thermo Scientific
CanoScan Toolbox 5.0	Canon
GraphPad Prism Version 8	GraphPad

2.1.12 Equipment

Table 13: Equipment used

Device	Manufacturer
Cell Counter	Bio-Rad
Incubator HeraCell 150i	Thermo Scientific
Microscope Ts2, TE2000-S	Nikon Eclipse
Cell Culture Centrifuge	Eppendorf
LightCycler®	Roche
Refrigerated Centrifuge	Beckman Coulter
Benchtop Centrifuge	Eppendorf
NanoDrop	Thermo Scientific
BioRad WB Incubator	Bio-Rad
iMark Microplate Reader	Bio-Rad
ChemiDoc Imaging System Version 2.3.0.07	Bio-Rad

2.2 Methods

2.2.1 Cell Culture

2.2.1.1 Cultivation of Urothelial Carcinoma Cells

Urothelial carcinoma cell lines were cultured in DMEM medium supplemented with heat-inactivated 10 % fetal calf serum (FCS). The cells were incubated at 37 °C with 5 % CO_2. Passage occurred biweekly, with cells being detached using trypsin and subsequently transferred to new culture flasks at a dilution ratio of 1:5 (RT-112) to 1:20 (UM-UC-3).

2.2.2 Cultivation of Uroepithelial Cells

The HBLAK cell line was cultured in epithelial cell culture medium and incubated at 37 °C with 5 % CO_2. Passage was conducted biweekly. Cells were detached using accutase, followed by centrifugation at 1.000 rpm for 5 minutes. The supernatant was resuspended, and the cell suspension was transferred to new culture flasks at a dilution ratio of 1:5.

2.2.2.1 Cell Counting

Cell viability and cell count were assessed during passage using Trypan Blue exclusion. The cell suspension was mixed with Trypan Blue in a 1:1 ratio and subsequently analyzed using an automated cell counter. The obtained cell count served as the basis for further experiments in 6- or 96-well plates.

2.2.2.2 Determination of IC_{50}-Values

The half-maximal inhibitory concentrations (IC_{50}) for the inhibitor THZ531 were determined. Tumor cell lines were seeded in 96-well plates and treated with various concentrations of THZ531. Eight dose points ranging from 100 to 5000 nM were tested. A DMSO control was included at the concentration equivalent to the highest dose point. Cells were treated in quadruplicates. Viability was assessed after 72 hours of incubation using the MTT assay, with data analysis and presentation conducted using GraphPad software.

For cisplatin and talazoparib IC_{50}-values previously determined within the research group were utilized (see Table 14).

Table 14: Half-maximal inhibitory concentrations of selected pharmaceuticals.

Cell Line	Cisplatin [µM]	Talazoparib [µM]
RT-112	10.5	25.5
RT-112 LTT	333	52.8
253J	4.5	0.68
253J LTT	83.9	4.9
T-24	3.5	0.8
T-24 LTT	100	0.12
J82	1.7	0.8
J82 LTT	18.8	0.13
UM-UC-3	4	-
VM-CUB1	4	-
HBLAK	5	1

2.2.2.3 Treatment with Pharmaceuticals

Table 15: Cell numbers per well. The table details the cell numbers plated in 96-well plates, with the corresponding cell number for 6-well plates being ten times higher.

Cell Line	96-Well [cells/well]
RT-112	4000
RT-112 LTT	10000
253J	3000
253J LTT	4500
T-24	1500
T-24 LTT	2500
J82	5000
J82 LTT	6000
UM-UC-3	2000
VM-CUB1	2000
HBLAK	5000

Cells designated for the study were plated in wells. The volume of the solution was 50 µl per well in 96-well plates and 2000 µl per well in 6-well plates. Cells were plated at varying concentrations according to their proliferation rates (see Table 15). In 6-well plates, the cell

density was ten times higher than in 96-well plates. After 24 hours, treatment with established dose points was administered. Cell viability was assessed after an additional 72 hours.
Certain sections of the study focused on the potential synergistic effects of combination therapy. For this purpose, cells were treated with combined pharmacological agents. Dose points were determined by combining multiples of the IC_{50}-values of both drugs. The dose points indicated with an X in Table 16 were administered to the cells. After 72 hours, cell viability was evaluated using the MTT assay. Synergistic effects were analyzed using CompuSyn software based on the Chou-Talalay method.

Table 16: Scheme of pharmacological combination therapy. The table illustrates combinations of equal multiples of the IC_{50}-values for two inhibitors/drugs.

x-fold IC_{50}	0.125	0.25	0.5	0.75	1	1.5
0.125	X					
0.25		X				
0.5			X			
0.75				X		
1					X	
1.5						X

2.2.2.4 Cell Viability Measurement

Following the successful treatment of cells with pharmacological inhibitors, cell viability was assessed using two distinct viability assays to quantify the effectiveness of the treatment.

2.2.2.4.1 MTT Assay

The MTT assay relies on the ability of living cells to reduce 3-(4,5-Dimethylthiazol-2-yl)-2,5-Diphenyltetrazolium Bromide (MTT) to formazan. After treatment, 10 µl of MTT reagent (5 mg/ml PBS) was added to the cells, where it was taken up by them. Metabolically active cells reduced MTT to formazan, resulting in the formation of blue formazan crystals. These crystals were dissolved with DMSO, and the absorbance was measured at 570 nm using a microplate reader. The absorbance measured was proportional to the number of viable cells.

2.2.2.4.2 CellTiterGlo® Luminescent Cell Viability Assay

Cell viability was measured using the CellTiterGlo® Luminescent Cell Viability Assay, which relies on a bioluminescence reaction. The light emission is ATP-dependent, and the intensity

of luminescence correlates with the amount of ATP and, consequently, the number of viable cells.

Initially, the provided buffer solution was mixed with the lyophilized substrate to prepare the reagent solution. After treatment in 96-well plates, 50 µl of substrate was added to the cells, initiating the bioluminescence reaction. The light intensity was recorded using a microplate reader.

2.2.2.5 siRNA Knockdown

The use of small interfering RNA (siRNA) results in the degradation of target mRNA, thereby preventing subsequent translation and enabling functional analyses of the gene product in subsequent experiments.

Transfection was performed using lipofectamine RNAiMAX in 6-well plates. This cationic lipid forms lipid nanoparticles with siRNA molecules, facilitating their entry into the cell interior by crossing the cell membrane. Each experiment spanned a duration of 96 hours. On day 1, target cells were seeded into 6-well plates. After 12 hours, transfection was carried out. In one vessel, 1 µl of siRNA (20 µM stock) was mixed with 249 µl of Optimem medium. In a separate vessel, 5 µl of Lipofectamine was mixed with 245 µl of Optimem medium. Both solutions were combined and incubated at room temperature for 15 minutes. The mixture was then pipetted into the wells. A negative control was performed using non-targeting siRNA.

The transfected cells were incubated for 24 hours to allow for siRNA uptake and mRNA degradation. The following day, the cells were plated into 96-well plates and treated with inhibitors. Two wells containing targeting and non-targeting siRNA were retained for subsequent evaluation of transfection efficiency. After an additional 72 hours, the experiments were assessed, and the remaining control cells were harvested. The success of transfection was evaluated using Western Blot and RT-qPCR.

2.2.2.6 Stable Overexpression

CDK12 overexpression was achieved using a pHAGE-based expression vector (vector ID: 116723 from Addgene), with the CDK12 insert subsequently subcloned into a pUC-derived vector for transfection. Cells were transfected using lipofection and selected with puromycin. The transfected cell lines were generated prior to this study and provided by the research group.

2.2.3 RNA Analysis

One section of this thesis investigates the mechanistic effects of pharmacological inhibitors, with a focus on gene expression analysis of various samples. RNA preparation for further molecular analysis is necessary, as described below.

2.2.3.1 RNA Extraction

RNA extraction was performed with trizol lysis followed by using the RNeasy Mini Kit from Qiagen.

Cells were harvested using trizol, and chloroform was added (200 µl chloroform per 1 ml trizol). Trizol denatures proteins and dissolves cellular components, with RNA remaining in the aqueous phase while proteins and DNA partition into the organic phase.

Following trizol lysis, the sample was centrifuged at 12.000 g for 15 minutes at 4 °C to separate the organic and aqueous phases. The aqueous phase, containing RNA, was carefully transferred to a new vessel. An equal volume of ethanol was added to precipitate the RNA from the aqueous phase. The mixture was then applied to the RNeasy Mini Kit columns, where RNA binds to the membrane and impurities are removed. The bound RNA was subsequently washed and eluted with 30-50 µl RNase-free water. RNA concentration was measured and documented using a Nanodrop spectrophotometer. If phenol contamination was detected from the absorption curves, the RNA sample was purified using the RNA Clean & Concentrate Kit from Zymo Research. For low RNA concentrations, samples were concentrated by evaporation to reduce the volume and increase the concentration.

2.2.3.2 Reverse Transcription

Reverse transcription generates a complementary DNA (cDNA) copy of mRNA, allowing the stabilization and storage of genetic information in a more stable double-stranded DNA format compared to RNA.

1 µg of RNA was reverse transcribed in a total volume of 12.5 µl. Each reaction included 1 µl of dNTP mix (10 mM), 0.25 µl of Oligo(dt) primers (0.5 µg/µl), and 0.25 µl of Random Hexamer primers (0.2 µg/µl). The samples were incubated at 65 °C for 5 minutes. Subsequently, RT buffer, 1 µl of Reverse Transcriptase (200 U/µl), and 0.5 µl of RNase Inhibitor (40 U/µl) were added. The resulting cDNA was diluted 1:20 and stored at -20 °C.

2.2.3.3 RT-qPCR

Quantitative Reverse Transcription Polymerase Chain Reaction (RT-qPCR) is a molecular biology technique used to detect and quantify RNA molecules in biological samples.

In the PCR reaction, 2 µl of the diluted cDNA was amplified using specific primers (100 µM stock, added at 0.05 µl each, resulting in a final concentration of 250 nM per primer) and Taq-DNA-polymerase, included in the Luna Master Mix at 10 µl per reaction. During PCR amplification, fluorescent probes were employed to quantify the amount of amplified DNA fragments in each reaction, thereby determining the original RNA quantity in the sample.

Raw data were presented as relative gene expression compared to TBP or SDHA. In some figures, the geometric mean of TBP and SDHA was used as a reference. The logarithmic fold change was calculated to represent genomic expression changes. A fold change with a value greater than 1 (indicating a doubling of gene expression) or less than -1 (indicating a halving of gene expression) is considered biologically significant. Each PCR reaction was conducted in triplicates.

2.2.4 Protein Analysis

2.2.4.1 Protein Extraction

Protein isolation was achieved using RIPA buffer from Cell Signaling, supplemented with protease and phosphatase inhibitors. After incubation with RIPA buffer, the sample was centrifuged at 12.000 g for 10 minutes at 4 °C, and the supernatant containing the proteins was carefully pipetted.

In certain experiments, γH2AX protein was examined. For these samples, prior to centrifugation, the samples were sonicated for 10 seconds three times at 40 % amplitude.

Protein concentration was determined using a BCA assay, which involves reacting BCA with copper ions from the reagent solutions to form a violet-blue color complex in the presence of proteins. The intensity of the color change is proportional to the protein concentration in the sample and was measured spectrophotometrically. A standard curve with known protein concentrations was prepared. The sample and standards were mixed with BCA reagent solutions and incubated. During incubation, copper (I) is reduced to copper (II) by the proteins, forming the color complex. Absorbance of the color complex at 595 nm was measured using a spectrophotometer. Protein concentrations of the samples were determined based on the calibration curve derived from the absorbance values of the standards. If the calculated values were outside the standard range, measurements were repeated with adjusted dilutions.

2.2.4.2 Western Blot

Western blotting enables the separation and identification of proteins based on their charge and size.

Extracted protein samples were denatured with β-Mercaptoethanol and SDS. 20 µg of protein was mixed with RIPA buffer to a total volume of 18 µl, with 6 µl of 4x concentrated Rotiload1 added. The protein samples were then denatured at 95 °C for 5 minutes.

The protein samples were loaded onto a polyacrylamide gel. The gels consisted of a stacking gel and a separating gel, which differed in polyacrylamide concentration. Typically, a 12 % gel was used in the experiments, while an 8% gel was employed for CDK12 detection. For the separation of particularly large proteins such as ATM and ATR a pre-cast gradient gel from

Invitrogen in the Mini Gel Tank from Thermo Fisher Scientific was utilized. Electrophoresis in the gradient gel was conducted at room temperature at 150 V for 90 minutes. For CDK12 detection, protein separation was performed on ice. After a 15-minute run at 70 V, the voltage was increased to 160 V for 90 minutes. For γH2AX and cleaved PARP detection, protein samples were separated on a 12 % gel at room temperature for 180 minutes at 80 V.

Transfer was carried out in the blotting tank at 180 mA for 120 minutes. A PVDF membrane was used for the transfer, whereas a nitrocellulose membrane was used for γH2AX detection. Both membranes were activated in methanol for one minute and then washed with Millipore water.

The membrane was blocked for one hour at room temperature with 5% milk. Incubation with the primary antibody was performed overnight at 4 °C. The primary antibody against γH2AX was dissolved in 5 % BSA, while other primary antibodies were dissolved in 5 % milk. The secondary antibody was diluted in the same medium as the primary antibody and incubated with the membrane at room temperature for one hour.

Detection was performed using ECL from Bio-Rad or Thermo Fisher Scientific. Densitometric analysis was not conducted.

2.2.4.3 Stripping

Stripping is a process used to remove antibodies from the membrane, allowing it to be reused for subsequent analyses with different antibodies. The stripping buffer was prepared with SDS, Tris-HCl, and water. The membrane was immersed in the buffer with 140 µl of 2-Mercaptoethanol added. It was incubated at 50 °C for 30 minutes, then washed. The membrane was subsequently blocked again with 5 % milk for one hour.

2.2.5 Statistics

Statistical analyses were performed using GraphPad Prism and Excel. Data are presented as mean ± standard deviation (SD). All experiments were carried out in at least three technical or biological replicates. For qPCR experiments, relative gene expression levels were calculated with TBP and/or SDHA serving as reference genes. In selected analyses, the geometric mean of both reference genes was applied. Gene expression changes are reported as logarithmic fold changes relative to control conditions.

Statistical significance was assessed using t-tests for pairwise comparisons or one-way ANOVA when more than two groups were compared. A p-value of < 0.05 was considered statistically significant. Levels of significance are indicated as follows: $p < 0.05$ (*), $p < 0.01$ (**), $p < 0.001$ (***), and not significant (n.s.)

3 Results

3.1 Molecular Response towards Short Term Treatment with Cisplatin

Unpublished data from the University Hospital Essen indicated that CDK12 protein levels increased in patient samples following cisplatin therapy. This suggested that CDK12 might play a role in the therapeutic response of urothelial carcinoma. The aim of the following experiments was therefore to further investigate these in vivo observations in cell culture models.

First, cisplatin-naive parental cell lines (PAR) and their long-term cisplatin-exposed sublines (LTT) were compared under untreated conditions in order to assess potential long-term effects of chronic cisplatin exposure on baseline CDK12 expression. Subsequently, the short-term effect of a 72-hour cisplatin treatment at the respective IC_{50} concentration (as shown in Table 14) on CDK12 expression was analyzed.

These analyses were performed using Western blotting. In further experiments, DNA repair genes that are partly regulated by CDK12 were examined by RT-qPCR.

3.1.1 Changes in CDK12 Protein Levels

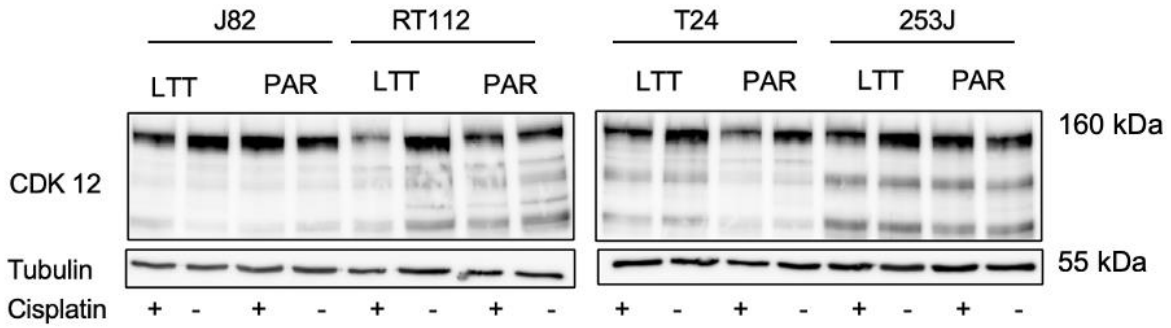

Figure 1: Protein levels of CDK12 after 72 hours of cisplatin exposure. The protein amount was measured using Western blot. Shown are the parental cisplatin-naive urothelial carcinoma cells (PAR) and their cisplatin-resistant sublines (LTT). Cisplatin treatment is indicated by a plus sign (+). Tubulin was used as a loading control. For the cisplatin concentrations applied, see Table 14.

The four urothelial carcinoma cell lines J82, RT-112, T24, and 253J (PAR), as well as their cisplatin-resistant sublines (LTT), were investigated. After 72 hours of cisplatin exposure (at IC_{50} dosage), CDK12 levels were measured by Western blot. Untreated LTT cells exhibited higher CDK12 protein levels compared to untreated parental cells.

Following cisplatin exposure, CDK12 protein amount decreased in all LTT lines after cisplatin treatment. In parental cells, the effect was more heterogeneous. In the J82 and 253J cell lines,

CDK12 content increased. In contrast, T24 cells showed a decrease in CDK12, while the protein content in RT-112 remained approximately constant.

In summary, the LTT cell lines exhibited higher basal CDK12 levels and responded to short-term cisplatin exposure with a downregulation of CDK12. The parental cell lines, in contrast, displayed a more heterogeneous behavior. These results are consistent with clinical observations.

3.1.2 Gene Expression Changes of DNA Damage Repair Genes

To further characterize the functional context, genes with a central role in the DNA damage response and, in particular, homologous recombination were analyzed. The selection included *BRCA1, BRCA2, RAD51 and RAD51C* as mediators of homologous recombination, *POLH* and *POLQ* as representatives of alternative repair mechanisms, *FANCD2* as a key molecule of the Fanconi anemia pathway, and the signaling kinases *ATR* and *ATM* (see 1.2). Gene expression was measured by RT-qPCR. Both LTT and parental cells were exposed to cisplatin for 72 hours at their respective IC_{50} doses (for concentrations see Table 14) prior to RNA extraction.

The following gene expression changes are presented as fold changes, which have been determined logarithmically. A fold change with a value greater than 1 (indicating a doubling of gene expression) or less than -1 (indicating a halving of gene expression) is considered biologically significant.

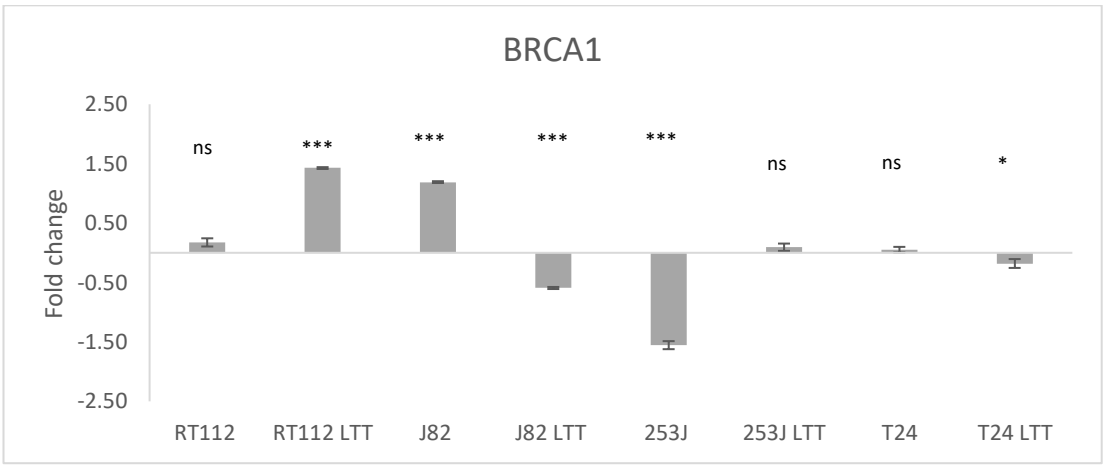

Figure 2: Logarithmic fold change of *BRCA1* after 72 hours of cisplatin exposure. The fold change was calculated as the logarithmic quotient (base 2) of the relative gene expression of treated versus untreated cells (measured by qPCR). *SDHA* and *TBP* were used as housekeeping genes; the geometric mean was calculated. Shown are the parental cisplatin-naive urothelial carcinoma cells and their cisplatin-resistant sublines (LTT). Bars represent mean ± SD of three technical replicates obtained from one biological sample per condition. Statistical comparisons between treated and untreated samples were performed using an unpaired two-tailed t-test. For the cisplatin concentrations applied, see Table 14.

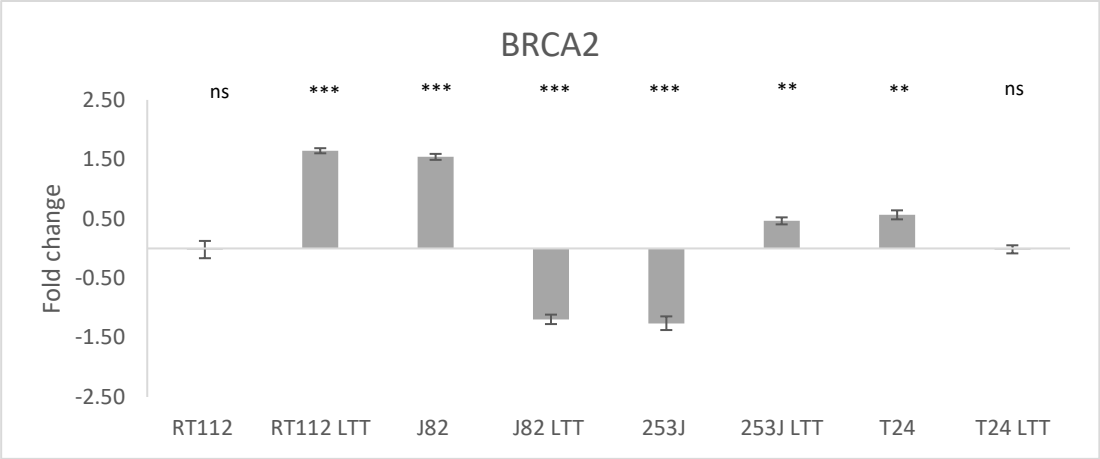

Figure 3: Logarithmic fold change of *BRCA2* after 72 hours of cisplatin exposure. The fold change was calculated as the logarithmic quotient (base 2) of the relative gene expression of treated versus untreated cells (measured by qPCR). *SDHA* and *TBP* were used as housekeeping genes; the geometric mean was calculated. Shown are the parental cisplatin-naive urothelial carcinoma cells and their cisplatin-resistant sublines (LTT). Bars represent mean ± SD of three technical replicates obtained from one biological sample per condition. Statistical comparisons between treated and untreated samples were performed using an unpaired two-tailed t-test. For the cisplatin concentrations applied, see Table 14.

In Figures 2 and 3, the gene expression changes of urothelial carcinoma cells for the genes *BRCA1* and *BRCA2* after cisplatin treatment are illustrated. Both genes displayed parallel expression changes in the respective cell line.

Both genes showed upregulation in the RT-112-LTT and J82 cell lines. Cisplatin-treated RT-112-LTT cells exhibited a 1.4-fold increase in *BRCA1* expression and a 1.6-fold increase in *BRCA2* expression. J82 cells responded to cisplatin with a 1.2-fold rise in *BRCA1*- and 1.5-fold in *BRCA2* expression.

Notably, RT112-LTT responded with a marked upregulation of both *BRCA* genes compared to the parental cell line. In contrast, J82-LTT displayed the opposite pattern, with a downregulation of *BRCA1* and *BRCA2*. The remaining cell lines showed fold change values that were not significant. Overall, RT112-LTT exhibited the expected behavior after cisplatin exposure, with an increase in the expression of genes involved in homologous recombination.

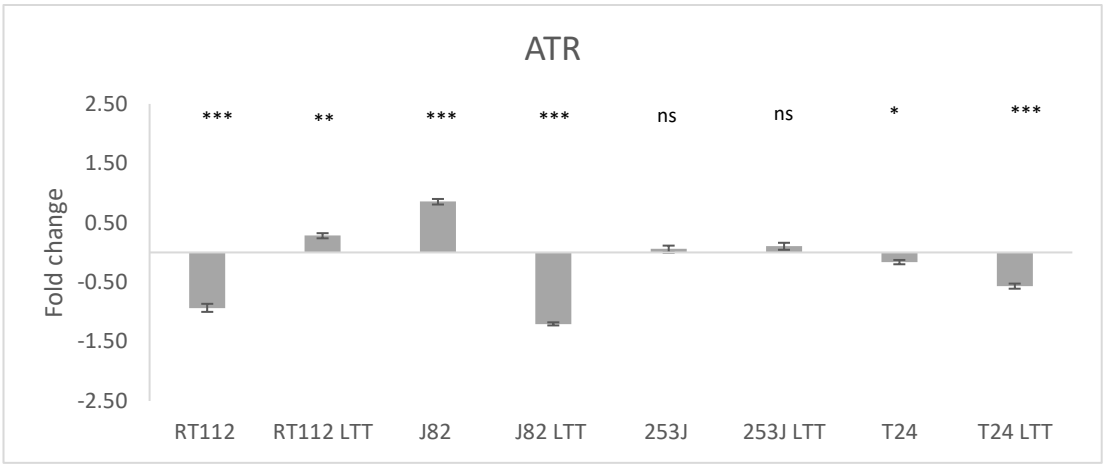

Figure 4: Logarithmic fold change of *ATR* after 72 hours of cisplatin exposure. The fold change is calculated as the logarithmic quotient (base 2) of the relative gene expression of treated versus untreated cells (measured by qPCR). *SDHA* and *TBP* were used as housekeeping genes; the geometric mean was calculated. Shown are the parental cisplatin-naive urothelial carcinoma cells and their cisplatin-resistant sublines (LTT). Bars represent mean ± SD of three technical replicates obtained from one biological sample per condition. Statistical comparisons between treated and untreated samples were performed using an unpaired two-tailed t-test. For the cisplatin concentrations applied, see Table 14.

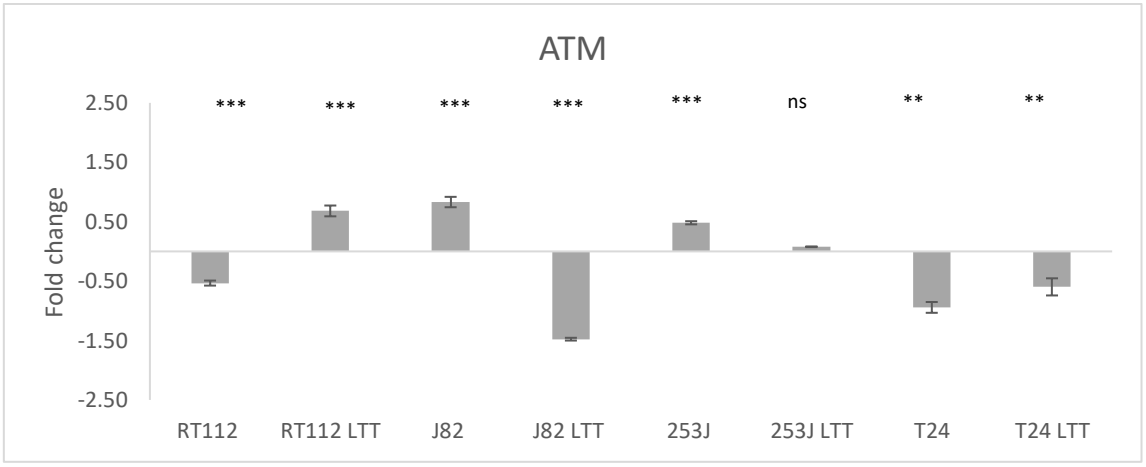

Figure 5: Logarithmic fold change of *ATM* after 72 hours of cisplatin exposure. The fold change was calculated as the logarithmic quotient (base 2) of the relative gene expression of treated versus untreated cells (measured by qPCR). *SDHA* and *TBP* were used as housekeeping genes; the geometric mean was calculated. Shown are the parental cisplatin-naive urothelial carcinoma cells and their cisplatin-resistant sublines (LTT). Bars represent mean ± SD of three technical replicates obtained from one biological sample per condition. Statistical comparisons between treated and untreated samples were performed using an unpaired two-tailed t-test. For the cisplatin concentrations applied, see Table 14.

The gene expression changes of the signaling molecules *ATR* and *ATM* are illustrated in Figures 4 and 5.

Following cisplatin exposure, *ATR* expression decreased by a factor of -1.2 and ATM expression by a factor of -1.5 in J82-LTT cells.

In the RT112-LTT cell line, *ATR* expression was reduced by approximately half, while *ATM* showed only a minor downregulation. In contrast, T24 exhibited a halving of *ATM* expression, whereas *ATR* did not display any significant change. The remaining cell lines showed no biologically relevant alterations in either kinase. Overall, no enhanced signal of *ATR* or *ATM* regulation was observed following cisplatin exposure. The regulation of ATR and ATM after cisplatin treatment appeared heterogeneous, with no consistent pattern across all cell lines.

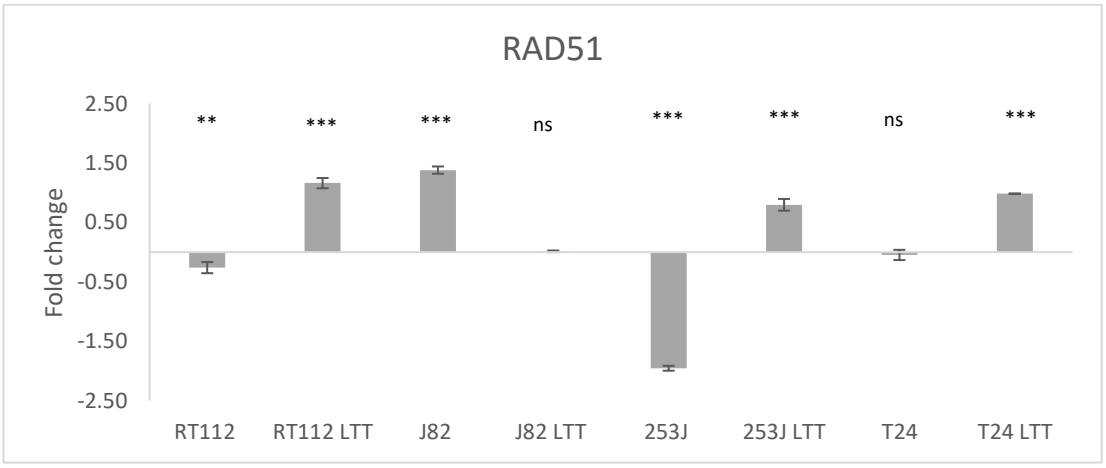

Figure 6: Logarithmic fold change of *RAD51* after 72 hours of cisplatin exposure. The fold change was calculated as the logarithmic quotient (base 2) of the relative gene expression of treated versus untreated cells (measured by qPCR). *SDHA* and *TBP* were used as housekeeping genes; the geometric mean was calculated. Shown are the parental cisplatin-naive urothelial carcinoma cells and their cisplatin-resistant sublines (LTT). Bars represent mean ± SD of three technical replicates obtained from one biological sample per condition. Statistical comparisons between treated and untreated samples were performed using an unpaired two-tailed t-test. For the cisplatin concentrations applied, see Table 14.

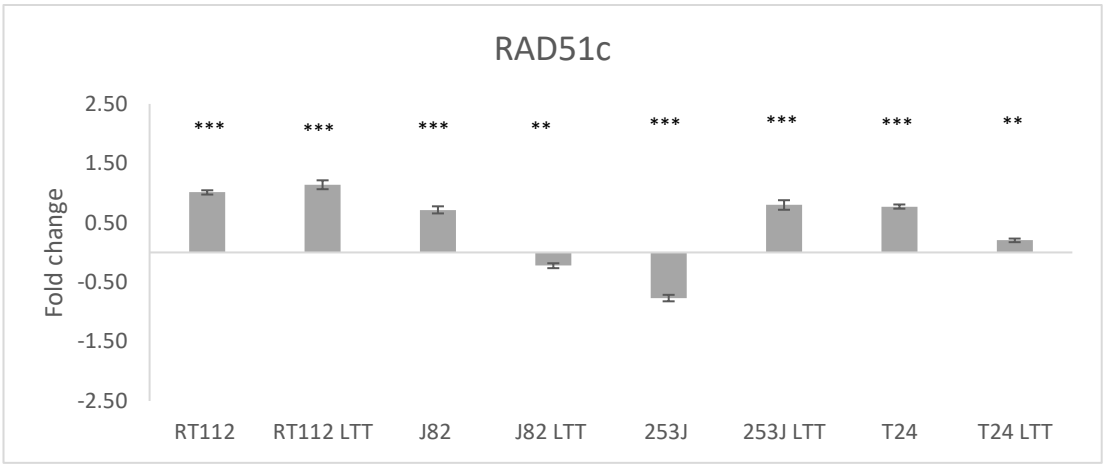

Figure 7: Logarithmic fold change of *RAD51c* after 72 hours of cisplatin exposure. The fold change was calculated as the logarithmic quotient (base 2) of the relative gene expression of treated versus untreated cells (measured by qPCR). *SDHA* and *TBP* were used as housekeeping genes; the geometric mean was calculated. Shown are the parental cisplatin-naive urothelial carcinoma cells and their cisplatin-resistant sublines (LTT). Bars represent mean ± SD of three technical replicates obtained from one biological sample per condition. Statistical comparisons between treated and untreated samples were performed using an unpaired two-tailed t-test. For the cisplatin concentrations applied, see Table 14.

Figures 6 and 7 illustrate the expression changes of the DNA repair proteins *RAD51* and *RAD51c* after 72 hours of cisplatin exposure. *RAD51* and *RAD51C* are essential mediators of homologous recombination. According to current knowledge, they are not directly subject to transcriptional regulation by CDK12, but they remain crucial components of the DNA damage response. Therefore, their expression after cisplatin exposure was compared between parental and LTT cells.

For *RAD51C*, a clear upregulation was observed in the RT112 cell lines, exceeding the predefined biological cut-off. In the remaining cell lines, changes remained below this threshold, although some of them reached statistical significance.

For *RAD51*, a more heterogeneous pattern emerged. In RT112-LTT and J82 parental cells, biologically relevant upregulation was detected, whereas 253J parental cells showed a marked downregulation. In T24-LTT, the value was approximately 0.98, narrowly below the cut-off, but reached high statistical significance, suggesting a relevant tendency toward upregulation. In the other cell lines, some significant changes were observed, but they remained below the biological threshold.

Overall, these findings indicate a consistent signal of enhanced *RAD51C* and *RAD51* expression in RT112-LTT, while the other LTT sublines exhibited only moderate, albeit statistically supported, alterations.

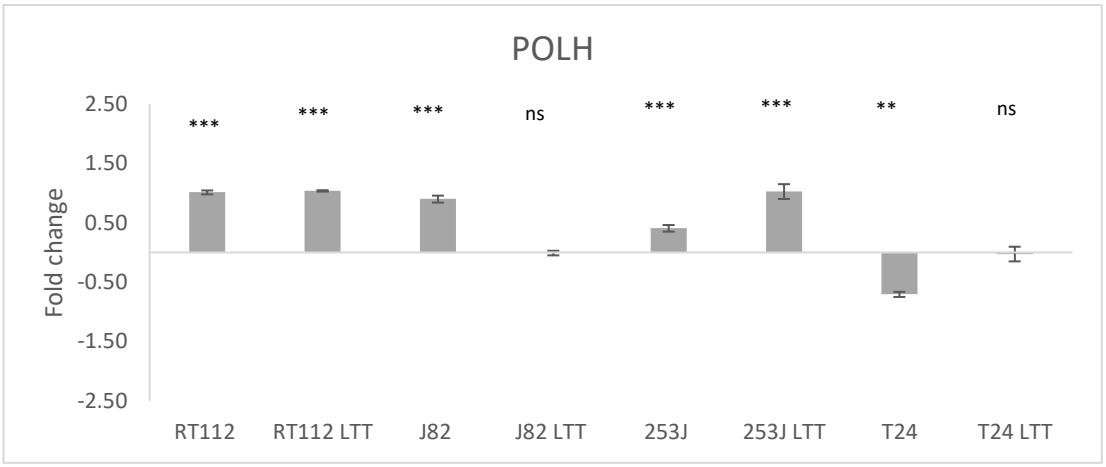

Figure 8: Logarithmic fold change of *POLH* after 72 hours of cisplatin exposure. The fold change was calculated as the logarithmic quotient (base 2) of the relative gene expression of treated versus untreated cells (measured by qPCR). *SDHA* and *TBP* were used as housekeeping genes; the geometric mean was calculated. Shown are the parental cisplatin-naive urothelial carcinoma cells and their cisplatin-resistant sublines (LTT). Bars represent mean ± SD of three technical replicates obtained from one biological sample per condition. Statistical comparisons between treated and untreated samples were performed using an unpaired two-tailed t-test. For the cisplatin concentrations applied, see Table 14.

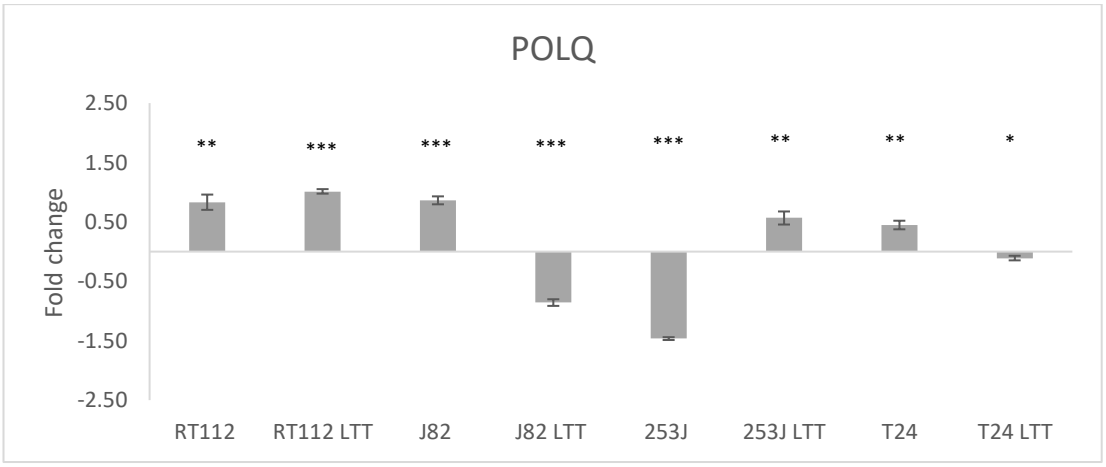

Figure 9: Logarithmic fold change of *POLQ* after 72 hours of cisplatin exposure. The fold change was calculated as the logarithmic quotient (base 2) of the relative gene expression of treated versus untreated cells (measured by qPCR). *SDHA* and *TBP* were used as housekeeping genes; the geometric mean was calculated. Shown are the parental cisplatin-naive urothelial carcinoma cells and their cisplatin-resistant sublines (LTT). Bars represent mean ± SD of three technical replicates obtained from one biological sample per condition. Statistical comparisons between treated and untreated samples were performed using an unpaired two-tailed t-test. For the cisplatin concentrations applied, see Table 14.

The expression of *POLH* and *POLQ* was analyzed, as their gene products play a central role in alternative DNA repair mechanisms. The expression changes after cisplatin exposure were analyzed by PCR and are presented in Figures 8 and 9.

POLH showed a marked upregulation above the log_2FC cut-off of 1 in the RT112 cell lines (parental and LTT) as well as in 253J-LTT, indicating biological relevance. In J82 parental cells, a strong increase was also observed (0.90), which narrowly missed the cut-off but was highly significant. The remaining cell lines displayed only moderate changes that, although statistically supported, did not reach biological relevance.

For *POLQ*, a more heterogeneous pattern was observed. In RT112-LTT, expression levels exceeded the cut-off (1.01) and were thus biologically relevant, whereas RT112 parental cells showed a moderate but significant upregulation (0.83). In contrast, 253J parental cells exhibited a pronounced downregulation (−1.46), clearly below the biological threshold. The other cell lines showed only minor or sub-threshold changes, some of which reached statistical significance.

In summary, RT112 cells responded consistently with an upregulation of *POLH* and *POLQ*, whereas 253J parental cells were characterized by a marked downregulation of *POLQ*. In the remaining cell lines, expression changes were less pronounced and predominantly biologically irrelevant, although in part statistically significant.

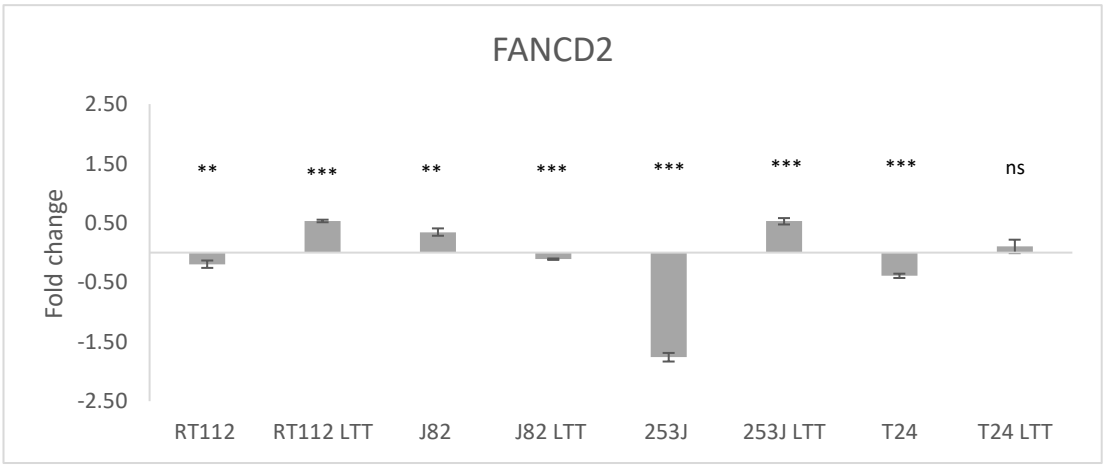

Figure 9: Logarithmic fold change of *FANCD2* after 72 hours of cisplatin exposure. The fold change was calculated as the logarithmic quotient (base 2) of the relative gene expression of treated versus untreated cells (measured by qPCR). *SDHA* and *TBP* were used as housekeeping genes; the geometric mean was calculated. Shown are the parental cisplatin-naive urothelial carcinoma cells and their cisplatin-resistant sublines (LTT). Bars represent mean ± SD of three technical replicates obtained from one biological sample per condition. Statistical comparisons between treated and untreated samples were performed using an unpaired two-tailed t-test. For the cisplatin concentrations applied, see Table 14.

The expression of *FANCD2,* a key factor of the Fanconi anemia pathway and closely linked to homologous recombination, was examined after cisplatin exposure.

In most cell lines, changes in *FANCD2* expression were moderate and did not exceed the predefined biological cut-off, although several of them reached statistical significance (e.g.,

RT112 LTT, J82, 253J LTT). A notable exception was observed in 253J parental cells, which showed a marked downregulation (−1.76), indicating biological relevance.
In summary, while *FANCD2* expression was only moderately altered in most models, 253J parental cells displayed a pronounced downregulation, suggesting a cell line–specific response within the Fanconi anemia repair pathway.

Taken together, the expression profiles show that long-term cisplatin exposed LTT cells do not exhibit a uniform regulatory pattern across DNA repair genes despite their elevated basal CDK12 levels. Instead of a consistent upregulation of homologous recombination, the LTT models responded in a distinctly cell-line dependent manner. This was particularly evident for *BRCA1* and *BRCA2*, which displayed parallel regulation within each model but frequently responded in opposite directions between parental and LTT cells. RT112-LTT showed a pronounced upregulation of multiple homologous recombination genes as well as alternative repair genes, whereas J82-LTT downregulated the same targets, and 253J-LTT activated only a subset of repair mechanisms. This heterogeneity indicates that elevated CDK12 levels do not automatically translate into enhanced transcription of DNA repair genes under acute cisplatin exposure. Rather, cisplatin resistance appears to rely on a broader reorganization of the DNA damage response, with individual cell lines engaging different combinations of repair programs. Overall, the findings support a model in which chronic cisplatin exposure promotes heterogeneous and multifactorial adaptations in the DNA repair landscape.

3.2 Response of Urothelial Carcinoma Cells to the CDK12-Inhibitor THZ531

From the previous sections it becomes evident that the cisplatin-resistant sublines (LTT) exhibit higher CDK12 protein levels compared to their parental counterparts. In the following, the sensitivity to the CDK12 inhibitor THZ531 was examined, with a particular focus on whether LTT cells display increased sensitivity and whether this correlates with CDK12 protein levels.

3.2.1 IC_{50}-Values for Urothelial Carcinoma Cells

A

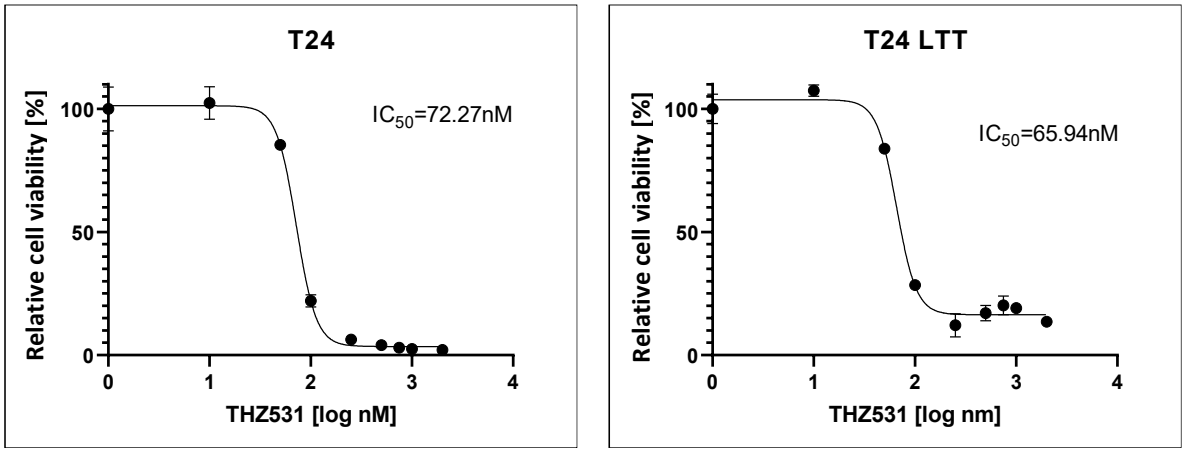

B

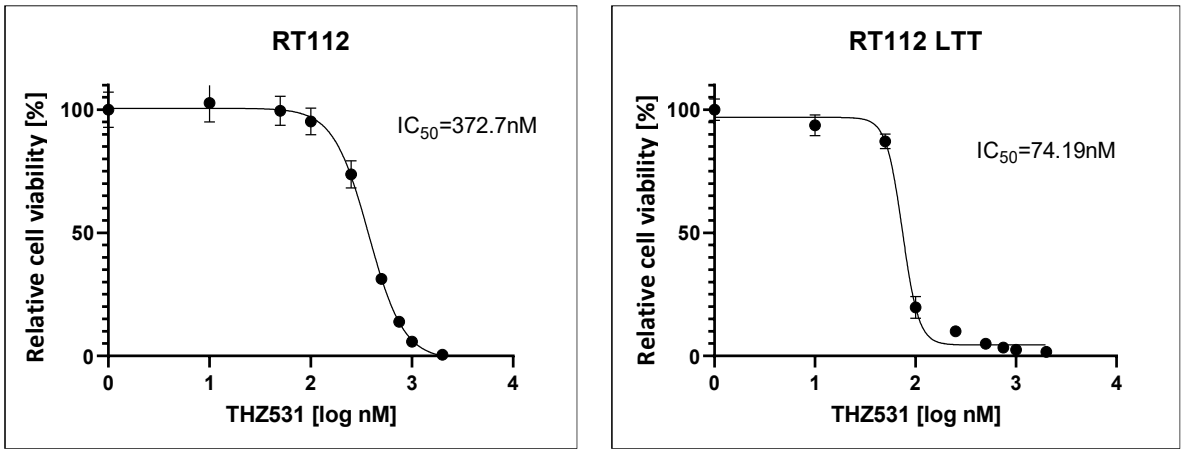

C

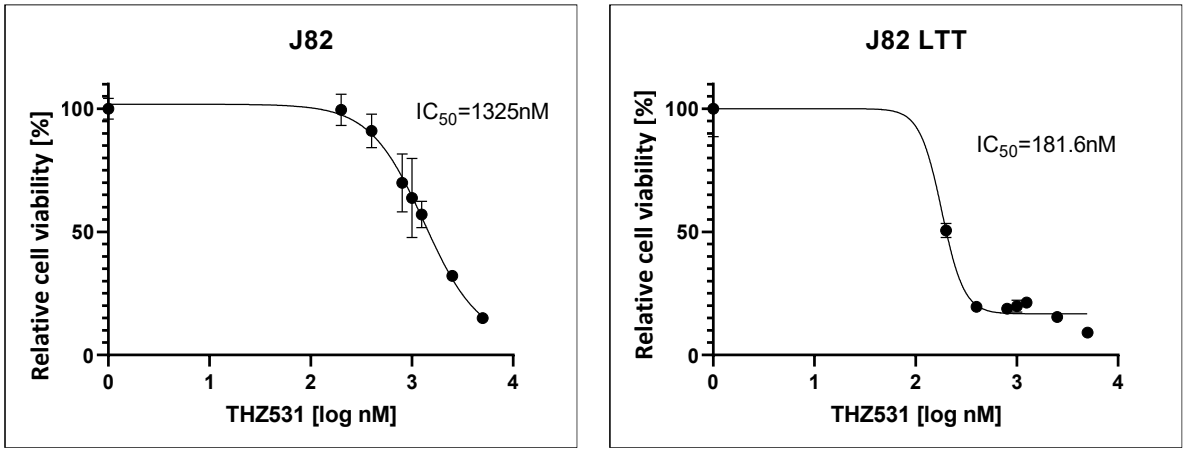

D

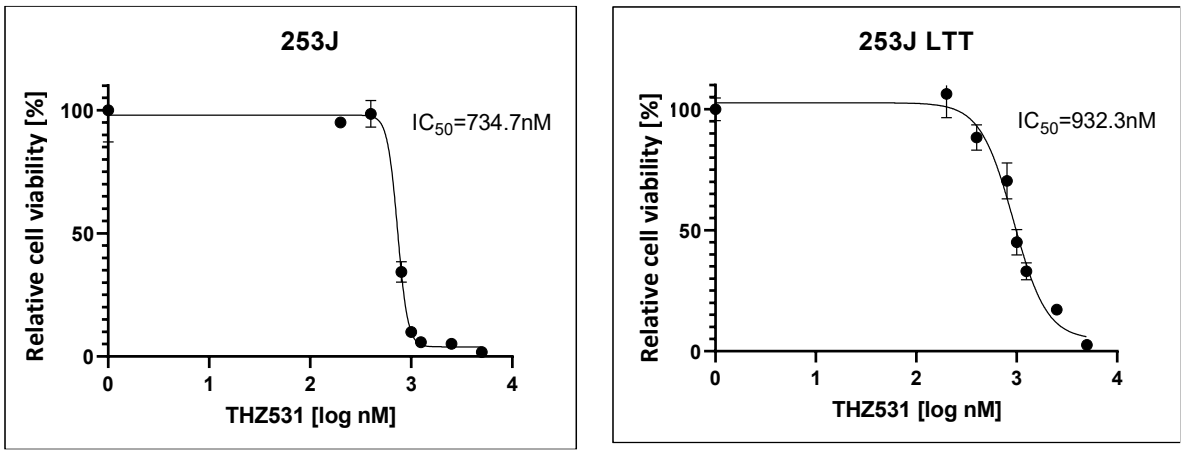

Figure 11: Half-maximal inhibitory doses (IC_{50}) for THZ531 in urothelial carcinoma cell lines. Figure 11 shows the IC_{50}-values for the pharmacological inhibitor THZ531 across various urothelial carcinoma cell lines. The values are presented pairwise for the parental urothelial carcinoma cell lines and their cisplatin-resistant sublines (LTT). Cell viability was assessed using an MTT assay following 72 hours of THZ531 exposure. The data were analyzed, and IC50-values were calculated using GraphPad Prism. Each concentration point represents the mean ± SD of four biological replicates derived from one biological sample per condition. IC_{50} values were calculated using non-linear regression analysis in GraphPad Prism.

IC_{50}-values for the pharmacological inhibitor THZ531 were determined for the depicted cell lines. Figure 11 shows the IC_{50}-values for cisplatin-naive cell lines compared directly with those of their cisplatin-resistant sublines (LTT).

It is evident that, except for 253J (D), the half-maximal inhibitory doses for the LTTs were lower than those for the parental cell lines. Specifically, the IC_{50}-value for J82-LTT (C) was seven times lower than that of the parental J82 cell line. Overall, the IC_{50}-values were in a low range, with RT112-LTT and T24-LTT achieving their half-maximal inhibitory doses below 100

nM. J82 had the highest IC_{50}-value with 1.3 µM. Both T24 parental and LTT cells are remarkably sensitive towards THZ531.

3.2.2 Normal Cell Toxicity of THZ531

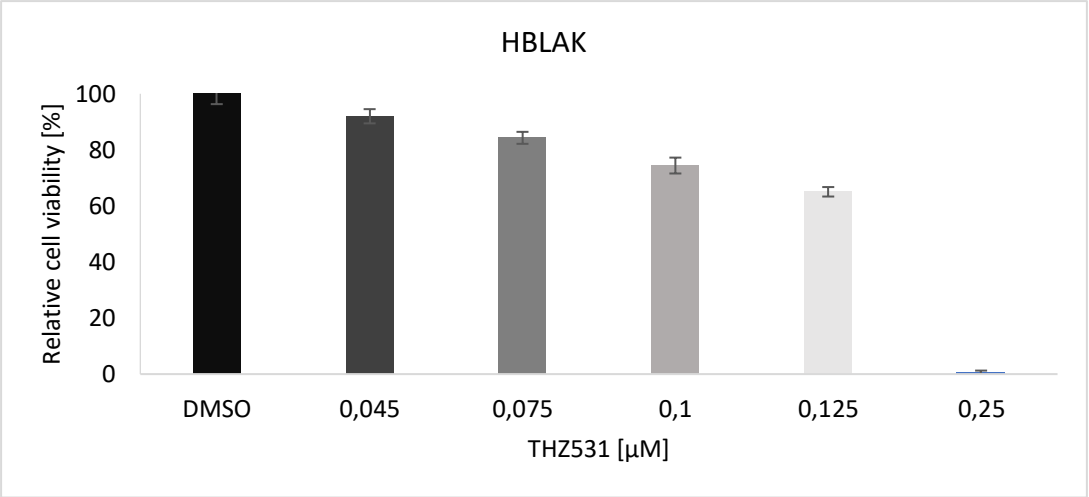

Figure 12: Effect of THZ531 on uroepithelial cells (HBLAK). Cell viability was assessed using the CellTiter-Glo assay after 72 h of THZ531 exposure. Each concentration was measured in biological triplicates, and values are shown as mean ± SD of one biological sample per condition. The IC_{50} value (204 nM) was determined using non-linear regression analysis in GraphPad Prism.

The figure above shows the viability profile for THZ531-treated immortalized uroepithelial cells (HBLAK).

For HBLAK cells (Figure 12), it was observed that at a concentration of 0.125 µM THZ531, approximately 65 % of the cells remained viable. Increasing the dose to 0.25 µM resulted in a rapid decline in cell viability to near 0 %. The calculated IC_{50}-value for HBLAK cells is 204 nM. When comparing the IC_{50}-values of the tumor cells with those of the immortalized uroepithelial cells (HBLAK), three of the four cisplatin-resistant LTT cell lines (RT112-LTT, T24-LTT, J82-LTT) exhibited lower IC_{50}-values than HBLAK, indicating a higher sensitivity toward THZ531. Among the parental cell lines, only T24 showed an IC_{50} below the HBLAK reference value.

3.2.3 DNA Damage and Apoptosis Induction in LTTs

It was observed that, with the exception of 253J, the LTT cells were more sensitive to pharmacological inhibition with THZ531. The subsequent experimental setups were therefore designed to address this finding. Specifically, we investigated the effect of THZ531 on the cells, focusing on whether it induces apoptosis or exerts its impact through alternative mechanisms affecting the cell cycle.

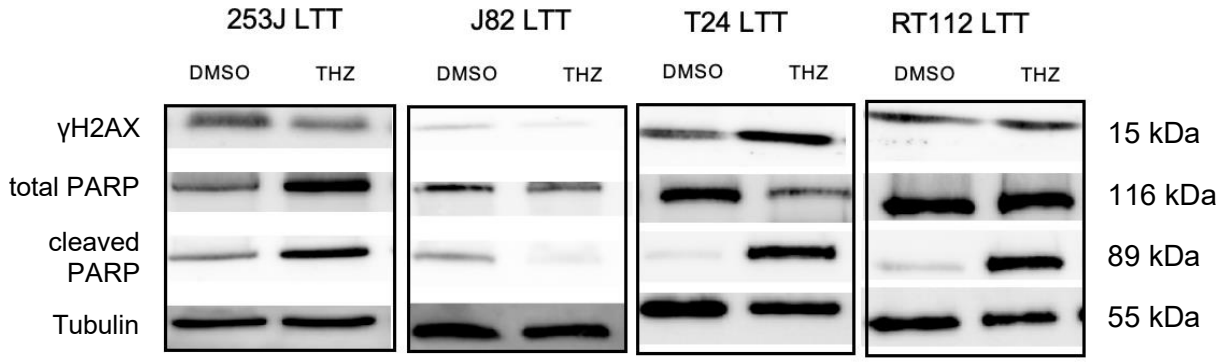

Figure 13: Effect of THZ531 on DNA damage and apoptosis induction. The impact of THZ531 on DNA damage and apoptosis induction was assessed. Protein levels were measured using Western blot. The figure reveals the cisplatin-resistant sublines (LTT) of established urothelial carcinoma cell lines, each treated with THZ531 for 72 hours (THZ). The control treatment was performed with DMSO. Tubulin was used as the loading control.

The effect of THZ531 on apoptosis and DNA damage was investigated using Western blot analysis, as shown in Figure 13. Apoptosis was monitored by assessing PARP cleavage, with cleaved PARP measured relative to total PARP.

The analysis revealed that the cell lines T24-LTT and RT112-LTT exhibited increased PARP cleavage in response to THZ531, suggesting enhanced apoptosis. In contrast, J82-LTT and 253J-LTT cells did not show a significant increase in PARP cleavage.

Regarding DNA damage, T24-LTT cells displayed elevated γH2AX levels, which may indicate increased DNA damage or reflect apoptotic processes. In the remaining cell lines, γH2AX levels remained largely unchanged following THZ531 treatment. To more precisely differentiate between DNA damage and apoptosis-associated changes, complementary analyses such as immunofluorescence staining of γH2AX would be required.

3.2.4 Changes in the Expression of DNA Damage Repair Genes Following THZ531 Treatment

It has been described in the literature that CDK12, through the transcriptional regulation of DNA repair genes, plays an essential role in controlling DNA damage responses. Pharmacological inhibition of CDK12 can therefore serve as a therapeutic approach by reducing the repair capacity of the cell and inducing a so-called BRCAness-phenotype (see 1.3.2). Against this background, the present study analyzed the expression of DNA repair genes involved in homologous recombination as well as alternative repair pathways after 72 hours of treatment with the CDK12 inhibitor THZ531 at the IC_{50} concentration (as displayed in Figure 11) using qPCR. The following gene expression changes are presented as fold changes, which have been determined logarithmically. A fold change with a value greater than 1 (indicating a

doubling of gene expression) or less than -1 (indicating a halving of gene expression) is considered biologically significant.

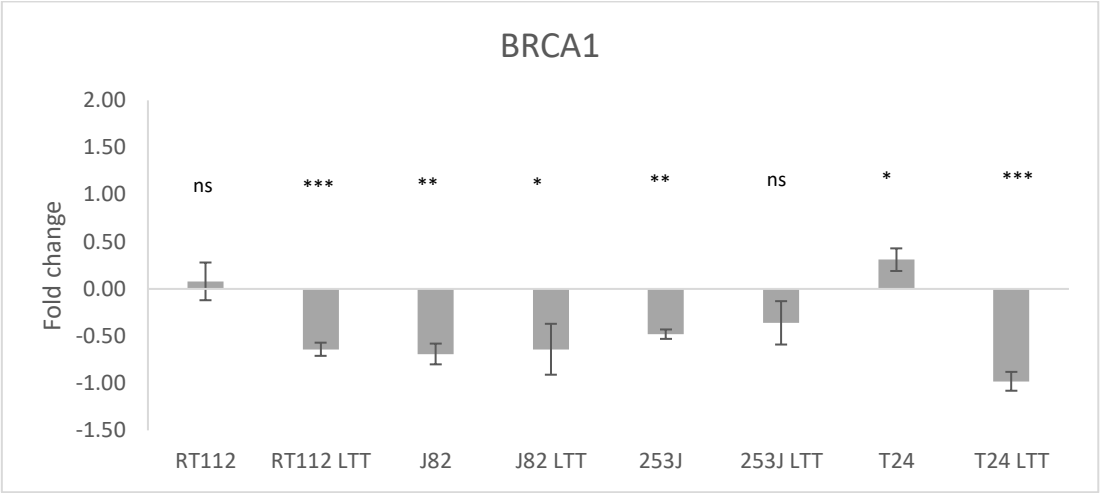

Figure 14: Logarithmic fold change of *BRCA1* after 72 hours of THZ531 exposure. The fold change was calculated as the logarithmic quotient (base 2) of the relative gene expression of treated versus untreated cells (measured by qPCR). *TBP* was used as a housekeeping gene. Shown are the parental cisplatin-naive urothelial carcinoma cells and their cisplatin-resistant sublines (LTT). Bars represent mean ± SD of three technical replicates obtained from one biological sample per condition. Statistical comparisons between treated and untreated samples were performed using an unpaired two-tailed t-test. For the THZ531 concentrations applied, see Figure 11.

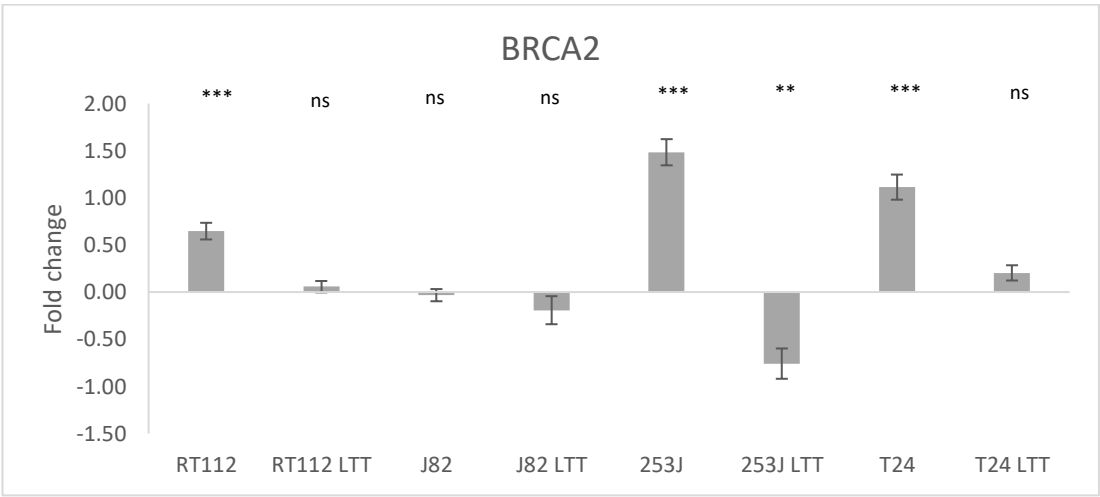

Figure 15: Logarithmic fold change of *BRCA2* after 72 hours of THZ531 exposure. The fold change was calculated as the logarithmic quotient (base 2) of the relative gene expression of treated versus untreated cells (measured by qPCR). *TBP* was used as a housekeeping gene. Shown are the parental cisplatin-naive urothelial carcinoma cells and their cisplatin-resistant sublines (LTT). Bars represent mean ± SD of three technical replicates obtained from one biological sample per condition. Statistical comparisons between treated and untreated samples were performed using an unpaired two-tailed t-test. For the THZ531 concentrations applied, see Figure 11.

Figures 14 and 15 illustrate the gene expression changes for *BRCA1* and *BRCA2* in urothelial carcinoma cells following treatment with THZ531.

For *BRCA1*, the data suggested a general tendency toward downregulation. In most cell lines, fold changes remained between −1 and +1, indicating no biologically relevant alteration. Nevertheless, T24-LTT cells showed a marked decrease (−0.98), corresponding to approximately a halving of *BRCA1* expression and thus representing a near-threshold biologically relevant reduction.

For *BRCA2*, biologically relevant upregulations were detected in 253J parental (1.48) and T24 parental (1.11). In RT112 parental cells, *BRCA2* expression increased significantly; however, the change did not exceed the biological cut-off and was therefore not considered biologically relevant. In 253J LTT cells, a moderate reduction (−0.76) was observed, which was statistically significant but likewise did not reach the threshold for biological relevance. The remaining models did not show biologically relevant changes.

THZ531 treatment induced a general downregulation trend for *BRCA1* and selective upregulation of *BRCA2* in 253J and T24 parental cells, while most other changes were statistically significant but not biologically relevant.

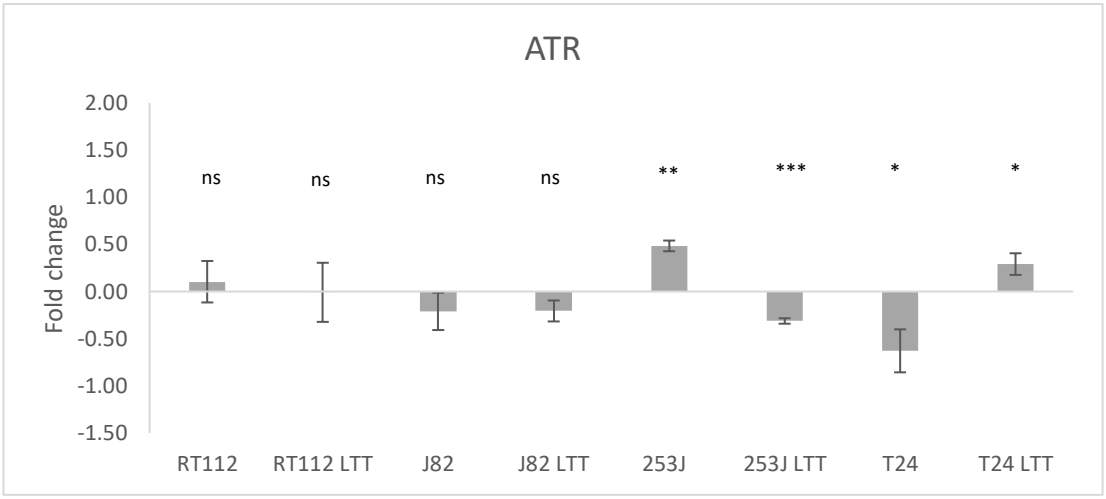

Figure 16: Logarithmic fold change of *ATR* after 72 hours of THZ531 exposure. The fold change was calculated as the logarithmic quotient (base 2) of the relative gene expression of treated versus untreated cells (measured by qPCR). *TBP* was used as a housekeeping gene. Shown are the parental cisplatin-naive urothelial carcinoma cells and their cisplatin-resistant sublines (LTT). Bars represent mean ± SD of three technical replicates obtained from one biological sample per condition. Statistical comparisons between treated and untreated samples were performed using an unpaired two-tailed t-test. For the THZ531 concentrations applied, see Figure 11.

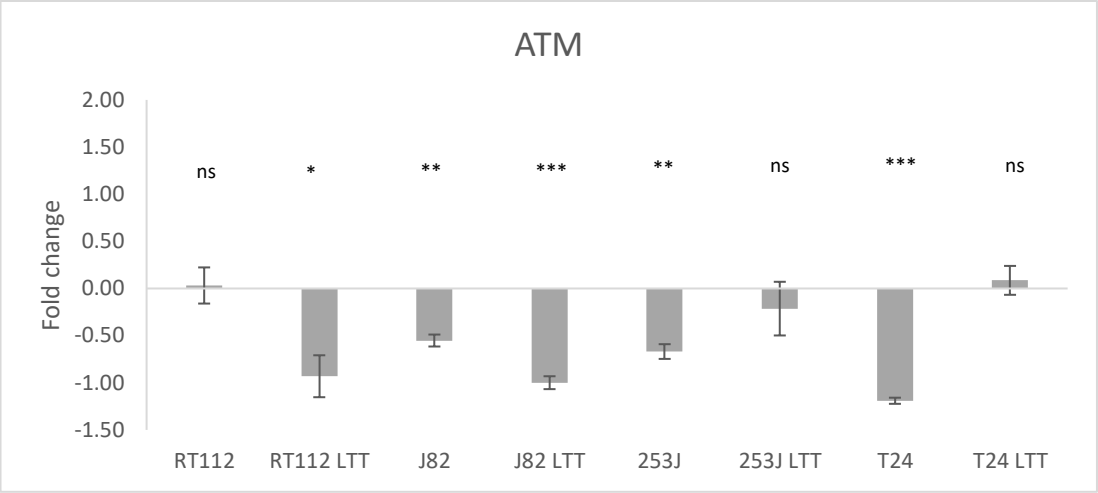

Figure 17: Logarithmic fold change of *ATM* after 72 hours of THZ531 exposure. The fold change was calculated as the logarithmic quotient (base 2) of the relative gene expression of treated versus untreated cells (measured by qPCR). *TBP* was used as a housekeeping gene. Shown are the parental cisplatin-naive urothelial carcinoma cells and their cisplatin-resistant sublines (LTT). Bars represent mean ± SD of three technical replicates obtained from one biological sample per condition. Statistical comparisons between treated and untreated samples were performed using an unpaired two-tailed t-test. For the THZ531 concentrations applied, see Figure 11.

The alterations in the gene expression of the signaling molecules *ATR* and *ATM* are graphically represented in Figures 16 and 17.

For *ATR*, no biologically relevant changes were observed across the analyzed cell lines. Several models displayed statistically significant but moderate alterations, such as a slight upregulation in 253J parental cells (0.48) and reductions in T24 (−0.63) and J82 (−0.21), yet all values remained below the biological threshold.

For *ATM*, more pronounced effects were detected. T24 parental cells exhibited a biologically relevant downregulation (−1.19). J82 LTT cells showed a near-threshold reduction (−0.99), and RT112 LTT cells displayed a significant decrease (−0.93). Although both values formally remained just below the cut-off, they may still be regarded as biologically relevant due to their statistical significance. In the remaining cell lines, changes were statistically significant but biologically not relevant. Across all models, *ATM* expression consistently tended toward downregulation following THZ531 treatment.

In summary**,** THZ531 treatment induced no relevant regulation of *ATR*, while *ATM* expression was reduced in several models. The strongest and biologically relevant decrease was observed in T24 parental cells, with J82 LTT and RT112 LTT also showing meaningful downregulation. Overall, the pattern of *ATM* regulation resembled the changes observed for *BRCA1*, suggesting a related response profile.

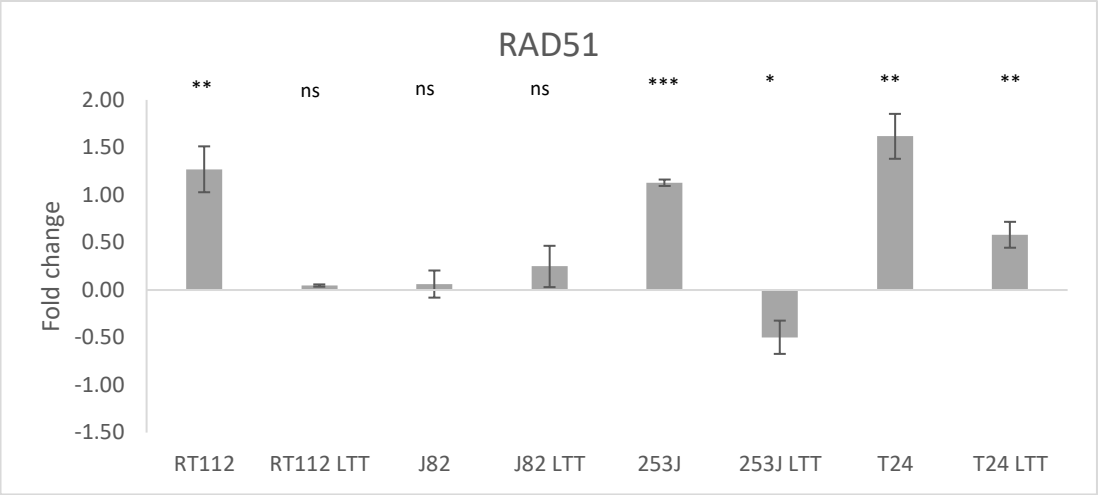

Figure 18: Logarithmic fold change of *RAD51* after 72 hours of THZ531 exposure. The fold change was calculated as the logarithmic quotient (base 2) of the relative gene expression of treated versus untreated cells (measured by qPCR). *TBP* was used as a housekeeping gene. Shown are the parental cisplatin-naive urothelial carcinoma cells and their cisplatin-resistant sublines (LTT). Bars represent mean ± SD of three technical replicates obtained from one biological sample per condition. Statistical comparisons between treated and untreated samples were performed using an unpaired two-tailed t-test. For the THZ531 concentrations applied, see Figure 11.

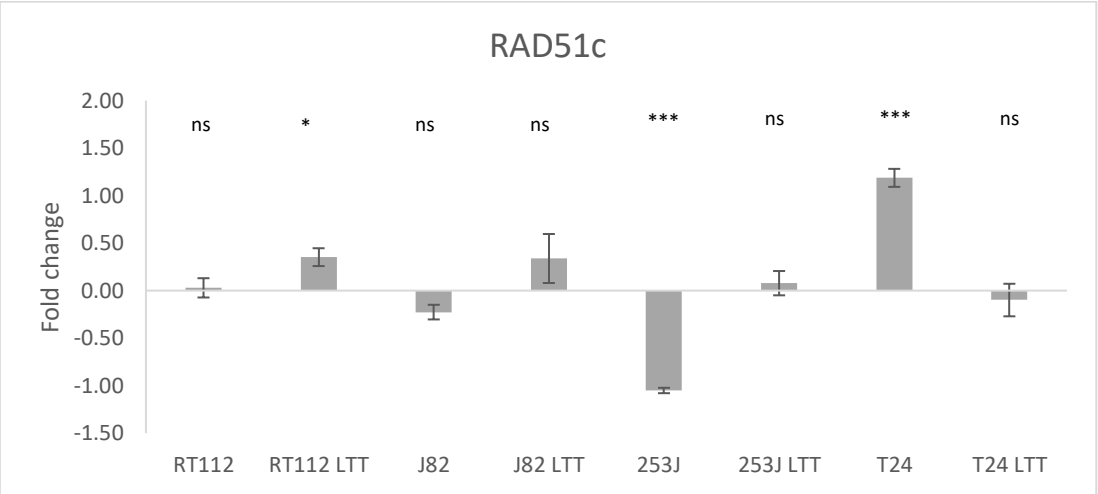

Figure 19: Logarithmic fold change of *RAD51c* after 72 hours of THZ531 exposure. The fold change was calculated as the logarithmic quotient (base 2) of the relative gene expression of treated versus untreated cells (measured by qPCR). *TBP* was used as a housekeeping gene. Shown are the parental cisplatin-naive urothelial carcinoma cells and their cisplatin-resistant sublines (LTT). Bars represent mean ± SD of three technical replicates obtained from one biological sample per condition. Statistical comparisons between treated and untreated samples were performed using an unpaired two-tailed t-test. For the THZ531 concentrations applied, see Figure 11.

Figures 18 and 19 illustrate the changes in expression levels of the DNA repair proteins *RAD51* and *RAD51c* following 72 hours of THZ531 exposure. For *RAD51*, biologically relevant upregulation was detected in T24 parental (1.62) and RT112 parental (1.27) cells. In all other models, expression changes remained below the threshold of biological relevance. The overall

response pattern of *RAD51* thus closely resembled that of *BRCA2*, indicating a similar regulation under CDK12 inhibition.

For *RAD51c*, a biologically relevant upregulation was observed in T24 parental cells (1.19). In contrast, the remaining cell lines showed only moderate changes, some of which were statistically significant but not biologically relevant. Interestingly, in several models *RAD51* and *RAD51c* exhibited opposing behaviors, suggesting differential regulation of these two homologous recombination factors.

In summary**,** *RAD51* and *BRCA2* responded in a concordant manner, particularly in parental T24 and RT112 cells, whereas *RAD51c* displayed in part opposite regulation. Moreover, parental and LTT cells appeared to differ in their response, with more pronounced upregulation observed in the parental lines.

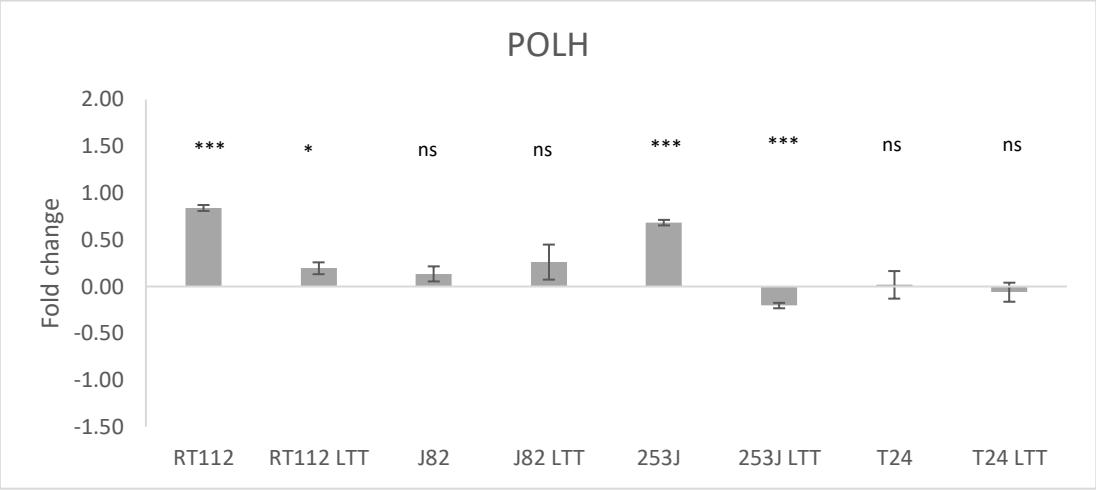

Figure 20: Logarithmic fold change of *POLH* after 72 hours of THZ531 exposure. The fold change was calculated as the logarithmic quotient (base 2) of the relative gene expression of treated versus untreated cells (measured by qPCR). *TBP* was used as a housekeeping gene. Shown are the parental cisplatin-naive urothelial carcinoma cells and their cisplatin-resistant sublines (LTT). Bars represent mean ± SD of three technical replicates obtained from one biological sample per condition. Statistical comparisons between treated and untreated samples were performed using an unpaired two-tailed t-test. For the THZ531 concentrations applied, see Figure 11.

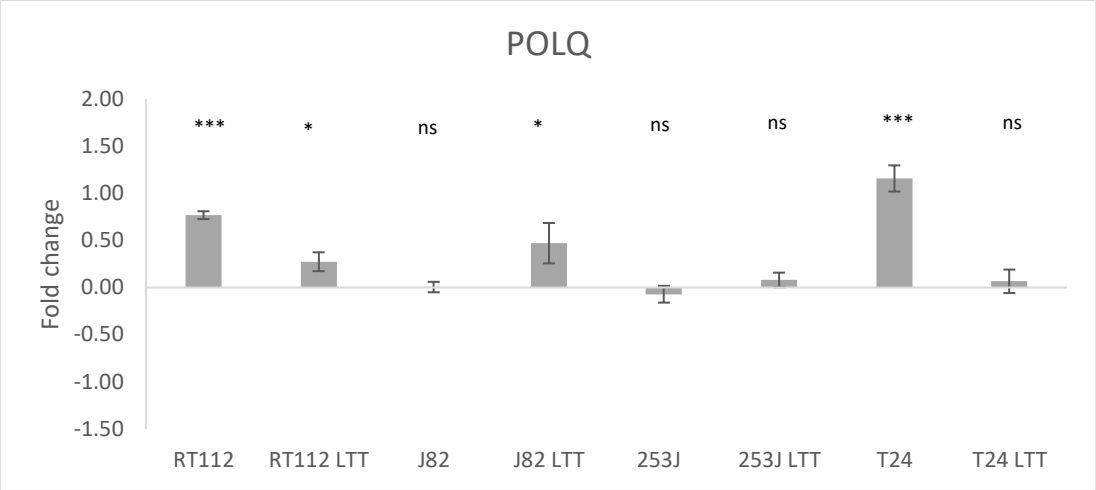

Figure 21: Logarithmic fold change of *POLQ* after 72 hours of THZ531 exposure. The fold change was calculated as the logarithmic quotient (base 2) of the relative gene expression of treated versus untreated cells (measured by qPCR). *TBP* was used as a housekeeping gene. Shown are the parental cisplatin-naive urothelial carcinoma cells and their cisplatin-resistant sublines (LTT). Bars represent mean ± SD of three technical replicates obtained from one biological sample per condition. Statistical comparisons between treated and untreated samples were performed using an unpaired two-tailed t-test. For the THZ531 concentrations applied, see Figure 11.

Figures 20 and 21 summarize the changes in expression levels of DNA polymerases POLH and POLQ following THZ531 treatment.

For *POLH*, no biologically relevant changes were observed in any of the analyzed cell lines. Several models showed moderate but statistically significant increases, most notably RT112 parental (0.84) and 253J parental (0.68), while the remaining cell lines exhibited only minor changes. Overall, *POLH* expression was only modestly affected by THZ531 treatment.

For *POLQ,* a more pronounced effect was detected in T24 parental cells, which showed a biologically relevant upregulation (1.16). RT112 parental (0.77) and J82 LTT (0.47) also demonstrated moderate, statistically significant increases that remained below the biological cut-off. 253J parental cells displayed a modest but significant downregulation (−0.67), while all other cell lines showed only minor changes.

THZ531 treatment resulted in moderate, sub-threshold changes in *POLH* expression across all models, whereas *POLQ* was clearly induced only in T24 parental cells, with other cell lines exhibiting smaller, statistically significant but biologically less relevant alterations.

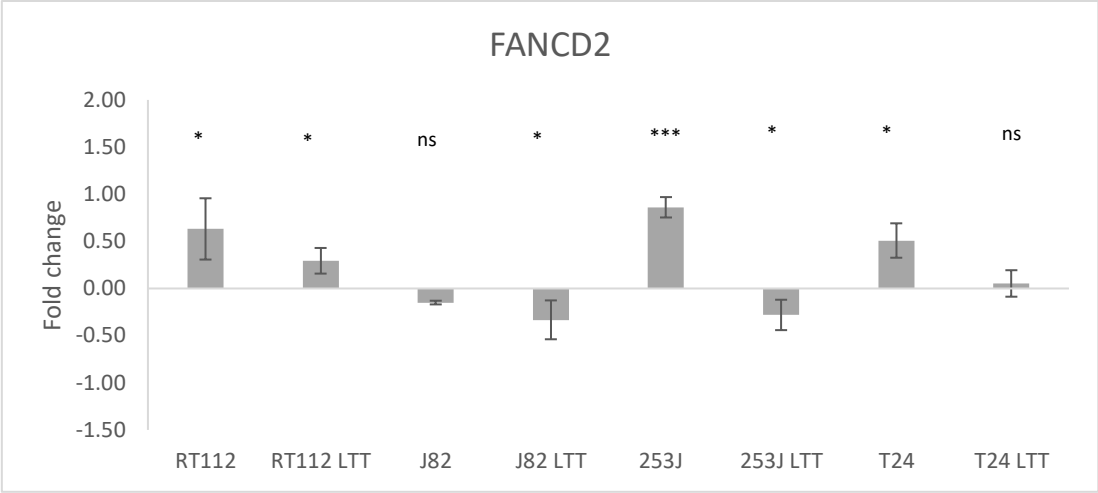

Figure 22: Logarithmic fold change of *FANCD2* after 72 hours of THZ531 exposure. The fold change was calculated as the logarithmic quotient (base 2) of the relative gene expression of treated versus untreated cells (measured by qPCR). *TBP* was used as a housekeeping gene. Shown are the parental cisplatin-naive urothelial carcinoma cells and their cisplatin-resistant sublines (LTT). Bars represent mean ± SD of three technical replicates obtained from one biological sample per condition. Statistical comparisons between treated and untreated samples were performed using an unpaired two-tailed t-test. For the THZ531 concentrations applied, see Figure 11.

Figure 22 illustrates the fold change in *FANCD2* expression in urothelial carcinoma cells following THZ531 exposure.

For all cell lines, the observed fold changes ranged between -1 and 1, indicating that the changes in *FANCD2* expression were biologically insignificant. The strongest increases were detected in 253J parental cells (0.86) and RT112 parental cells (0.63), both indicating a measurable but sub-threshold induction.

Under THZ531 treatment, the DNA repair genes displayed a heterogeneous and clearly cell-line-specific response pattern. Core signaling and recognition factors of the DNA damage response were predominantly downregulated, whereas selected homologous recombination components showed moderate upregulation, particularly in the parental cell lines. Repair mechanisms outside of homologous recombination remained largely stable and exhibited only minor changes. Parental and LTT cells differed markedly: parental models showed stronger and more variable transcriptional changes, while LTT cells displayed overall attenuated responses. Thus, THZ531 induces a selective, cell-line-dependent modulation of the DNA repair machinery without causing a uniform or global suppression of the investigated repair pathways.

3.3 Modulation of CDK12 and its Impact on Cisplatin Response

To characterize the role of CDK12 in the response of urothelial carcinoma cells to cisplatin, three complementary experimental approaches were employed. The aim was to determine whether, and to what extent, the expression level of CDK12 modulates the cellular reaction to cisplatin.

In the first approach, stable overexpression of CDK12 using a plasmid vector was established to create a setting with elevated CDK12 levels. This was intended to assess whether increased CDK12 expression alters cisplatin-induced gene regulation and whether this provides evidence for CDK12-dependent resistance.

In the second approach, siRNA-mediated knockdown of CDK12 was performed to induce a functional loss. This allowed evaluation of whether reduced CDK12 expression affects the regulation of DNA repair genes and the cellular response to cisplatin.

In the third approach, pharmacological inhibition was applied using the selective CDK12 inhibitor THZ531, either alone or in combination with cisplatin. This was designed to determine whether pharmacological blockade induces effects like genetic knockdown. In addition, it was investigated whether the lethal doses of cisplatin and THZ531 vary depending on CDK12 status.

Taken together, these three experimental strategies provide complementary perspectives on cisplatin response: gain of function and amplification (CDK12 overexpression), loss of function (CDK12 knockdown), and pharmacological blockade (THZ531). Direct comparison of these conditions was intended to elucidate the role of CDK12 as a modulator of cisplatin sensitivity and to explore potential therapeutic implications.

3.3.1 The Effects of CDK12 Overexpression

From previous data on the THZ531 sensitivity of cisplatin-resistant cells, it was suggested that susceptibility to THZ531 might depend on CDK12 expression levels. To further investigate this relationship, a cell model with stable CDK12 overexpression was used. The cell lines employed for this purpose had been generated by the research group prior to this work.

First, CDK12 overexpression was confirmed by Western blot analysis. Subsequently, THZ531 sensitivity was assessed in relation to CDK12 levels. In the following sections, the damage response to cisplatin under conditions of CDK12 overexpression was also analyzed. The aim of these experiments was to assess whether CDK12 overexpression confers protection against cisplatin-induced damage by promoting an enhanced activation of DNA repair pathways.

3.3.1.1 Validation of Overexpression

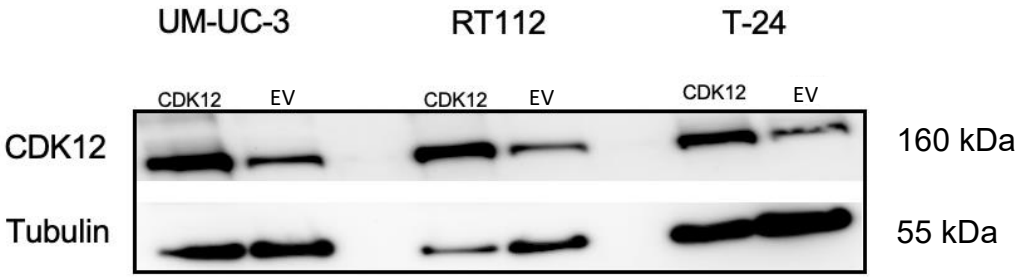

Figure 23: Validation of CDK12 overexpression by Western blot. This figure presents the validation of CDK12 overexpression in cell lines through Western blot analysis. The cell lines expressing CDK12 via vector plasmid transfection (CDK12) are compared with control cells that were transfected with an empty vector (EV). Tubulin was used as a loading control.

As part of the project, cells were stimulated to achieve stable CDK12 overexpression using a vector plasmid. The overexpression was validated by Western blot analysis, as depicted in Figure 23. The figure presents samples from cells overexpressing CDK12 (CDK12) and cells transfected with an empty vector (EV).

The Western blot analysis reveals distinct differences in band intensities across the three cell lines studied. Elevated levels of CDK12 were observed in all three cell lines following transfection.

3.3.1.2 Response to the Inhibitor THZ531

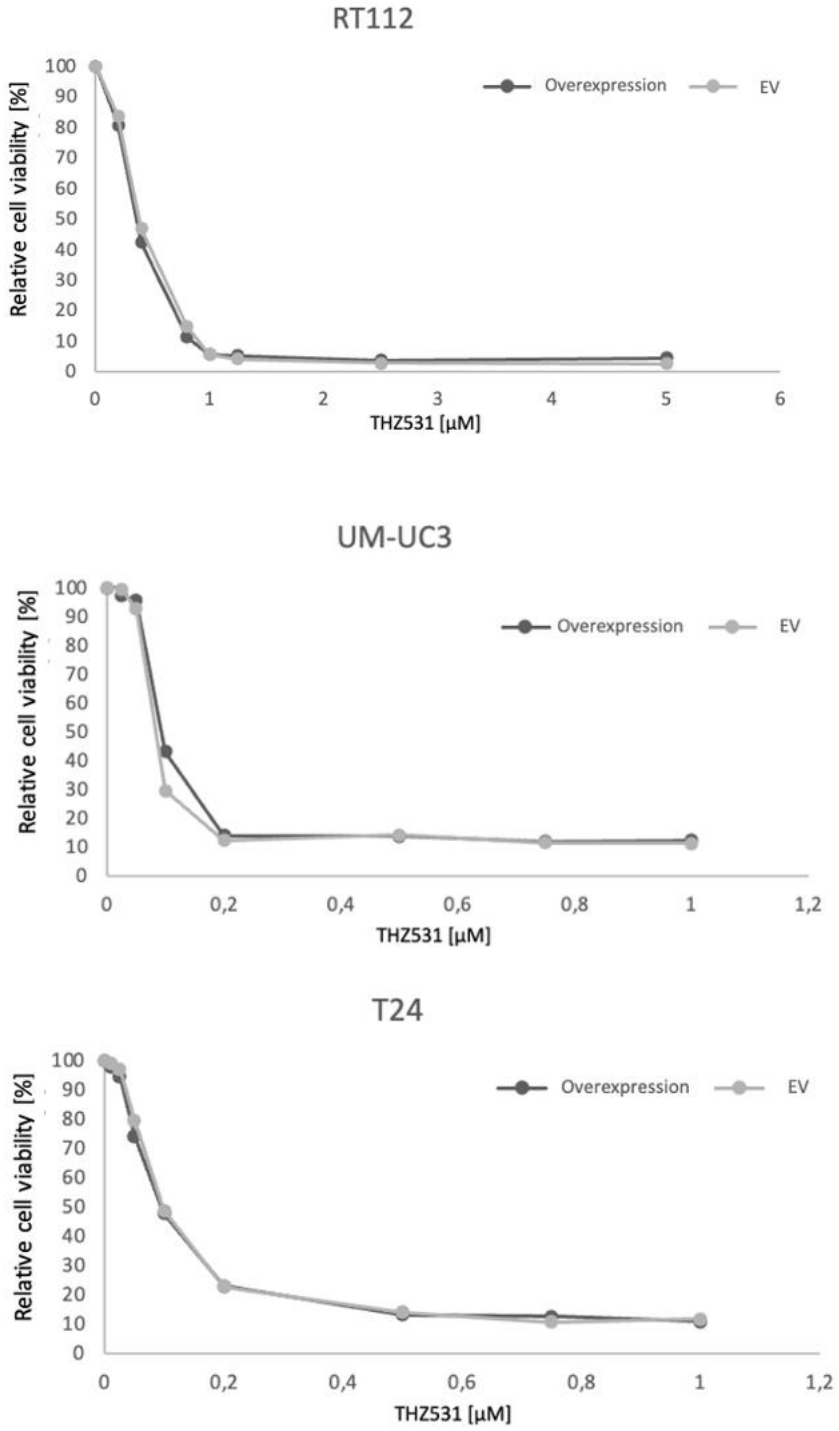

Figure 24: Response to THZ531 in CDK12-overexpressing cells compared to cells with empty vector. This figure illustrates the response of CDK12-overexpressing cells (Overexpression) to THZ531 compared to cells transfected with an empty vector (EV). Cell viability was measured using an MTT assay after 72 hours of THZ531 exposure. Each concentration point represents the mean of four biological replicates. Standard deviations were not plotted because replicate variability was negligible and, given the mechanistic focus of this experiment, error bars would not have provided additional interpretative value.

The three panels in Figure 24 present the response of tumor cells to the inhibitor THZ531 under two experimental conditions: with CDK12 overexpression and without. The analysis was conducted for three cell lines.

The dose-response curves are nearly identical for both conditions across all three cell lines. The half-maximal inhibitory concentrations were achieved at approximately the same dose points for both conditions. Specifically, RT112 cells exhibited an IC_{50}-value of approximately 400 nM, whereas UMUC-3 and T24 cells demonstrated IC_{50}-values in the vicinity of 100 nM. These findings suggest that THZ531 sensitivity is largely independent of CDK12 abundance.

3.3.1.3 Impact on DNA Damage and Apoptosis Induction

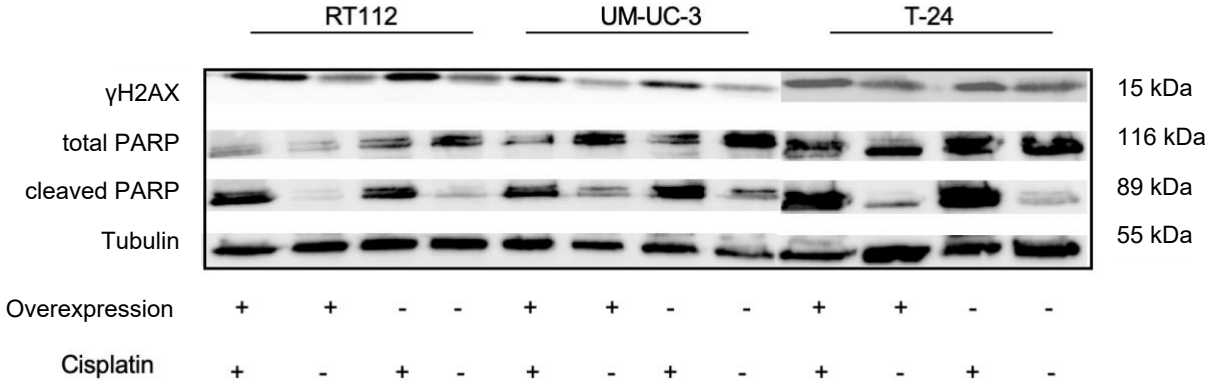

Figure 25: DNA damage and apoptosis induction in CDK12-overexpressing cells following 72 hours of cisplatin exposure. Western Blot detection of γH2AX and PARP cleavage as apoptosis marker in urothelial carcinoma cells with CDK12 overexpression (+) compared to cells transfected with an empty vector (-). Cisplatin treatment is indicated by a plus sign (+). Tubulin was used as the loading control. For the cisplatin concentrations applied, see Table 14.

Figure 25 illustrates the analysis of PARP cleavage and DNA damage in CDK12-overexpressing cells following cisplatin exposure. Cells transfected with an empty vector served as controls.

All three cell lines demonstrated PARP cleavage and increased levels of phosphorylated H2AX, indicative of DNA double-strand breakage, in response to cisplatin treatment, irrespective of CDK12 expression levels.

When comparing the cell lines, it is observed that the response to cisplatin was not significantly altered by the levels of CDK12 expression. The intensity of the cleaved PARP and γH2AX bands remained consistent within each cell line, regardless of variations in CDK12 levels.

RT-112 cells exhibited a more pronounced effect in H2AX phosphorylation following cisplatin treatment compared to UMUC-3 and T-24 cells. T-24 cells already displayed indications of DNA damage in the untreated state, with γH2AX bands only marginally less intense compared to those observed after cisplatin treatment.

Cisplatin induced comparable levels of DNA damage and apoptosis irrespective of CDK12 overexpression. No reduction in γH2AX formation or PARP cleavage was observed in CDK12-overexpressing cells, indicating that elevated CDK12 levels did not diminish the extent of cisplatin-induced cellular damage.

3.3.1.4 Changes in the Expression of DNA Damage Repair Genes Following Cisplatin Treatment

Because CDK12 is described as a transcriptional regulator of numerous DNA repair genes, we investigated how CDK12 overexpression influences the cisplatin-induced damage response. The same key genes involved in homologous recombination, the Fanconi anemia pathway, and alternative repair mechanisms were analyzed as in the previous approaches. The following gene expression changes are presented as fold changes, which have been determined logarithmically.

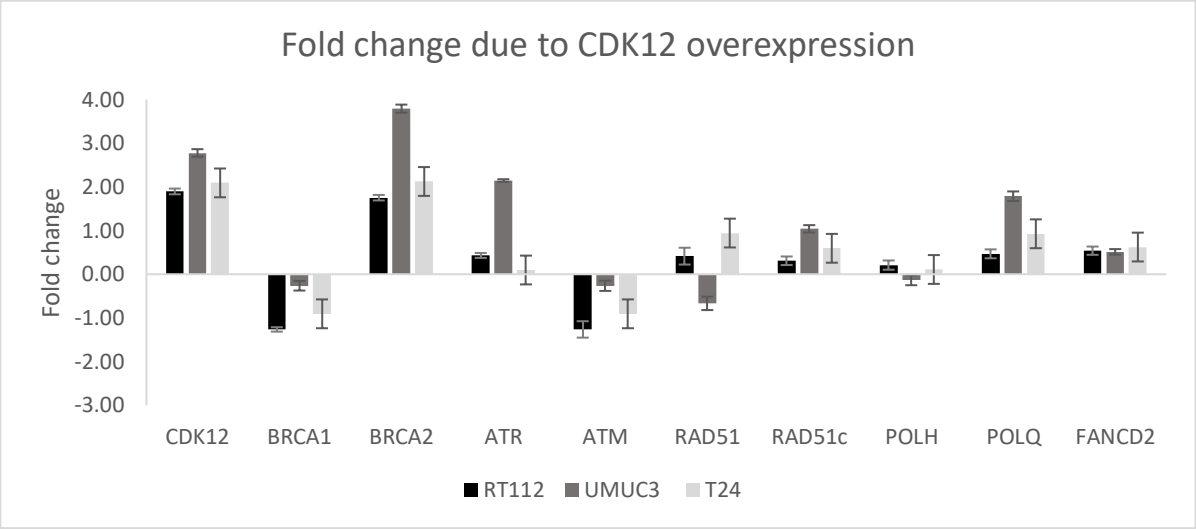

Figure 26: Logarithmic fold change in DNA damage repair genes in CDK12-overexpressing cells compared to cells with empty vector. This figure presents the fold change in DNA damage repair genes in untreated CDK12-overexpressing cells relative to cells transfected with an empty vector. The fold change is calculated as the logarithmic ratio (base 2) of the relative gene expression between treated and untreated cells, as measured by qPCR. *TBP* was utilized as the housekeeping gene. Bars represent mean ± SD of three technical replicates obtained from one biological sample per condition.

Figure 26 shows the fold changes in DNA damage response gene expression following stable CDK12 overexpression in the urothelial carcinoma cell lines RT112, UMUC3, and T24. *CDK12* expression was strongly increased in all three models, confirming successful overexpression.

The largest transcriptional effects were observed for *BRCA2,* which was strongly upregulated in all cell lines, most prominently in UMUC3 (nearly 4-fold). *BRCA1*, in contrast, showed a

mild but consistent downregulation. Among the signaling kinases, *ATR* displayed moderate induction, whereas *ATM* was modestly reduced.

For the remaining DNA repair factors, expression changes were generally moderate, although *POLQ* showed a noticeable increase in UMUC3.

Overall, CDK12 overexpression resulted in a strong *BRCA2* induction, while most other DNA repair genes exhibited only minor transcriptional changes.

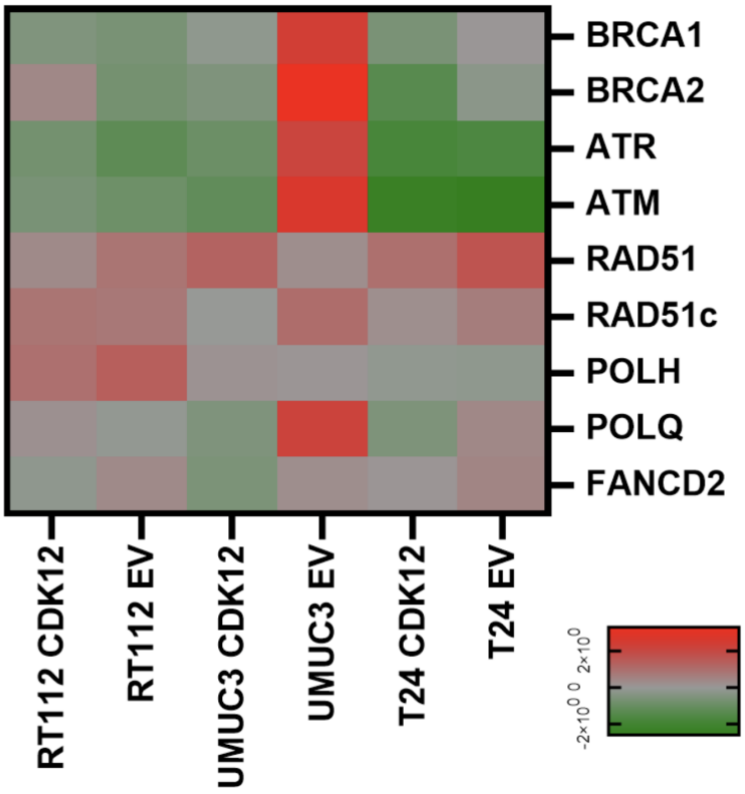

Figure 27: Heatmap of gene expression changes in CDK12-overexpressing urothelial carcinoma cells following cisplatin treatment. Fold changes (log_2) of DNA damage response and repair genes are shown for three urothelial carcinoma cell lines (RT112, UMUC3, T24) with stable CDK12 overexpression (CDK12) compared to their respective empty-vector controls (EV). Each value represents the mean of three technical replicates from one biological sample per condition. Fold changes were calculated relative to the corresponding untreated controls (no cisplatin exposure). Red indicates upregulation, green indicates downregulation, and grey reflects minimal or no change. Color intensity corresponds to the magnitude of expression change as defined by the scale bar. For the cisplatin concentrations applied, see Table 14.

The heatmap in Figure 27 illustrates the cisplatin-induced changes in the expression of key DNA repair genes in urothelial carcinoma cell lines with CDK12 overexpression compared with their respective empty-vector controls.

In UMUC3, the most pronounced divergent pattern was observed. Whereas the empty-vector cells showed a marked upregulation of several repair genes following cisplatin treatment, most notably *BRCA1, BRCA2, ATR,* and *ATM*, the CDK12-overexpressing cells of the same line exhibited an opposite response, with a clear downregulation of these genes. This opposing expression profile affected both homologous recombination factors and central signaling kinases and represented the most striking divergence among all analyzed models. Notably, UMUC3 demonstrated an inverse regulatory pattern under CDK12 overexpression compared with the control condition, contrary to the expected enhanced activation of DNA repair genes at elevated CDK12 levels.

In RT112, the expression changes were overall more moderate. Most transcriptional alterations in CDK12-overexpressing cells were concordant with those observed in empty-vector controls. An exception was *BRCA2*, which was upregulated in CDK12-overexpressing cells while showing a slight decrease in the control condition. All other genes displayed only minor differences between the two conditions.

T24 similarly exhibited an overall attenuated response, comparable to RT112. Most expression changes occurred in the same direction in both empty-vector and CDK12-overexpressing cells, without clear or consistent divergences. The only notable exception was *POLQ*, which showed an opposite regulatory pattern between the two conditions.

Because UMUC3 displayed the most pronounced and opposing transcriptional response under CDK12 overexpression, Western blot analyses for ATR and ATM were performed to determine whether the observed gene expression changes were also reflected at the protein level and to provide an additional layer of validation for the qPCR findings.

Figure 28 reveals that CDK12-overexpressing UMUC-3 cells displayed reduced levels of ATM and ATR proteins following cisplatin treatment. In untreated UMUC-3 cells, ATR and ATM protein levels were elevated in those with CDK12 overexpression.

A similar trend was observed in T-24 cells. Untreated T-24 cells with CDK12 overexpression had increased levels of ATM and ATR. After cisplatin treatment, both proteins were downregulated in the CDK12-overexpressing T-24 cells. In contrast, T-24 cells with normal CDK12 expression showed a decrease in ATM protein levels in response to cisplatin, while ATR levels remained unchanged.

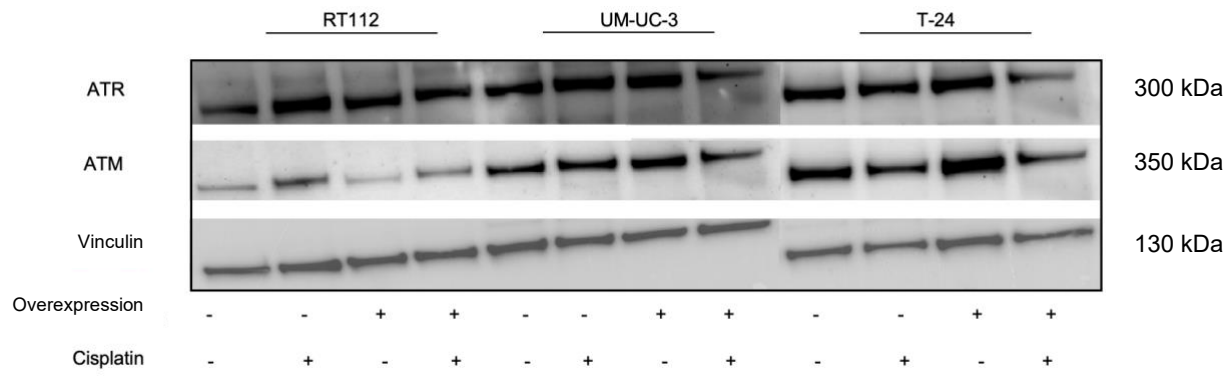

Figure 28: ATR and ATM protein levels in CDK12-overexpressing cells following cisplatin exposure. Protein quantities were assessed using Western blot analysis. The figure displays urothelial carcinoma cells with CDK12 overexpression (+) and cells transfected with an empty vector (-). Cisplatin treatment is denoted by a plus sign (+). Vinculin was used as the loading control. For the cisplatin concentrations applied, see Table 14.

The data collectively indicate that CDK12-overexpressing cells consistently showed a basal upregulation of *BRCA2*. Following cisplatin exposure, UMUC3 was the only cell line in which CDK12 overexpression was associated with a marked downregulation of key DNA damage response genes. These effects were not observed in RT112 or T24, where expression changes were generally moderate and showed no clear association with CDK12 levels.

3.3.2 Effects of CDK12 Knockdown

To investigate the opposite regulatory effect, a transient siRNA-mediated knockdown of CDK12 was performed in three tumor cell lines. The selection of cell lines differed from the overexpression model: RT112 and UMUC3 were included again, as UMUC3 had shown an unexpected transcriptional response to cisplatin in the previous experiments. In addition, VMCUB1 was incorporated into the analysis because preliminary data from the research group indicated that this cell line exhibits one of the highest basal CDK12 protein levels, making it particularly suitable for assessing the impact of CDK12 depletion.

The underlying question was whether the loss of CDK12 alters the extent of cisplatin-induced DNA damage. Specifically, it was examined whether cells with reduced CDK12 levels display increased sensitivity to cisplatin, potentially as a consequence of diminished DNA repair capacity. Analogous to the overexpression experiments, the degree of DNA damage and apoptosis induction was assessed by Western blot analysis. Furthermore, changes in the expression of key DNA repair genes following cisplatin exposure were quantified using RT-qPCR.

3.3.2.1 Knockdown Validation

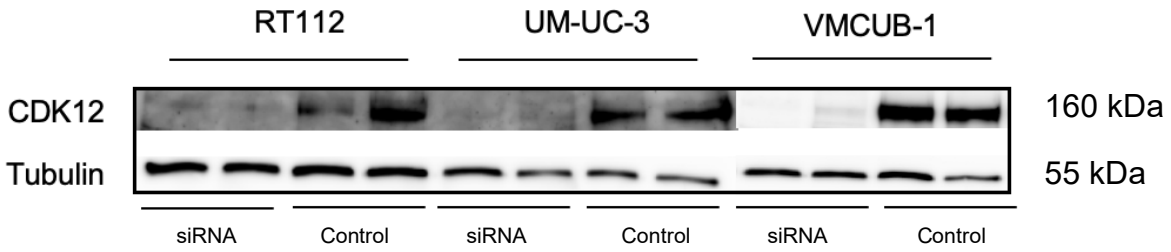

Figure 29: Validation of CDK12 siRNA knockdown after 96 hours using Western blot analysis. The figure shows urothelial carcinoma cell lines with CDK12 protein levels in cells subjected to siRNA knockdown (siRNA). Cells transfected with non-targeting siRNA are labeled as Control. Tubulin was used as the loading control.

In the subsequent experimental setups, a CDK12 knockdown was performed for 96 hours using CDK12-targeting siRNA. The control was conducted with non-targeting siRNA. The success of the transfection was confirmed by Western blot analysis, as shown in Figure 29. For all three cell lines, it was evident that CDK12 mRNA degradation was effectively achieved. On the protein level, CDK12 was barely detectable.

3.3.2.2 Response to Cisplatin

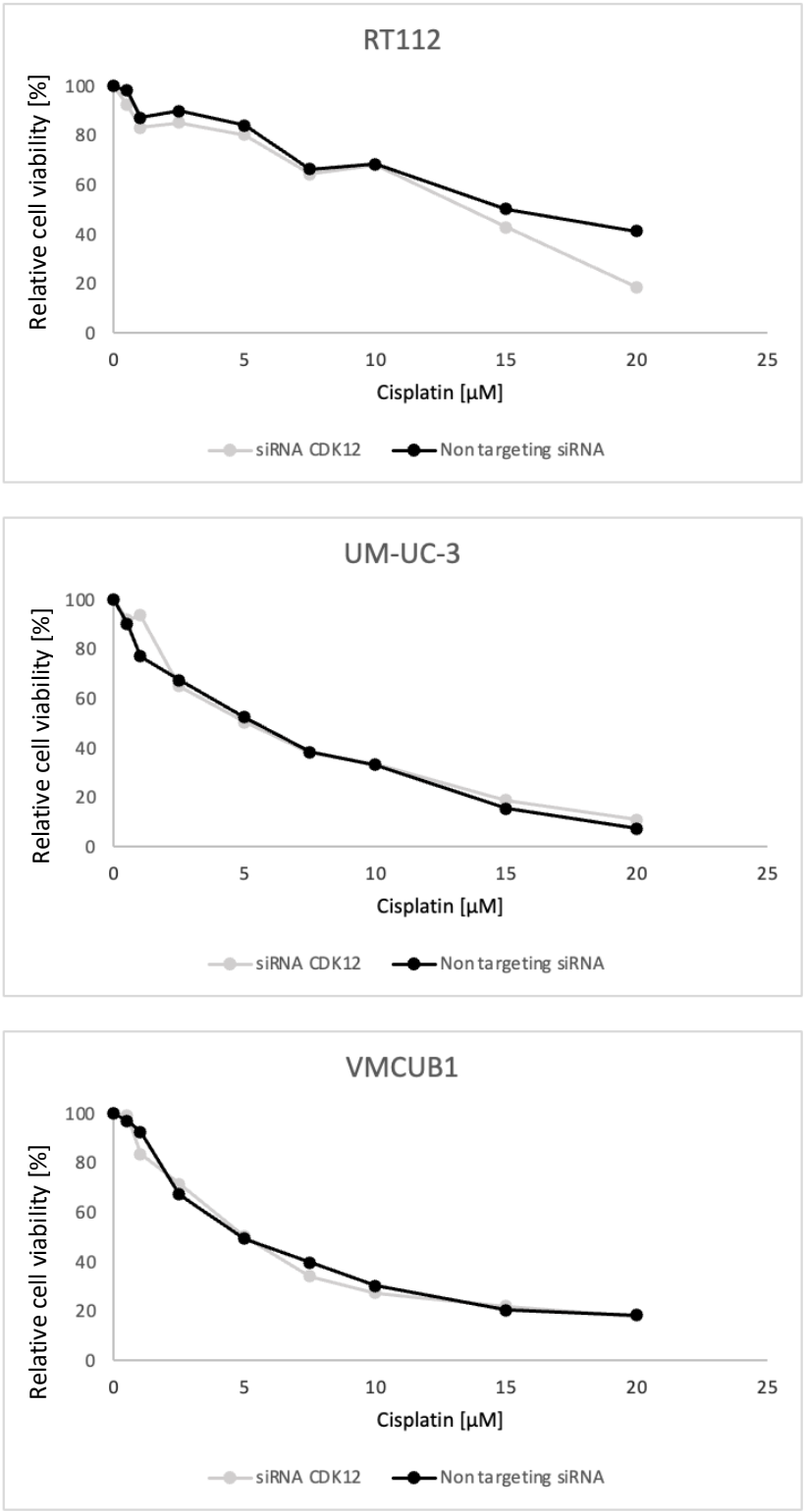

Figure 30: The effect of CDK12 on cisplatin response assessed through siRNA knockdown. Cell viability was measured using an MTT assay following 72 hours of cisplatin exposure. The figure shows three urothelial carcinoma cell lines subjected to CDK12 siRNA knockdown and the corresponding control cells (non-targeting siRNA). Each concentration point represents the mean of four biological replicates. Standard deviations were not plotted because replicate variability was negligible and, given the mechanistic focus of this experiment, error bars would not have provided additional interpretative value.

The dose response curves depicted in Figure 30 illustrate the response of urothelial carcinoma cells to cisplatin with and without CDK12 siRNA knockdown. In all three graphs, the dose response curves are nearly identical, indicating that both the CDK12 siRNA knockdown cells and the control cells (non-targeting siRNA) exhibit similar responses to increasing cisplatin concentrations. The half-maximal inhibitory concentration (IC_{50}) for the UMUC-3 and VMCUB-1 cell lines is approximately 5 µM under both conditions. For the RT-112 cell line, the IC_{50} is approximately 14 µM for both conditions.

Taken together, these findings indicate that the cellular response to cisplatin, exemplary for DNA-damaging agents, is independent of CDK12 expression levels, as no differences were observed between CDK12-depleted and control cells.

3.3.2.3 Impact on DNA Damage and Apoptosis Induction

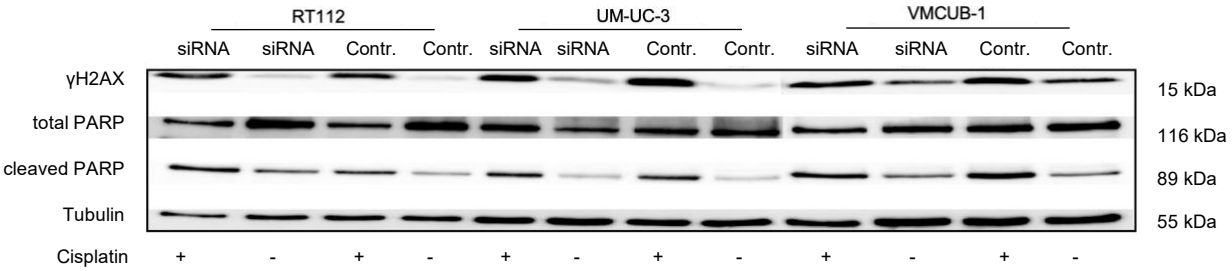

Figure 31: DNA damage and apoptosis induction by cisplatin following CDK12 siRNA knockdown. Protein levels were assessed using Western blot analysis. The figure shows three urothelial carcinoma cell lines subjected to CDK12 knockdown (siRNA) and control cells treated with non-targeting siRNA (Control). Samples are presented with cisplatin treatment (+) and without cisplatin treatment (-). The bands shown are for phosphorylated H2AX (γH2AX) as a DNA damage marker, cleaved PARP as an apoptosis marker, and total PARP as a loading control. Tubulin was used as the general loading control. For the cisplatin concentrations applied, see Table 14.

The Western blot image presented in Figure 31 demonstrates the impact of CDK12 siRNA knockdown on DNA damage and apoptosis induction in three urothelial carcinoma cell lines. The results indicate that all treated cells exhibited increased PARP cleavage and DNA damage in response to cisplatin. The bands for cleaved PARP and γH2AX are more intense in all cisplatin-treated samples.

In UMUC-3 control cells, the γH2AX band is more pronounced compared to CDK12 knockdown cells following cisplatin treatment. A similar trend is observed in VMCUB1 cells. Notably, the tubulin band in the cisplatin-treated VMCUB1 knockdown sample is weaker than in other VMCUB1 samples, which may limit the interpretability of the γH2AX band in this context. Untreated VMCUB1 cells already exhibit faint γH2AX bands.

Although γH2AX levels differed slightly between UMUC-3 and VMCUB1 samples, cisplatin-induced DNA damage was not enhanced by CDK12 knockdown. If anything, γH2AX appeared

more pronounced in control cells. Overall, the extent of DNA damage and apoptosis induction was comparable between knockdown and control conditions.

3.3.2.4 Changes in the Expression of DNA Damage Repair Genes Following Cisplatin Treatment

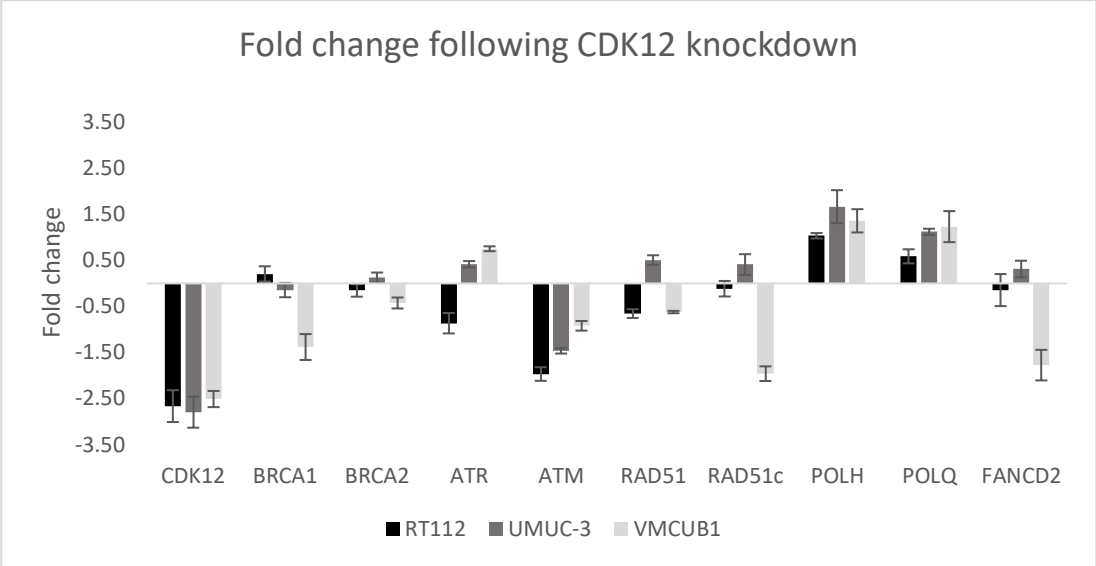

Figure 32: Logarithmic fold change in DNA damage repair genes after CDK12 siRNA knockdown compared to non-targeting control. This figure depicts the logarithmic fold change (log_2FC) in the expression of key DNA damage repair genes following transient CDK12 knockdown by siRNA. Gene expression levels in CDK12-silenced cells were compared with those in cells transfected with a non-targeting control siRNA. Relative transcript levels were determined by qPCR using *TBP* as the housekeeping gene. Positive values indicate upregulation upon CDK12 knockdown, whereas negative values represent downregulation. Bars represent mean ± SD of three technical replicates obtained from one biological sample per condition.

Figure 32 illustrates the fold changes in DNA damage repair genes following siRNA-mediated CDK12 knockdown in RT112, UMUC-3, and VMCUB1 cells.

CDK12 itself was strongly reduced in all three cell lines, confirming an efficient knockdown at the mRNA level.

Across the remaining genes, a cell line dependent pattern emerged. *BRCA1* expression decreased markedly in VMCUB1, whereas *BRCA2* remained largely unchanged across all models. The signaling kinase *ATM* showed a consistent downregulation in all three cell lines, representing the most uniform effect observed. *RAD51c* was reduced specifically in VMCUB1, while *RAD51* showed only minor changes.

In contrast to these reductions, the alternative repair polymerases *POLH* and *POLQ* were upregulated under knockdown conditions in all cell lines, indicating a compensatory transcriptional response. *FANCD2* displayed moderate alterations, particularly a decrease in VMCUB1.

Overall, CDK12 knockdown resulted in a heterogeneous transcriptional profile characterized by repression of selected homologous recombination and signaling genes together with induction of alternative repair polymerases.

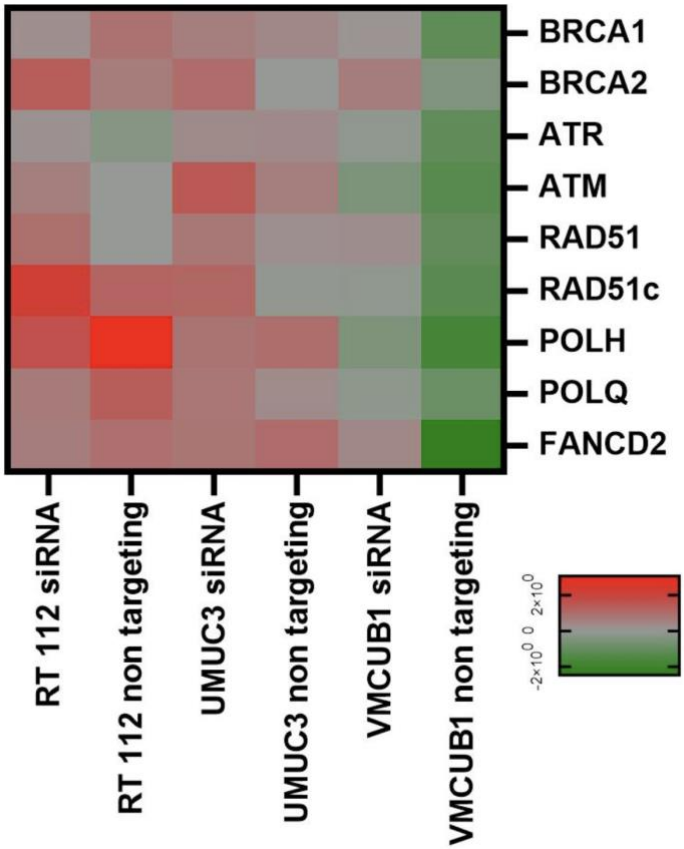

Figure 33: Heatmap of gene expression changes in CDK12-knockdown urothelial carcinoma cells following cisplatin treatment. Fold changes (log_2) of DNA damage response and repair genes are shown for three urothelial carcinoma cell lines (RT112, UMUC3, VMCUB1) after transient siRNA-mediated CDK12 knockdown (siRNA) compared to their respective non-targeting siRNA controls (non-targeting). Each value represents the mean of three technical replicates from one biological sample per condition. Fold changes were calculated relative to the corresponding untreated controls (no cisplatin exposure). Red indicates upregulation, green indicates downregulation, and grey reflects minimal or no change. Color intensity corresponds to the magnitude of expression change as defined by the scale bar. For the cisplatin concentrations applied, see Table 14.

The heatmap in Figure 33 depicts the changes in the expression of key DNA repair genes following CDK12 siRNA knockdown and subsequent cisplatin treatment, compared with the respective non-targeting controls. In RT112, CDK12 knockdown followed by cisplatin exposure resulted in a moderate upregulation of several repair factors, including *BRCA2, RAD51c,* and *POLH*. UMUC3 likewise showed a general tendency toward upregulation of the analyzed genes after knockdown and cisplatin treatment, representing a pattern opposite to that observed in the overexpression model. In contrast, VMCUB1 exhibited a pronounced cisplatin-

induced downregulation of multiple repair genes in the non-targeting control, whereas no substantial expression changes were detected after CDK12 knockdown. Overall, the cisplatin-induced transcriptional responses in the siRNA setting were markedly weaker than in the overexpression model. Most changes remained within a fold change range of −1 to +1 and were moderate in magnitude, without consistent divergent patterns across the three cell lines.

3.3.3 Effects of Pharmacological CDK12 Inhibition Combined with Cisplatin

The previous sections have outlined the impacts of CDK12 modulation. Using Western blot analysis, DNA damage and apoptosis induction by cisplatin, depending on CDK12 protein levels, were investigated. Subsequently, the effects on the expression of DNA repair genes were analyzed by qPCR. The following section will address how these effects are influenced by pharmacological CDK12 inhibition. To ensure consistency and comparability across experimental conditions, the pharmacological inhibition experiments were conducted in the same cell lines used for the CDK12 overexpression model (RT112, UMUC3, T24). VMCUB1, included previously for the knockdown approach because of its high endogenous CDK12 abundance, was not part of this analysis.

3.3.3.1 Impact on DNA Damage and Apoptosis Induction

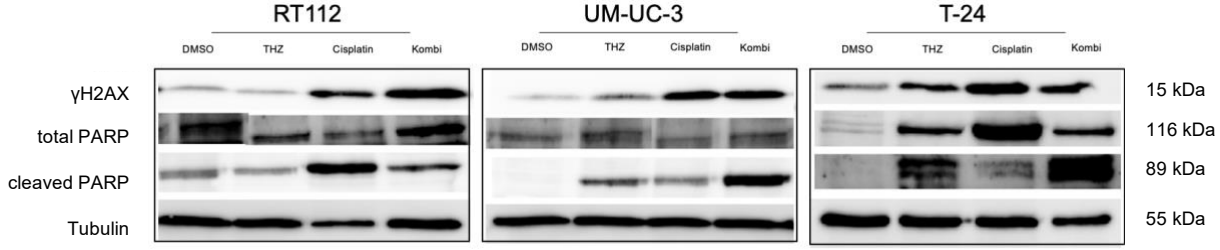

Figure 34: DNA damage and apoptosis induction in urothelial carcinoma cells following 48-hour combined exposure to cisplatin and THZ531 (both at IC_{50}-doses). Protein levels were measured using Western blot analysis. Tubulin was used as a loading control. The bands shown represent phosphorylated H2AX (γH2AX) as a marker of DNA damage, cleaved PARP as a marker of apoptosis, and total PARP as the corresponding loading control. For the drug concentrations applied, see Table 14 and Figure 11.

The effects of pharmacological CDK12 inhibition with THZ531 and cisplatin treatment on apoptosis induction and DNA damage were investigated using Western blot analysis (Figure 34).

Across all examined cell lines, increased H2AX phosphorylation was observed after cisplatin exposure. A THZ531 monotherapy induced slight H2AX phosphorylation in UMUC-3, while it led to a pronounced γH2AX band in T-24. The combined treatment resulted in enhanced H2AX phosphorylation compared to cisplatin monotherapy in RT112. Remarkably, THZ531 monotherapy did not cause increased PARP cleavage in the cell lines examined.

Following treatment with both agents, increased PARP cleavage was noted compared to monotherapy in UMUC-3 and T-24. In RT112, PARP cleavage was more pronounced after cisplatin exposure than after the combination therapy.

The loading control in RT112 and T-24 was not consistently represented. A thinner band was observed in cisplatin-treated RT112 cells and in combined treatment T-24 samples.

Overall, the data indicate a cell-line–dependent enhancement of apoptotic signaling under combined treatment. In UMUC-3 and T-24, the combination of cisplatin and THZ531 produced stronger γH2AX and PARP-cleavage signals than either agent alone, suggesting a potential synergistic effect.

3.3.3.2 Changes in the Expression of DNA Damage Repair Genes

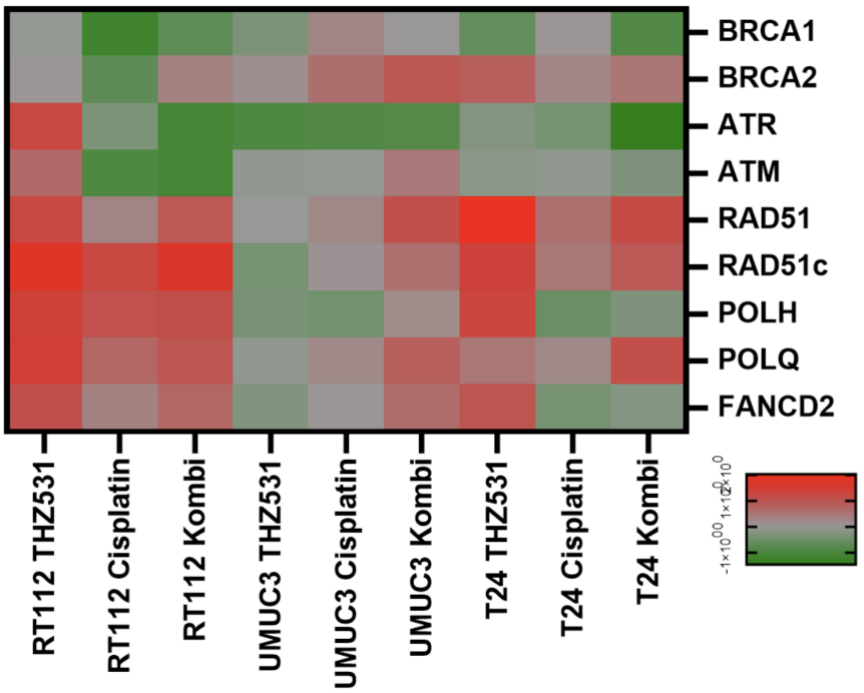

Figure 35: Heatmap of gene expression changes following treatment with THZ531, cisplatin, or the combination of both. Fold changes (log_2) of DNA damage response and repair genes are shown for three urothelial carcinoma cell lines (RT112, UMUC3, T24) following treatment with the CDK12 inhibitor THZ531 (THZ531), cisplatin (Cisplatin), or the combination of both agents (Kombi). Each value represents the mean of three technical replicates from one biological sample per condition. Fold changes were calculated relative to the corresponding untreated controls (no drug exposure). Red indicates upregulation, green indicates downregulation, and grey reflects minimal or no change. Color intensity corresponds to the magnitude of expression change as defined by the scale bar. For the drug concentrations applied, see Table 14 and Figure 11.

The heatmap (Figure 35) summarizes the transcriptional response of DNA repair genes in RT112, UMUC3, and T24 cells following treatment with THZ531, cisplatin, or the combination of both agents. Three aspects were evaluated: the effect of THZ531 monotherapy, cisplatin monotherapy, and combined treatment.

In RT112, THZ531 monotherapy induced a noticeable upregulation of most analyzed DNA repair genes. Cisplatin alone triggered a mixed response with both increases and decreases

depending on the gene. When both agents were combined, the expression pattern largely resembled that of THZ531 monotherapy, with only minor deviations. A notable exception was *ATR*, which showed a clearer downregulation under combination treatment compared with THZ531 alone.

In UMUC3, both THZ531 and cisplatin monotherapy produced only minimal changes in the expression of the assessed repair genes. In contrast, the combination treatment resulted in a tendency toward upregulation across several genes, indicating a more pronounced transcriptional activation than observed for either monotherapy.

In T24, the transcriptional responses to THZ531 and cisplatin were generally modest, like the patterns observed in RT112. No consistent differences could be identified between combination treatment and the respective monotherapies, except for *ATR*, which was downregulated in the combined condition.

Overall, although Western blot data suggested enhanced PARP cleavage under combination treatment in UMUC3 and T24, the gene expression data did not reveal a corresponding suppression of DNA repair capacity. In this experimental setting, combined THZ531 and cisplatin treatment did not lead to a consistent or generalized downregulation of DNA repair genes and thus did not provide a conclusive mechanistic explanation at the transcriptional level.

3.4 Effectiveness of Combination Therapy with THZ531 and Cisplatin

For the cisplatin-resistant LTT cell lines, THZ531 proved to be highly toxic, in some cases even at very low concentrations. In contrast, the parental cell lines, except for T24, required substantially higher half-maximal inhibitory doses. The findings from the previous section suggested that a synergistic effect between THZ531 and cisplatin may be present, particularly in T24 cells.

To further investigate potential synergy and explore whether Cisplatin could be used to reduce the required THZ531 dose and thereby improve therapeutic tolerability. The combination of THZ531 and cisplatin was examined in the J82 and 253J cell lines. These two cell lines exhibited the highest IC_{50} values for THZ531 among the parental lines, making them especially relevant candidates for testing dose-reduction strategies through combination treatment.

The diagram presented in Figure 36 illustrates the dose response curves of J82 cells (A) and 253J cells (B) following combined treatment with THZ531 and cisplatin. The x-axis represents concentrations expressed as multiples of the respective IC_{50} values determined for each drug in single-agent treatment. For combination treatment, both drugs were applied at fixed ratios based on their individual IC_{50} values.

In the J82 cell line, cisplatin monotherapy resulted in a continuous decrease in viability, reaching the IC_{50}-value. The response to THZ531 was less pronounced compared to cisplatin. The combination treatment led to the most significant reduction in viability. It was evident for each dosage point that the combination treatment caused a greater reduction in viability than the single-agent treatments.

A similar pattern was observed for the 253J cell line. The half-maximal inhibitory concentration for cisplatin was achieved. THZ531 also resulted in a less pronounced reduction in viability compared to cisplatin. The combination treatment had a more substantial effect on cell viability than either monotherapy.

A

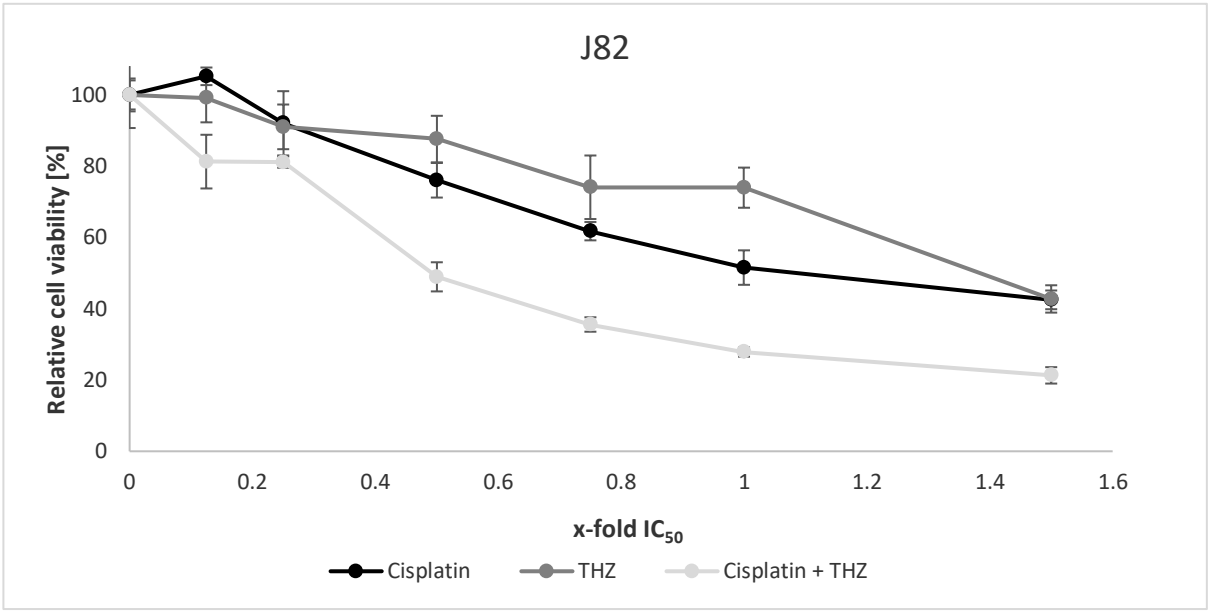

B

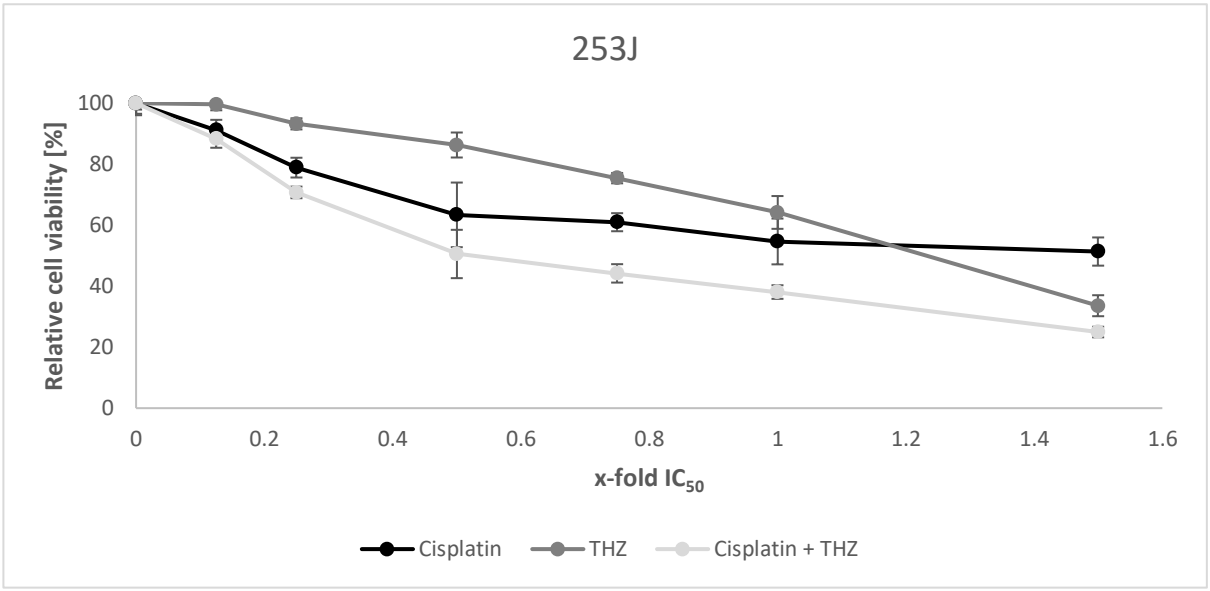

Figure 36: Combined treatment with THZ531 (THZ) and cisplatin. The dose response curves of the urothelial carcinoma cell lines J82 (A) and 253J (B) are presented following individual and combined treatments with both agents. Cell viability was assessed using the MTT assay after 72 hours of exposure. Each concentration point represents the mean ± SD of four biological replicates derived from one biological sample per condition. For the drug concentrations applied, see Table 14 and Figure 11. Combination treatments were performed at fixed ratios based on the respective IC50 values derived from these data.

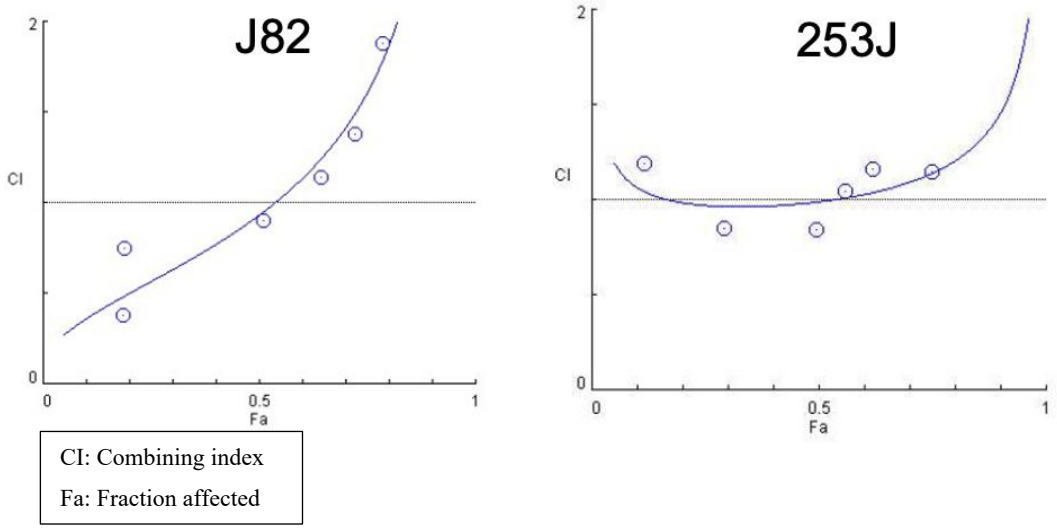

Figure 37: Synergistic effects of combination therapy with THZ531 and cisplatin in the J82 and 253J cell lines. The Combination Indices (CI) are shown, calculated according to the Chou-Talalay method. The dose points represent multiples of both agents. A CI value less than 1 indicates synergy, a CI value greater than 1 indicates an antagonistic effect, and a CI value of 1 represents an additive effect. The Fraction Affected (Fa) denotes the proportion of cells impacted by the treatment.

The results observed in Figure 36 were analyzed using the Chou-Talalay method to assess the synergistic effects of the combination treatment which is displayed in Figure 37.

For the J82 cell line, it was found that the 0.125- and 0.25-fold IC_{50}-doses exhibited synergy between THZ531 and cisplatin, with a Fraction Affected (Fa) of approximately 20 %. The combined 0.5-fold IC_{50}-dose also demonstrated synergy, with a CI value close to 1 and a Fraction Affected of 50 %. Antagonistic effects were observed for the remaining dose points, as indicated by CI values greater than 1.

In the 253J cell line, synergistic effects were observed only at the 0.25- and 0.5-fold IC_{50}-doses, with Fractions Affected of 30 % and 50 %, respectively.

While synergy was observed at several dose points, the effect remained moderate. Moreover, when compared with the IC_{50} values of HBLAK cells, the synergistic doses remained well above the levels tolerated by non-malignant uroepithelial cells, limiting the translational potential of the combination at these concentrations.

3.5 Effectiveness of Combination Therapy with THZ531 and Talazoparib

Talazoparib is a PARPi. The literature describes that pharmacological inhibition of CDK12 can exert synergistic effects with PARP inhibitors. Several preclinical studies have shown that combined blockade of CDK12 and PARP markedly reduces cell viability across different tumor entities. Moreover, pharmacological CDK12 inhibition has been reported to overcome both acquired and intrinsic resistance to PARP inhibitors by re-sensitizing tumor cells to PARPi-induced DNA damage (see 1.3.2). Against this background, the present study investigated whether the combination of talazoparib and THZ531 also produces synergistic effects in urothelial carcinoma cells. As in the previous experimental approach, 253J and J82 were selected because both cell lines exhibited the highest IC_{50} values for THZ531. Their high baseline tolerance to pharmacological CDK12 inhibition makes them particularly relevant for identifying potential synergy, as a combination treatment could reduce the required drug concentrations and thereby improve therapeutic feasibility. The inclusion of the T24 cell line was based on earlier findings demonstrating pronounced sensitivity to THZ531 and indications of synergistic activity in combination with cisplatin, making T24 a suitable model to further investigate the interaction between CDK12 and PARP inhibition.

3.5.1 Impact on Cell Viability

Using MTT assays, the effects of combined treatment with THZ531 and talazoparib on cell viability in the J82, 253J, and T24 cell lines were evaluated. The dose response curves are illustrated in Figure 38. The x-axis represents concentrations expressed as multiples of the respective IC_{50} values determined for each drug in single-agent treatment. For combination treatment, both drugs were applied at fixed ratios based on their individual IC_{50} values.

In the J82 cell line, both monotherapies resulted in a reduction of cell viability. The half-maximal inhibitory concentration for THZ531 was overestimated, while that for talazoparib was underestimated in this experimental setup. The combination treatment led to a more pronounced decrease in cell viability compared to either monotherapy. In the 253J cell line, talazoparib monotherapy initially caused a substantial decrease in cell viability; however, further dose escalation did not result in additional reductions in survival. THZ531 monotherapy produced a continuous decline in viability, with a 50 % survival rate observed at the IC_{50}-value. Similar to J82 cells, the combination treatment yielded the most significant reduction in cell viability. For T24 cells, a reduction of approximately 40 % in viability was observed at a low dose of talazoparib (0.125-fold IC_{50}), with this effect diminishing at higher doses. THZ531

treatment at lower doses (up to 0.5-fold IC_{50}) did not lead to a significant decrease in cell viability compared to the DMSO control, with the half-maximal dose being slightly overestimated. The combination of both agents resulted in the greatest reduction in cell viability. Notably, THZ531 at very low concentrations did not exhibit cytotoxicity in T24 cells, yet the combination with talazoparib still produced a synergistic reduction in viability.

The data from the combination treatments (Figure 38) were analyzed for their synergistic effects using the Chou-Talalay method. The results are presented in Figure 39.
In the J82 cell line, all dose points in the combination treatment exhibited synergistic effects (CI < 1). The Fraction Affected (Fa) increased with higher dosages.
A similar pattern was observed for the 253J cell line. All tested dose points in the combination treatment were synergistic. Treatment with the 0.125-fold IC_{50} of both drugs affected 50 % of the cells' viability (Fa: 0.5). The Fraction affected also increased with increasing dosage, with CI values predominantly below 0.5.
For the T24 cell line, synergistic effects were noted within the range of 0.125- to 0.5-fold IC_{50} doses. CI values were below 1 but above 0.5. At the 0.125-fold IC50 dose, the Fraction affected was 50 % and increased with higher dosages. Starting from the 0.75-fold IC_{50} dose, the effects of both agents became additive or antagonistic.
In summary, synergy was observed across all evaluated dose points in 253J and J82 cells. Despite this, the high THZ531 IC_{50} of J82 implies that even an eighth of its IC_{50} remains pharmacologically too high to be clinically meaningful as it is too toxic for HBLAK. Nevertheless, the consistent synergistic interactions across J82, 253J, and T24 demonstrate that, on a mechanistic level, the combination of talazoparib and THZ531 exerts synergistic effects in urothelial carcinoma cells, aligning with previously reported findings in other tumor entities.

A

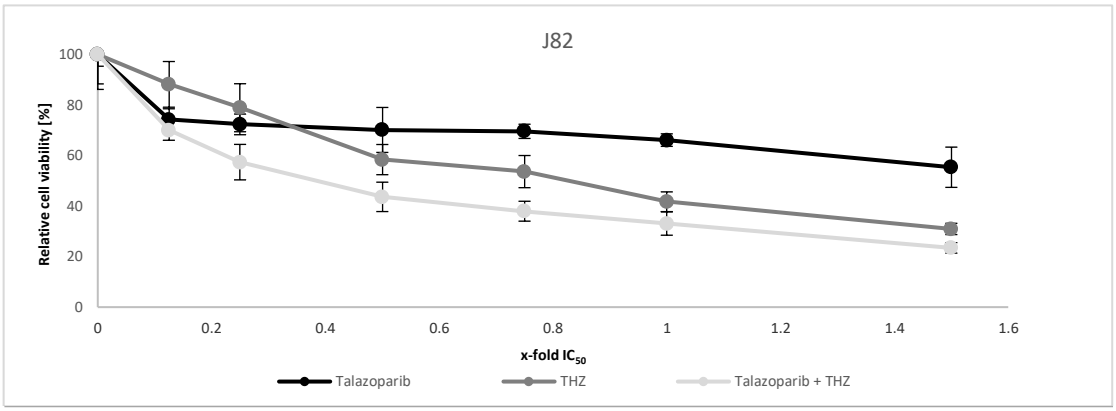

B

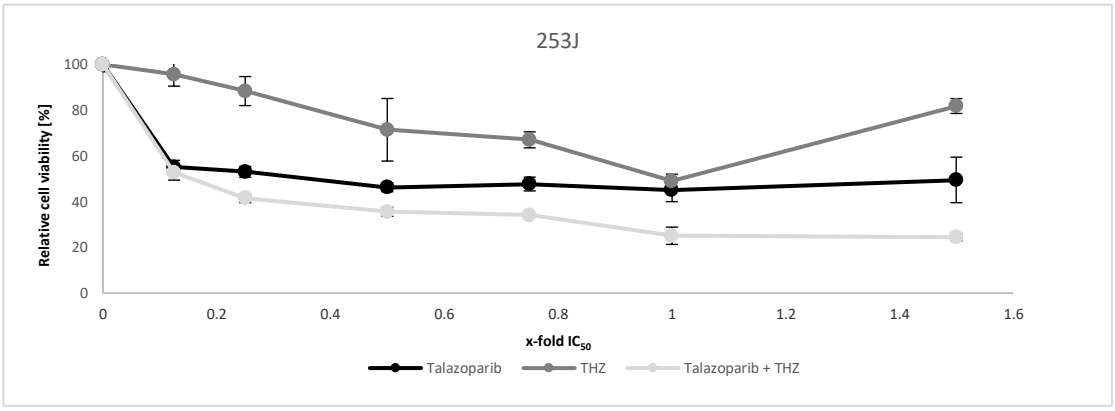

C

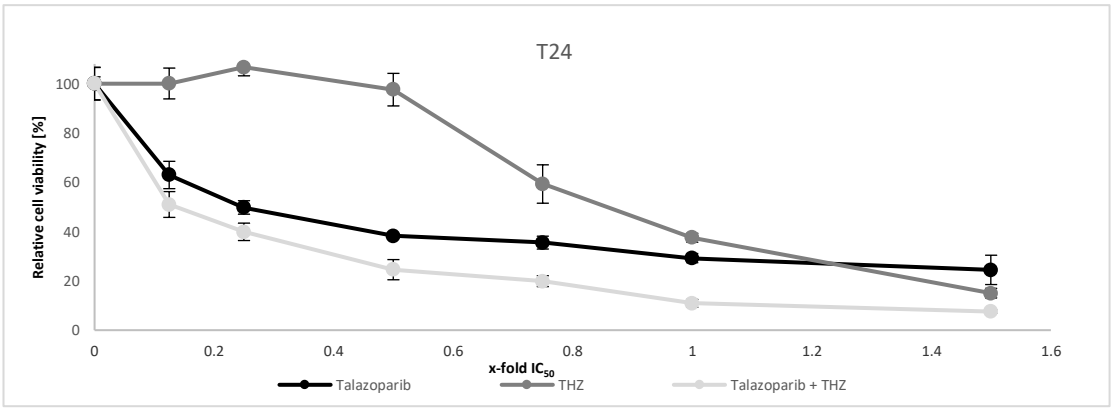

Figure 38: Combined treatment with THZ531 (THZ) and talazoparib. The dose response curves for the urothelial carcinoma cell lines J82 (A), 253J (B), and T24 (C) are shown following individual and combined treatments with both agents. Cell viability was evaluated using the MTT assay after 72 hours of exposure. Each concentration point represents the mean ± SD of four biological replicates derived from one biological sample per condition. For the drug concentrations applied, see Table 14 and Figure 11. Combination treatments were performed at fixed ratios based on the respective IC50 values derived from these data.

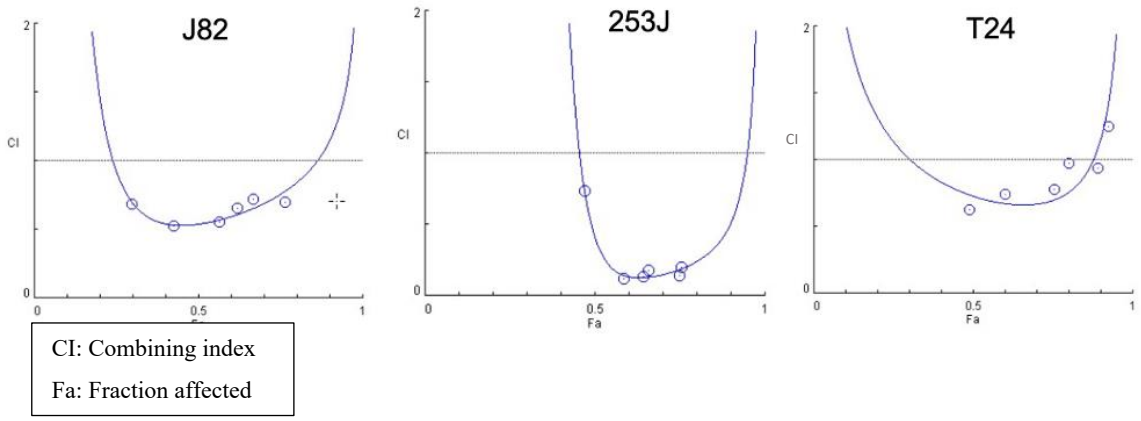

Figure 39: Synergistic effects of combination therapy with THZ531 and talazoparib in the J82, 253J, and T24 cell lines. The Combination Indices (CI) are displayed, calculated using the Chou-Talalay method. The dose points represent multiples of both agents. A CI value below 1 indicates a synergistic effect, a CI value above 1 indicates an antagonistic effect, and a CI value of 1 signifies an additive effect. The Fraction Affected (Fa) denotes the proportion of cells impacted by the treatment.

3.5.2 DNA Damage and Apoptosis Induction

Due to the synergistic effects observed with the combination of THZ531 and talazoparib, the impact of this treatment on DNA damage levels and apoptosis was examined by Western blot analysis to determine whether the observed cytotoxicity is mediated through apoptosis induction and is shown in figure 40.

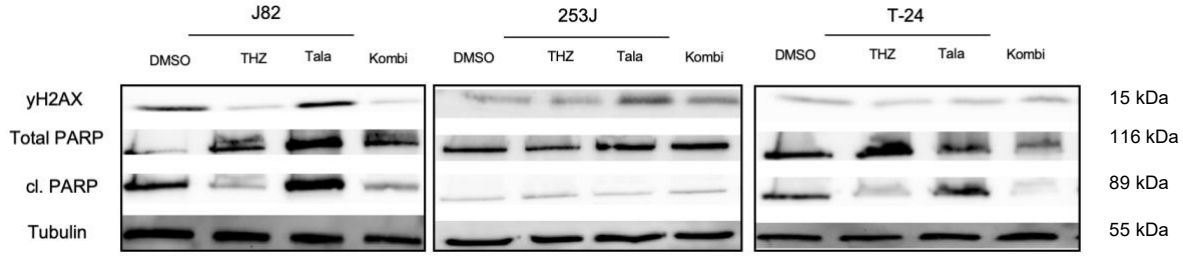

Figure 40: DNA damage and apoptosis induction by THZ531 (THZ) and talazoparib (Tala) in urothelial carcinoma cells. Protein levels were assessed using Western blotting. Loading control was performed with Tubulin. The bands shown include phosphorylated H2AX (γH2AX) as a marker of DNA damage, cleaved PARP as a marker of apoptosis, and total PARP as the corresponding loading control. For the drug concentrations applied, see Table 14 and Figure 11.

J82 and 253J cells exhibited increased H2AX phosphorylation in response to talazoparib, indicated by more intense γH2AX bands. No evidence of DNA damage was observed in THZ531-treated samples across all three cell lines. PARP cleavage was observed in J82 and T24 cells following talazoparib monotherapy, although a stronger cleaved PARP band was noted even in the DMSO control. This effect was not apparent in cells treated with the

combination therapy. In 253J cells, increased PARP cleavage was not detected in any of the treated samples.

Taken together, none of the three examined cell lines demonstrated an increase in PARP cleavage or H2AX phosphorylation under the combination treatment, suggesting that the synergistic reduction in viability is not mediated by enhanced apoptosis induction.

4 Discussion

Cisplatin-based chemotherapy remains a cornerstone in the treatment of advanced urothelial carcinoma, yet intrinsic and acquired resistance limit its long-term clinical benefit [49, 50]. In recent years, therapeutic options have expanded substantially with the introduction of immune checkpoint inhibitors and antibody drug conjugates, yet cisplatin continues to form the backbone of systemic therapy for most patients [18, 50]. Understanding the molecular determinants of cisplatin sensitivity and resistance therefore remains a central research objective. Growing body of literature has implicated CDK12, a transcriptional regulator of long genes enriched for DNA repair functions, in modulating the cellular response to DNA damage [40]. In several tumor entities, CDK12 inhibition alter DNA repair dependencies and influence response to chemotherapeutic agents and PARP inhibitors [44, 45]. Conversely, CDK12 amplification or hyperactivity has been linked to therapy resistance and aggressive tumor biology [51]. Functional data on CDK12 in urothelial carcinoma have been limited.

4.1 Correlation between Patient Data and In-vitro Findings

In tissue microarray analyses, it was observed that urothelial carcinoma patients responded to neoadjuvant cisplatin-based chemotherapy with an increase in CDK12 levels, suggesting a potential role for CDK12 as a predictive biomarker [43]. To evaluate this observation in vitro, parental and LTT cell lines were analyzed for their CDK12 protein levels under basal conditions and after 72 hours of cisplatin exposure.

The analyses demonstrated that LTT cells exhibit an elevated CDK12 protein level compared to their parental cells, mirroring the increase observed in responsive patient tumors following neoadjuvant therapy. Short-term cisplatin exposure resulted in heterogeneous CDK12 regulation: CDK12 decreased in T24 cells, increased in J82 and 253J cells, and remained unchanged in RT112 cells. In LTT cells, short-term cisplatin exposure led to a reduction in CDK12 levels, highlighting the distinct regulatory dynamics between acute and chronic treatment conditions.

These findings can be interpreted considering clinical chemotherapy schedules. Neoadjuvant chemotherapy for urothelial carcinoma typically involves the administration of cisplatin over 3-4 chemotherapy cycles, with each cycle lasting several weeks [7]. This corresponds to a prolonged, intermittent cisplatin exposure for the tumor tissue, which is best mimicked by the LTT model. Accordingly, the elevated CDK12 expression observed in LTT cells may reflect an adaptive response to sustained DNA damage pressure, consistent with the patient data.

Furthermore, patient data suggest a correlation between CDK12 levels and therapy response or overall survival. Untreated patients with high CDK12 levels had longer overall survival compared to those with low CDK12 levels. Concurrently, CDK12 appeared to be an unfavorable prognostic marker when a poor response to chemotherapy was observed [43]. This suggests a dual role for CDK12 in the context of urothelial carcinoma. This seemingly paradoxical observation can be explained by the context-dependent function of CDK12: Genomic instability is considered one of the hallmarks of cancer [52]. Since CDK12 regulates the transcription of numerous DNA-repair genes, one may assume that higher CDK12 activity contributes to a more stable genomic landscape [53, 54]. Tumors with greater genomic stability may, in principle, exhibit a lower capacity for evolutionary diversification and accumulate fewer mutations, potentially resulting in a slower progression and overall, less aggressive phenotype. Within this framework, it is conceivable that higher CDK12 expression, by supporting transcriptional programs that maintain genomic integrity, correlates with a more favorable clinical outcome in untreated patients.

Under the selective pressure of cytotoxic therapy, however, these functional implications may reverse. Cisplatin exerts its antitumor activity through the induction of persistent DNA damage [55]. A pronounced CDK12-dependent repair capacity could, at least hypothetically, reduce the efficiency of this damage by maintaining sufficient expression of key DNA repair pathways and facilitating the removal of cisplatin-induced lesions. In this therapeutic context, robust DNA repair may therefore become disadvantageous (for the patient) and contribute to reduced treatment sensitivity. This survival advantage may also preserve the possibility for further cellular adaptation due to chemotherapy like those described by Galluzzi et al. [20].

Overall, this model suggests that the same biological property, effective DNA repair, may lead to a more favorable course in the absence of therapy but to diminished sensitivity to cisplatin under treatment conditions. This interpretation remains hypothetical and serves as a conceptual framework to explain the divergent clinical outcomes observed in our cohort.

Although the proposed model suggests that high CDK12 levels may contribute to enhanced genomic stability and thereby potentially support a more indolent course in untreated conditions, it is important to note that there is currently no tumor entity in which high CDK12 expression has been clearly established as an independent favorable prognostic factor (as of December 2025).

Recent articles further emphasize the dual function of CDK12. It can function as a tumor suppressor, CDK12 contributes to the maintenance of genomic integrity, whereas in certain

contexts, increased CDK12 activity can exert oncogenic effects and promote resistance to DNA-damaging therapies [56].

Additional support for this context dependency comes from other tumor entities. In HER2-positive breast cancer, CDK12 is frequently co-amplified due to its genomic proximity, and in this specific molecular setting, increased CDK12 levels are associated with more aggressive tumor behavior [57]. Conversely, inactivating CDK12 alterations in prostate cancer define a clinically aggressive subtype characterized by high Gleason grade, early metastatic presentation, and poor responses to hormonal agents, taxanes, and PARP inhibitors [58]. Although these findings cannot be directly extrapolated to urothelial carcinoma, they illustrate that CDK12-dependent cellular programs can exert variable effects on tumor biology across different genomic environments.

Nevertheless, these mechanistic insights provide a coherent framework to partially explain the divergent prognostic associations observed in untreated versus chemotherapy-exposed tumors.

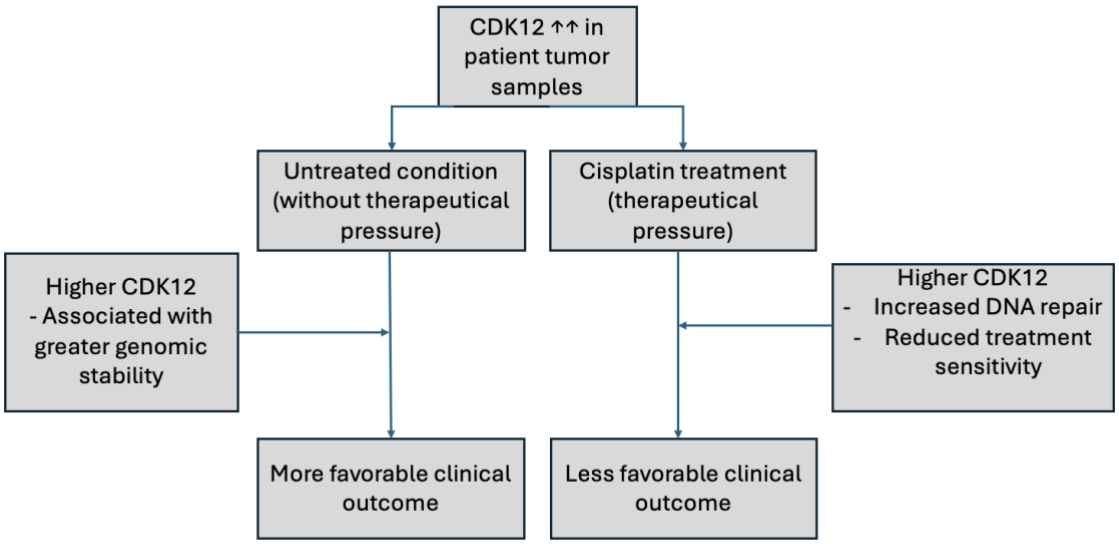

Figure 41: Hypothetical model illustrating the context-dependent interpretation of elevated CDK12 levels in urothelial carcinoma. This schematic presents a conceptual, hypothesis-based framework to interpret the divergent associations of high CDK12 expression observed in patient samples. The proposed model suggests that elevated CDK12 levels may reflect greater genomic stability under untreated conditions and could be associated with more favorable clinical outcomes. Under cisplatin treatment, however, higher CDK12 expression may hypothetically support increased DNA repair activity and potentially contribute to reduced treatment sensitivity, corresponding to less favorable outcomes. Importantly, this diagram does not represent proven causal relationships but rather a theoretical interpretation intended to contextualize the findings from patient data and in-vitro models.

4.2 CDK12-dependent DNA Damage Response in LTTs

Given that CDK12 is considered a central transcriptional regulator of numerous DNA repair genes and that LTT cell lines consistently exhibited elevated CDK12 protein levels, the question arose whether this was functionally associated with an enhanced DNA damage response [37]. It was hypothesized that increased CDK12 expression in cisplatin-resistant cells might promote augmented activation of homologous recombination mechanisms and thereby contribute to an increased repair capacity. Against this background, the expression of key homologous recombination genes and additional DNA repair pathways was systematically analyzed following cisplatin exposure.

Building on these considerations, the LTT models provide further insights into the relationship between CDK12 and the DNA damage response. Although all LTT cell lines showed uniformly elevated CDK12 protein levels, cisplatin exposure did not result in a consistent upregulation of homologous recombination genes. Instead, the transcriptional response varied markedly between the different models, indicating that high CDK12 expression alone is insufficient to predict the activation pattern of individual DNA repair pathways.

In several LTT models, cisplatin exposure was associated with an upregulation of selected homologous recombination genes. This was most pronounced in RT112-LTT, which upregulated both *BRCA1* and *BRCA2* and additionally displayed a consistent tendency toward activation of further repair-related transcripts. This behavior aligns with the hypothesis that elevated CDK12 levels may support the transcription of certain DNA repair factors [37].

However, this pattern was not observed across all models. J82-LTT responded to cisplatin exposure with a marked downregulation of several homologous recombination-associated genes, suggesting that the regulation of the DNA damage response in cisplatin-tolerant cells is not determined by CDK12 alone.

The remaining LTT models exhibited predominantly moderate or cell line-specific changes without a uniform activation profile. While individual genes, such as *RAD51c* in RT112-LTT or *POLH* in multiple models, were significantly upregulated, other repair pathways remained largely unchanged. The observed changes were therefore functionally relevant but not consistently restricted to homologous recombination.

This pronounced heterogeneity demonstrates that elevated CDK12 levels do not automatically translate into enhanced transcription of DNA repair genes under acute cisplatin exposure. Instead, cisplatin resistance appears to arise from a complex, multifactorial reorganization of the DNA damage response as already described in literature, in which CDK12 plays a contributory but not exclusively determinative role [20, 22].

These observations are consistent with findings by Skowron et al., who likewise reported a complex and heterogeneous adaptation of DNA repair programs across different LTT models, without a uniform regulatory pattern [21].

4.3 Mechanisms of CDK12 Modulation

Against the background of elevated CDK12 levels observed in the LTT models, and considering the central role of CDK12 as a transcriptional regulator of numerous DNA repair genes, the question arose as to what isolated functional contribution CDK12 makes to the DNA damage response and cisplatin sensitivity of urothelial carcinoma cells [37]. To investigate this relationship independently of the complex long-term adaptations present in the LTT models, three complementary experimental systems were employed: stable CDK12 overexpression, siRNA-mediated knockdown, and pharmacological inhibition using THZ531. These approaches allow a systematic analysis of the immediate consequences of altered CDK12 activity and enable assessment of whether CDK12 modulation influences the expression of DNA repair genes, the induction of DNA damage, or apoptosis following cisplatin exposure.

4.3.1 CDK12 overexpression

4.3.1.1 Functional Consequences of CDK12 Overexpression

To determine how an isolated increase in CDK12 affects the basal expression of key DNA repair genes, a stable overexpression model was established. The analysis of CDK12 overexpression showed that an isolated increase in CDK12 induces some basal changes in the expression of DDR genes, but does not generate a consistent pattern indicative of an enhanced DNA repair capacity. In all three models, *BRCA2* was markedly upregulated under untreated conditions, reflecting the established role of CDK12 as a transcriptional regulator of long DNA repair genes [37, 38]. Additional genes such as *ATR* and *RAD51c* were moderately induced, whereas *BRCA1* tended to be reduced across all models.

4.3.1.2 CDK12-dependent Stress Response under Cisplatin Exposure

After cisplatin exposure, no uniform or CDK12-dependent activation pattern was observed. RT112 and T24 responded largely similarly to their respective control cells under CDK12 overexpression; differences were moderate and limited to individual genes such as *BRCA2* or *POLQ*. This suggests that CDK12 overexpression alone is insufficient to substantially modulate the DNA damage response under conditions of acute DNA damage.

In contrast, UMUC-3 displayed a distinctly divergent behavior. Whereas control cells showed a marked induction of key DNA damage repair genes (*BRCA1/2*) and the signaling kinases *ATR* and *ATM* following cisplatin treatment, CDK12-overexpressing UMUC-3 cells responded with

a pronounced downregulation of these factors. Western blot analyses confirmed the qPCR results for ATR and ATM. Reduced protein levels were likewise observed in CDK12-overexpressing cells after cisplatin exposure.

The observation that CDK12-overexpressing UMUC-3 cells upregulate selected DNA repair genes under basal conditions, but downregulate these same factors upon cisplatin exposure, can be interpreted within a dynamic, stress-dependent regulatory framework.

When CDK12 is elevated under untreated conditions, it enables increased transcription of selected CDK12-dependent DNA damage repair genes, particularly long genes such as *BRCA2*. This pattern is consistent with the established role of CDK12 as a regulator of transcriptional elongation of long DNA repair genes [37]. An increased basal expression of certain DNA damage repair factors can therefore, in principle, contribute to an enhanced readiness for repair. When cells are exposed to acute cisplatin-induced genotoxic stress, however, cellular priorities may shift. Under such conditions, the cell must repair DNA damage efficiently while avoiding unnecessary strain on the energy-intensive transcriptional and translational machinery. The literature describes that cells downregulate global transcriptional programs under severe DNA damage to prevent transcription-repair-conflicts, for example the accumulation of aberrant RNA species and additional DNA damage arising from stalled polymerases [59].

Accordingly, when cisplatin induces acute DNA damage, a downregulation of central DNA damage repair genes, including those that were upregulated as a result of CDK12 overexpression, occurs only in UMUC-3.

This regulatory pattern may allow UMUC-3 to maintain a form of functional "repair homeostasis," in which CDK12-mediated basal transcriptional advantages coexist with stress-dependent attenuation mechanisms. In this model, cells balance the need for sufficient repair capacity with the necessity of preventing a dysregulated and dysfunctional DNA damage repair activation.

Although hypothetical, this model offers a mechanistically coherent explanation for the uniquely opposing regulatory behavior observed in UMUC-3.

This regulatory behavior in UMUC-3, although observed under acute CDK12-dependent stress conditions, conceptually aligns with the heterogeneity described by Skowron et al. in long-term cisplatin-adapted models. While Skowron et al. investigated stable, selectively acquired resistance phenotypes in LTT cells, their data likewise demonstrate that cisplatin-induced adaptations do not occur in a uniform direction. Instead, individual DNA repair pathways may be either upregulated or actively suppressed, as exemplified by the downregulation of mismatch repair components in J82-LTT, which the authors interpret as a mechanism to prevent "futile

repair cycles" [21]. Although mechanistically distinct, both settings underscore that DNA damage responses to cisplatin are fundamentally non-linear, context-dependent, and can involve adaptive suppression of specific repair axes rather than global enhancement of repair capacity.

4.3.1.3 Impact on Apoptosis and DNA Damage by Cisplatin

To complement the transcriptional analyses, the impact of CDK12 overexpression on cisplatin-induced DNA damage and apoptosis was examined using γH2AX and cleaved PARP. Across all three cell lines, cisplatin treatment led to detectable γH2AX induction and PARP cleavage, and these responses occurred to a comparable extent in CDK12-overexpressing cells and their empty-vector controls. While γH2AX does not allow precise quantification of the absolute damage burden [60], the consistent induction of γH2AX and cleaved PARP across conditions suggests that CDK12 overexpression did not markedly alter the qualitative DNA damage response or apoptosis initiation under the experimental conditions used. These findings support the notion that CDK12 overexpression alone is insufficient to substantially modify the early cellular damage response to cisplatin as already mentioned above.

4.3.2 CDK12 Knockdown

4.3.2.1 Functional Consequences of CDK12 Knockdown

To assess whether reduced CDK12 levels sensitize urothelial carcinoma cells to cisplatin and functionally attenuate DNA repair capacity, a siRNA-mediated knockdown approach was established. Based on the known role of CDK12 as a regulator of long DNA damage repair genes, a decrease in homologous recombination capacity and a corresponding increase in cisplatin sensitivity had been expected [37].

Basal gene expression changes following CDK12 depletion were modest. Only VMCUB1 cells showed a consistent reduction of *BRCA2* and *RAD51C*, while the remaining cell lines exhibited largely unchanged expression profiles. The only uniform finding across all models was a downregulation of *ATM*. Conversely, *POLH* was reproducibly upregulated in all knockdown lines. Although *POLH* is not known to be transcriptionally regulated by CDK12, its induction is compatible with a compensatory shift towards translesion synthesis in the context of reduced homologous recombination capacity [32].

4.3.2.2 CDK12-dependent Stress Response under Cisplatin Exposure

After cisplatin exposure, the transcriptional responses were highly cell line dependent. RT112 cells were able to induce *BRCA2*, *RAD51* and additional DNA repair genes despite reduced CDK12 levels, suggesting that CDK12 depletion alone is not sufficient to functionally impair

the homologous recombination response. UMUC3 cells showed a similar, albeit less pronounced pattern with moderate induction of *BRCA2*, *RAD51* and *ATM*. VMCUB1 knockdown cells displayed virtually no adaptive transcriptional response to cisplatin. Overall, the magnitude of all transcriptional changes remained within a narrow logarithmic fold change range and thus limits mechanistic interpretation.

A notable observation was the substantial difference between the control groups of the two experimental systems. Empty-vector controls (overexpression setting) exhibited markedly stronger induction of DNA damage repair genes than non-targeting siRNA controls (knockdown setting). Such discrepancies are consistent with reports that lipofectamine-mediated transfection and non-targeting siRNAs can trigger cellular stress responses and globally dampen transcription [61]. These confounding factors likely contribute to the attenuated cisplatin response in non-targeting siRNA controls and must be considered when interpreting the data.

Notably, the direction of the cisplatin-induced response differed between the overexpression and knockdown systems in UMUC-3. CDK12-overexpressing UMUC3 cells displayed a marked decrease in *BRCA2*, *ATR* and *ATM* after cisplatin exposure, whereas CDK12-depleted UMUC3 cells showed the opposite trend with a relative induction of these factors. A reciprocal pattern of the DNA damage response is observed that may depend on CDK12 levels, but is restricted to a single investigated cell line.

4.3.2.3 Impact on Apoptosis and DNA Damage by Cisplatin

Importantly, functional readouts did not indicate increased cisplatin sensitivity in urothelial carcinoma cells following CDK12 depletion. Cisplatin-induced DNA damage, reflected by γH2AX accumulation, was comparable between knockdown and control cells. Likewise, cleaved PARP levels indicated similar degrees of apoptosis induction across all conditions. Although γH2AX is not an absolute quantitative measure of DNA damage [60], the concordant patterns of γH2AX and PARP cleavage across cell lines strongly suggest that CDK12 knockdown does not substantially alter cisplatin susceptibility under the tested conditions.

Consistent with these findings, dose-response analyses revealed virtually identical IC_{50} values for cisplatin in CDK12-depleted and control cells, indicating that reducing CDK12 expression does not translate into measurable differences in drug sensitivity.

Comparable findings have been reported in other tumor types. In ovarian cancer, a CRISPR-mediated CDK12 knockout also failed to increase sensitivity to DNA-damaging agents [62], reinforcing the biological plausibility of our results. These findings emphasize that CDK12 acts

as a modulatory rather than determinant factor of the cisplatin response in urothelial carcinoma cells.

4.3.3 Pharmacological CDK12 Inhibition

After evaluating the effects of genetic CDK12 modulation, through both overexpression and siRNA-mediated knockdown, the next question was whether acute pharmacological inhibition of CDK12 produces functional consequences distinct from those observed under chronic alterations of CDK12 abundance. Specifically, the aim was to determine whether inhibition of CDK12 kinase activity itself, independent of transcriptional adaptations induced by long-term modulation, affects DNA-damage induction and the expression of key DNA repair genes. To address this, the covalent CDK12/13 inhibitor THZ531 was employed to assess whether acute kinase blockade enhances the cellular response to cisplatin and generates a functional pattern different from the genetic perturbation models [36].

The results revealed that pharmacological inhibition of CDK12 produces a distinct pattern compared with genetic modulation.

In contrast to the overexpression and knockdown models, pharmacological CDK12 inhibition generated a more uniform pattern of molecular and cellular effects across several urothelial carcinoma cell lines. Treatment with the covalent CDK12/13 inhibitor THZ531 together with cisplatin resulted in a cell line dependent enhancement of DNA damage and apoptosis. This was reflected by increased γH2AX phosphorylation in RT112 and UMUC3, and by stronger PARP cleavage in UMUC3 and T24, compared with either monotherapy alone. These findings indicate that pharmacological CDK12 inhibition can potentiate cisplatin toxicity, at least in a subset of models.

Despite the enhanced γH2AX and PARP-cleavage signals observed under combination treatment, the transcriptional response did not reveal a corresponding suppression of DNA repair gene transcription. THZ531 monotherapy induced moderate upregulation of DNA damage repair genes in RT112 but had minimal effects in UMUC3 and T24. The cisplatin and THZ531 combination produced no coherent transcriptional signature across cell lines. Notably, the combination did not consistently downregulate *BRCA1/2*, *ATR*, or other genes of homologous recombination, suggesting that the functional sensitization observed in the combined treatment cannot be explained by transcriptional repression of DNA damage repair genes, as it has been reported for other tumor entities [44, 45].

The only recurring pattern across two cell lines was a reduction in *ATR* expression under the combination condition, although the magnitude of change remained modest.

Importantly, only pharmacological inhibition sensitized cells to treatment with cisplatin. CDK12 knockdown did not alter cisplatin IC_{50} values, γH2AX levels, or PARP cleavage, supporting the notion that partial depletion of CDK12 is insufficient to compromise cisplatin tolerance. In ovarian cancer, a CRISPR-mediated CDK12 knockout also failed to increase sensitivity to DNA-damaging agents [62]. These findings underline that genetic loss of CDK12 does not inherently induce chemosensitization, whereas acute pharmacological inhibition can potentiate cisplatin effects**.**

Because THZ531 acts as a covalent inhibitor of both CDK12 and CDK13, its cellular effects extend beyond transcriptional elongation of long DNA damage repair genes [36, 63]. Wu et al. described a role of CDK13 in translational regulation and proposed a broader connection to global protein synthesis, with potential implications for tumorigenesis and tumor progression [63]. The original THZ531 developers already pointed out that the compound may exert additional target-related effects, which could help explain such broader cellular responses [36]. In addition, previous work has shown that CDK12 contributes to maintaining transcriptional homeostasis, suggesting that its inhibition may have broader cellular consequences beyond DNA damage repair gene expression [57, 64, 65]. THZ531 may affect CDK12-independent cellular functions that were not examined in this study and could thereby exert additional cytotoxic effects in combination with cisplatin.

Table 17: Overview of experimental findings following CDK12 overexpression, CDK12 knockdown, and pharmacological inhibition with THZ531 in urothelial carcinoma cells.

	CDK12 Overexpression	CDK12 Knockdown	Pharmacological inhibition (THZ531)
Basal CDK12 expression	↑↑↑	↓↓↓	Reduced activity
Basal expression of DNA damage repair genes	*BRCA2* ↑, *ATR* ↑	*ATM* ↓, *BRCA1* ↓ in VMCUB1 *POLH* ↑, *POLQ* ↑	No consistent pattern across cell lines
Cisplatin induced DNA damage and apoptosis	Comparable to empty vector control	Comparable to non targeted control cells	Increased γH2AX and PARP cleavage in some cell lines
Cisplatin induced DNA damage repair gene expression	Partly inverse regulation in UMUC-3 (Homologous recombination genes ↓)	Moderate effects, potentially attributable to transfection-related stress.	Mostly moderate, cell line dependent changes
Cisplatin IC_{50}	Not assessed	Unchanged	Not assessed
Mechanistic interpretation	CDK12 overexpression influences HR-gene expression, but does not reduce Cisplatin-mediated damage	Loss of CDK12 does not lead to Cisplatin sensitivity. Loss of CDK12 may enhance alternative repair pathways	THZ531 and Cisplatin increases DNA damage and apoptosis in some cell lines, possibly via additional CDK13-related or off-target mechanisms

4.4 Significance of CDK12 in Cisplatin Resistance of Urothelial Carcinoma

Taken together, the patient cohort and in-vitro data consistently indicate that CDK12 is involved in the cisplatin response of urothelial carcinoma, but does not act as a singular driver of sensitivity or resistance. In patient tumors, CDK12 levels increased during neoadjuvant cisplatin-based chemotherapy, and long-term cisplatin adapted LTT cell lines recapitulated this increase, supporting the interpretation that CDK12 upregulation reflects an adaptive response to sustained genotoxic pressure in urothelial carcinoma cells [43].

However, neither CDK12 overexpression nor siRNA-mediated depletion produced functional evidence for altered cisplatin susceptibility. While cisplatin IC_{50} values were directly assessed in the knockdown model where CDK12 depletion failed to increase sensitivity, both modulation strategies showed comparable γH2AX accumulation and PARP cleavage after cisplatin exposure. Together, these findings indicate that variation in CDK12 abundance alone is insufficient to meaningfully modify the acute cellular response to cisplatin.

The heterogeneity observed in our models aligns with the broader CDK12 literature, which does not support a single, linear role for CDK12 in cancer biology. While CDK12 is well established as a transcriptional regulator of long DNA repair genes, including *BRCA1/2*, this functional axis alone does not predict its impact on tumor behavior or treatment response. Instead, CDK12 has emerged as a context-dependent modifier whose biological consequences vary widely across tumor types [38, 40, 53, 58].

In ovarian cancer, CDK12 loss leads to impaired transcription of long homologous recombination genes, yet does not consistently increase sensitivity to DNA-damaging agents [62]. In contrast, in HER2-positive breast cancer, CDK12 is frequently co-amplified and has been associated with increased proliferation, invasion, and poorer therapeutic response [51, 57]. Similarly, no amplification was observed in melanoma cells, but CDK12 hyperactivity was detected, leading to an inherent resistance to chemotherapeutic agents in *BRAF*-mutated melanoma cells [66]. These findings indicate that CDK12 dysregulation can have markedly different biological consequences across tumor types. Loss of CDK12 does not uniformly produce a chemosensitive phenotype, while increased CDK12 activity may contribute to a more aggressive or therapy-resistant phenotype in certain molecular settings.

Recent pan-cancer analyses reinforce this ambiguity. Lu et al. show that CDK12 expression correlates positively with tumor aggressiveness, immune infiltration or poor prognosis in some cancers, while displaying neutral associations in others [67]. No consistent pattern exists with respect to invasion depth, metastatic potential, or overall survival [67].

In this context, the elevated CDK12 levels observed in the LTT models are compatible with the broader literature, in which increased CDK12 activity is frequently associated with more aggressive tumor phenotypes and enhanced stress tolerance.

4.5 Mechanistic Effects of CDK12 Inhibitor THZ531

THZ531 is a covalent small-molecule inhibitor of the transcriptional kinases CDK12 and CDK13, designed to disrupt the transcriptional regulation of DNA-repair genes by targeting

RNA-Polymerase II–dependent processes [36]. In the performed overexpression models during this study, THZ531 sensitivity was independent of baseline CDK12 protein levels. Even cells with markedly elevated CDK12 did not show reduced susceptibility to the inhibitor. This indicates that THZ531 exerts its effects through mechanisms that extend beyond CDK12 abundance alone and warrants a closer examination of its impact on apoptosis and cell-cycle dynamics.

4.5.1 Effects on Cell Cycle and Apoptosis

The apoptotic effects of THZ531 varied markedly depending on cellular context and resistance status. In LTTs, THZ531 induced measurable apoptotic signaling, particularly in RT112-LTT and T24-LTT, where increased PARP cleavage was observed. J82-LTT and 253J-LTT, however, showed no substantial induction of apoptosis, underscoring the heterogeneity of the response. These findings indicate that cisplatin-tolerant cells may be differentially primed for CDK12/13 inhibition, although the underlying determinants remain unclear.

In contrast, in neither of the parental cell lines examined, THZ531 monotherapy induced PARP cleavage. Instead, THZ531 produced only modest H2AX phosphorylation, most prominently in T24.

In neuroblastoma cells, THZ531 has been shown to trigger apoptosis alongside a pronounced G2/M arrest [68], whereas prostate cancer models demonstrated impaired proliferation, increased G2/M accumulation, reduced S-phase progression and induction of apoptosis following CDK12 inhibition [69]. These observations align with the heterogeneous responses observed in our urothelial carcinoma models. This pattern suggests that THZ531 does not elicit a uniform mechanism of cytotoxicity. Pathways vary between tumor types and even between closely related urothelial cell lines.

However, for urothelial carcinoma cells, no definitive conclusion can be drawn as to whether THZ531-mediated growth inhibition is primarily driven by apoptosis or by cell-cycle arrest. Dedicated cell-cycle analyses, such as FACS-based phase profiling, were not performed in this study and would be required to accurately determine the underlying mechanism.

4.5.2 Effects on DNA Damage Response

To characterize the transcriptional consequences of CDK12 inhibition, THZ531 was applied to parental and LTT cell lines, and the expression of key DNA damage repair genes was quantified.

THZ531 caused heterogeneous but mostly modest transcriptional effects. The most consistent change was a reduction of *ATM*, while *ATR* was largely unchanged. *BRCA1* showed a global

downward trend across all cell lines, often modest and not always reaching biological cut-offs, whereas *BRCA2*, *RAD51*, and *RAD51c* were selectively upregulated in some parental models. *POLH/POLQ* changed only slightly. Overall, THZ531 did not uniformly suppress genes of homologous recombination as it was expected due to reports in the literature [38], but produced a cell-line-specific modulation of DNA damage repair genes.

Given this heterogeneity, our data do not provide sufficient evidence to conclude that THZ531 induces a BRCAness-like state in urothelial carcinoma. Although some features, such as *BRCA1* and *ATM* downregulation in selected models, resemble patterns described in BRCA-deficient systems, these effects were neither consistent nor robust across all cell lines. As such, alternative explanations, including broader transcriptional stress induced by CDK12/13 inhibition, remain equally plausible [36, 63].

The concept of pharmacologically induced BRCAness is, however, well supported in other tumor entities. Studies in triple-negative breast cancer and the multiple myeloma demonstrate that CDK12 inhibition can reduce homologous recombination capacity and sensitize cells to PARP inhibitors through BRCA-like transcriptional signatures [45, 70]. In contrast, our data in urothelial carcinoma reveal a more complex and attenuated response, suggesting that the extent to which CDK12 inhibition induces homologous recombination deficiency may be highly cell line dependent.

Taken together, while individual transcriptional changes in our models align with mechanisms described in BRCAness-inducing settings, the overall expression patterns do not justify inferring a genuine BRCAness phenotype in urothelial carcinoma. A definitive classification would require functional assays which were beyond the scope of this study.

4.5.3 Tolerability and Side Effects

The tolerability of THZ531 was evaluated in vitro using HBLAK urothelial cells, which demonstrated overall acceptable viability at lower concentrations. The calculated IC_{50} for HBLAK was approximately 204 nM; however, the transition between 0.125 µM and 0.25 µM resulted in an abrupt and disproportionately strong inhibition of cell growth. This steep dose–response relationship indicates a narrow therapeutic window and suggests that even minor dose escalations may rapidly shift the compound from a tolerable to a cytotoxic range.

Comprehensive toxicological characterization is currently lacking. No systematic analyses of cumulative toxicities, hematologic or gastrointestinal adverse effects are available. Likewise, long-term toxicity profiling of repeated dosing or combination strategies has not been performed. This creates substantial uncertainty regarding the clinical safety profile of THZ531.

Clinically established agents, such as CDK4/6 inhibitors (palbociclib, ribociclib, abemaciclib), are associated with dose-limiting toxicities, most notably hematologic adverse events (e.g., neutropenia) and gastrointestinal or hepatic toxicity [71]. Given this background, the current in-vitro data for THZ531 are insufficient to make reliable assumptions about tolerability in a physiological context. A deeper toxicological analysis, including in vivo pharmacokinetics, tissue-specific toxicity and long-term safety is required before clinical translation can be considered.

4.6 Therapeutic Potential of CDK12 Targeting by THZ531

CDK12 can be pharmacologically inhibited using the small-molecule inhibitor THZ531 [36]. Based on the observation that parental urothelial carcinoma cells exhibit substantially higher IC_{50} values than their cisplatin-resistant LTT counterparts, we explored strategies to reduce the required THZ531 dose while retaining therapeutic efficacy. The literature indicates synergistic interactions between CDK12 inhibition and DNA-damaging chemotherapy in several tumor types [44, 70]. In this study, it was therefore examined whether comparable synergistic effects occur in urothelial carcinoma and whether such interactions could enable meaningful dose reductions to improve tolerability.

4.6.1 THZ531 as a Monotherapy

THZ531 demonstrated notable potential as a monotherapy in cisplatin-resistant urothelial carcinoma cells. At relatively low concentrations, THZ531 induced marked apoptotic signaling in LTT models, as evidenced by strong PARP cleavage. In contrast, none of the parental, cisplatin-naive cell lines exhibited comparable apoptotic responses. This suggests a selective vulnerability of chemoresistant, stress-adapted tumor populations to pharmacological CDK12 inhibition.

A similar phenomenon has been described in hepatocellular carcinoma, where THZ531 monotherapy substantially reduced cell viability across multiple HCC cell lines [47]. Although these studies did not employ specifically engineered therapy-resistant sublines, the authors emphasize that HCC as a tumor entity is inherently difficult to treat due to its limited therapeutic options and adaptive survival mechanisms, features that resemble the challenges seen in LTT models [47].

In line with this observation, recent data from high-grade serous ovarian carcinoma demonstrate that THZ531 is highly effective even in carboplatin-resistant cellular models, further supporting the notion that CDK12/13 inhibition may preferentially target chemotherapy-resistant tumor states across different cancer types [72].

4.6.2 THZ531 in Combination Therapy

4.6.2.1 THZ531 in Combination with Cisplatin

Across the parental urothelial carcinoma models, the combination of THZ531 with cisplatin produced modest but reproducible synergistic effects. Although the magnitude of synergy was limited, these effects are mechanistically relevant, as they align with the Western blot data demonstrating enhanced γH2AX accumulation and increased PARP cleavage in T24 and UMUC-3 under combination treatment. This pattern suggests that CDK12 inhibition can augment cisplatin-induced DNA damage in selected models.

A clinical translation, however, remains uncertain. Even after dose reduction, the THZ531 concentrations required to achieve synergy in vitro remained well above the tolerability threshold of HBLAK cells, indicating that the therapeutic window is too narrow to justify combined dosing at the effective in-vitro levels. Thus, these findings should primarily be interpreted as mechanistic insights rather than therapeutically actionable dosing regimens.

While no quantitative conclusions can be drawn regarding dose reduction, these observations nevertheless hint at a potential cooperative effect between THZ531 and DNA-damaging agents, consistent with reports from other tumor models [44, 45].

Taken together, the data regarding cisplatin and THZ531 support the broader concept that CDK12 inhibition can sensitize urothelial carcinoma cells to genotoxic chemotherapy, although the detectable effects in vitro were modest and their therapeutic applicability limited by the narrow safety margin of THZ531.

4.6.2.2 THZ531 in Combination with Talazoparib

In contrast to the cisplatin data, the combination of THZ531 with the PARP inhibitor talazoparib produced clear and robust synergistic effects across all examined cell lines. In T24 cells, extremely low concentrations of THZ531, which had no measurable toxicity as monotherapy, became highly effective in combination with talazoparib. This indicates that THZ531, even at sub-cytotoxic doses, can prime cells for PARP inhibitor sensitivity, consistent with a partial, CDK12-dependent reduction of homologous recombination competence [44].

Interestingly, in none of the cell lines did the talazoparib/THZ531 combination induce detectable PARP cleavage. This suggests that the synergistic loss of viability is not mediated through apoptosis, but rather through cell-cycle arrest, senescence, or alternative stress-response pathways, all of which have been implicated in recent literature on CDK12 inhibition [47, 68, 69].

Given these observations, THZ531 emerges as a potent sensitizer to PARP inhibition, capable of lowering the effective talazoparib threshold even at doses of THZ531 that are otherwise non-

toxic. This effect aligns with findings in other tumor entities, such as triple-negative breast cancer and multiple myeloma, where CDK12 inhibition can induce or mimic BRCAness-like vulnerabilities [45, 70]. Nevertheless, in our models, the underlying mechanism remains unresolved, and definitive conclusions will require functional assays.

Finally, the data raise the possibility that sequential rather than simultaneous administration may further enhance the therapeutic window. This concept should be evaluated in future work, especially given the narrow tolerability range of THZ531.

4.6.3 Potential for Clinical Use and Implementation

The therapeutic utilization of CDK12 is an emerging concept with increasing translational relevance [39, 53]. While CDK4/6 inhibitors are already clinically established for breast cancer patient with metastatic disease, the development of selective CDK12 inhibitors is still in its early stages [39, 53, 73]. Dinaciclib, a multi-CDK inhibitor with activity against CDK12, has entered clinical evaluation, and first-in-class selective Cyclin K inhibitors are currently progressing toward phase I trials [74, 75].

THZ531 represents a potent covalent CDK12/13 inhibitor [36]. In our study, urothelial carcinoma cells, particularly LTTs, exhibited pronounced sensitivity to THZ531, suggesting that low-dose pharmacologic CDK12 inhibition might be clinically exploitable in relapse settings or in tumors with limited chemotherapeutic options. However, THZ531 also elicited cytotoxic effects independent of CDK12 protein abundance, indicating that its activity is only partially CDK12-driven. This lack of CDK12 dependency underscores a key limitation: no validated biomarker currently exists to predict therapeutic response to CDK12 inhibition. The identification of robust biomarker will therefore be crucial for clinical implementation. Recent publications emphasize that the function of CDK12 in cancer remains incompletely understood [56, 67].

Immune checkpoint inhibitors have become a standard component of systemic therapy for urothelial carcinoma [13, 17]. Insights from pan-cancer analyses suggest that CDK12 alterations may shape tumor immunogenicity, immune infiltration, and responsiveness to immune checkpoint inhibition [67]. While these findings cannot be directly extrapolated without dedicated studies in urothelial carcinoma, they highlight a potential avenue for integrating CDK12-targeted therapies with immunotherapy in the future.

Collectively, these observations underscore the translational potential of CDK12 as a therapeutic target and as a biomarker candidate. However, substantial preclinical and clinical validation is required before CDK12-directed therapies can be meaningfully incorporated into treatment algorithms for urothelial carcinoma.

4.7 Methodological Limitations

Several methodological limitations of the present study must be considered when interpreting the results.

First, all findings are based exclusively on in vitro models. No data from three-dimensional tumor systems or in vivo experiments are available. This limits the translational relevance of the results, as pharmacokinetic properties of THZ531, such as absorption, distribution, metabolism, and excretion, cannot be captured. Consequently, the conclusions regarding its potential clinical applicability remain constrained. However, recent work in high-grade serous ovarian carcinoma demonstrated that THZ531 exerts potent activity in patient-derived organoid models, indicating that at least in selected tumor entities, CDK12 inhibition can show robust efficacy in more physiologically relevant three-dimensional systems [72].

Second, the study lacks high-throughput analyses such as RNA sequencing or proteomics. Such approaches would be essential for a comprehensive understanding of the global transcriptional and signaling changes induced by CDK12 modulation or THZ531 treatment, especially in urothelial carcinoma cells. The qPCR data included in this work offer only a limited snapshot of selected DNA repair genes and do not reflect the full spectrum of CDK12-dependent gene regulation.

Third, CDK13, despite being a known target of THZ531, was not investigated [36, 72]. THZ531 covalently inhibits both CDK12 and CDK13 [36], and CDK13 is also involved in transcriptional regulation and RNA processing [63]. Off-target inhibition of CDK13 may therefore have influenced the observed effects. Without a differential assessment of CDK12 and CDK13, it remains unclear which findings are truly CDK12-specific.

Another limiting factor concerns the incomplete toxicological characterization. Although the tolerability of THZ531 was assessed in urothelial epithelial cells, systematic analyses of cumulative toxicities, particularly hematologic, neurotoxic, or synergistic toxicities in combination with cisplatin were not performed. Given that cisplatin is known to cause nephrotoxicity and ototoxicity, more comprehensive toxicity profiling would be required to evaluate the safety of potential combination therapies [76].

Finally, the role of Cyclin K, the obligate binding partner of CDK12 and CDK13, was not examined [37]. The FDA approved a clinical trial specifically targeting Cyclin K in the context of selective CDK12/13 inhibition [74]. Since Cyclin K is critical for the functional activity of both kinases, the lack of its assessment represents a relevant methodological gap.

In summary, future studies should incorporate in vivo models, high-throughput approaches, extended toxicity testing, and a dedicated analysis of CDK13 and Cyclin K.

4.8 Outlook

Despite substantial progress in understanding CDK12 biology, its exact contribution to urothelial carcinoma remains incompletely defined. The findings of this thesis underscore the need for a more detailed molecular characterization of CDK12, including its context-dependent functions, co-regulated pathways, and interaction with other determinants of DNA repair capacity and treatment response. Future studies should integrate genomic, transcriptomic, and functional analyses to delineate whether specific CDK12 alterations can serve as predictive or prognostic biomarkers.

Targeted therapies are increasingly shaping modern oncology [77]. In urothelial carcinoma, immune checkpoint inhibitors and antibody-drug conjugates have already expanded the therapeutic landscape [5, 13]. Given the central role of kinases in cell-cycle control, molecular kinase inhibitors have become indispensable across several cancer types, including chronic myeloid leukemia and colorectal cancer [78-80]. Similar strategies may also become relevant for urothelial carcinoma, provided that key regulatory molecules such as CDK12 are further elucidated.

A refined understanding of CDK12 dependency, synthetic lethal interactions, and stress-response pathways could pave the way for rationally designed targeted therapies. Ultimately, integrating CDK12-based biomarkers or inhibitors into personalized treatment concepts may help improve therapeutic precision and overcome resistance to established modalities such as cisplatin.

5 References

1. Robert-Koch-Institut. *Krebs in Deutschland 2019/2020*. 2023 28 July 2024]; Available from: https://www.krebsdaten.de/Krebs/DE/Content/Publikationen/Krebs_in_Deutschland/kid_2023/kid_2023_c67_harnblase.pdf?__blob=publicationFile#:~:text=Beim%20Harnblasenkrebs%20handelt%20es%20sich,der%201990er%20Jahre%20deutlich%20rückläufig.
2. Leitlinienprogramm Onkologie der Arbeitsgemeinschaft der Wissenschaftlichen Medizinischen Fachgesellschaften e.V. (AWMF), D.K.e.V.D.u.D.K.D. *S3-Leitlinie Früherkennung, Diagnose, Therapie und Nachsorge des Harnblasenkarzinoms*. 2016 28 July 2024]; Available from: https://www.leitlinienprogramm-onkologie.de/fileadmin/user_upload/Downloads/Leitlinien/Blasenkarzinom/LL_Harnblasenkarzinom_Langversion_1.1.pdf.
3. Tang, H., et al., *Pioglitazone and bladder cancer risk: a systematic review and meta-analysis.* Cancer Medicine, 2018. **7**(4): p. 1070-1080.
4. Travis, L.B., et al., *Bladder and Kidney Cancer Following Cyclophosphamide Therapy for Non-Hodgkin's Lymphoma.* Journal of the National Cancer institute, 1995.
5. Krauter, J., K. Gust, and S. Shariat, *Metastasiertes Urothelkarzinom – Spätlinientherapien.* Journal für Urologie und Urogynäkologie/Österreich, 2023. **30**(2): p. 60-65.
6. Siegel, R.L., et al., *Cancer statistics, 2022.* CA: A Cancer Journal for Clinicians, 2022. **72**(1): p. 7-33.
7. Leitlinienprogramm Onkologie der Arbeitsgemeinschaft der Wissenschaftlichen Medizinischen Fachgesellschaften e.V. (AWMF), D.K.e.V.D.u.D.K.D. *S3-Leitlinie Früherkennung, Diagnose, Therapie und Nachsorge des Harnblasenkarzinoms*. 2020 23 August 2024]; Available from: https://register.awmf.org/assets/guidelines/032-038OL1_S3_Harnblasenkarzinom_2020-04-verlaengert.pdf.
8. Sylvester, R., W. Oosterlinck, and A. van der Meijden, *A single immediate postoperative instillation of chemotherapy decreases the risk of recurrence in patients with stage Ta T1 bladder cancer: a meta-analysis of published results of randomized clinical trials.* Urological Survey, 2004.
9. Michael R Abern, R.A.O., Mark R Anderson, Edward N Rampersaud, Brant A Inman, *Perioperative Intravesical Chemotherapy in Non-Muscle-Invasive Bladder Cancer: A Systematic Review and Meta-Analysis.* 2013.
10. Nieuwenhuijzen, J.A., et al., *Survival after Bladder-Preservation with Brachytherapy versus Radical Cystectomy; A Single Institution Experience.* European Urology, 2005. **48**(2): p. 239-245.
11. von der Maase, H., et al., *Long-Term Survival Results of a Randomized Trial Comparing Gemcitabine Plus Cisplatin, With Methotrexate, Vinblastine, Doxorubicin, Plus Cisplatin in Patients With Bladder Cancer.* 2005.
12. De Santis, M., et al., *Randomized Phase II/III Trial Assessing Gemcitabine/Carboplatin and Methotrexate/Carboplatin/Vinblastine in Patients With Advanced Urothelial Cancer Who Are Unfit for Cisplatin-Based Chemotherapy: EORTC Study 30986.* Journal of Clinical Oncology, 2012. **30**(2): p. 191-199.
13. Balar, A.V., et al., *First-line pembrolizumab in cisplatin-ineligible patients with locally advanced and unresectable or metastatic urothelial cancer (KEYNOTE-052): a multicentre, single-arm, phase 2 study.* The Lancet Oncology, 2017. **18**(11): p. 1483-1492.

14. Balar, A.V., et al., *Atezolizumab as first-line treatment in cisplatin-ineligible patients with locally advanced and metastatic urothelial carcinoma: a single-arm, multicentre, phase 2 trial.* The Lancet, 2017. **389**(10064): p. 67-76.
15. Oing, C., et al., *Second Line Chemotherapy for Advanced and Metastatic Urothelial Carcinoma: Vinflunine and Beyond-A Comprehensive Review of the Current Literature.* 2016.
16. Raggi, D., et al., *Second-line single-agent versus doublet chemotherapy as salvage therapy for metastatic urothelial cancer: a systematic review and meta-analysis.* Annals of Oncology, 2016. **27**(1): p. 49-61.
17. Bellmunt, J., et al., *Pembrolizumab as Second-Line Therapy for Advanced Urothelial Carcinoma.* New England Journal of Medicine, 2017. **376**(11): p. 1015-1026.
18. Sarfaty, M. and J.E. Rosenberg, *Antibody-Drug Conjugates in Urothelial Carcinomas.* Current Oncology Reports, 2020. **22**(2).
19. Shruthi, S. and K. Bhasker Shenoy, *Cisplatin Resistance in Cancer Therapy: Causes and Overcoming Strategies.* ChemistrySelect, 2024. **9**(25).
20. Galluzzi, L., et al., *Molecular mechanisms of cisplatin resistance.* Oncogene, 2011. **31**(15): p. 1869-1883.
21. Skowron, M., et al., *Multifaceted Mechanisms of Cisplatin Resistance in Long-Term Treated Urothelial Carcinoma Cell Lines.* International Journal of Molecular Sciences, 2018. **19**(2).
22. Höhn, A., et al., *Distinct mechanisms contribute to acquired cisplatin resistance of urothelial carcinoma cells.* 2016.
23. Siddik, Z.H., *Cisplatin: mode of cytotoxic action and molecular basis of resistance.* Oncogene, 2003. **22**(47): p. 7265-7279.
24. Mah, L.J., A. El-Osta, and T.C. Karagiannis, *γH2AX: a sensitive molecular marker of DNA damage and repair.* Leukemia, 2010. **24**(4): p. 679-686.
25. Smith, H.L., et al., *DNA damage checkpoint kinases in cancer.* Expert Reviews in Molecular Medicine, 2020. **22**.
26. Li, X. and W.-D. Heyer, *Homologous recombination in DNA repair and DNA damage tolerance.* Cell Research, 2008. **18**(1): p. 99-113.
27. Roy, U. and E.C. Greene, *Demystifying the D-loop in DNA recombination.* Nature, 2020.
28. San Filippo, J., P. Sung, and H. Klein, *Mechanism of Eukaryotic Homologous Recombination.* Annual Review of Biochemistry, 2008. **77**(1): p. 229-257.
29. Tutt, A. and A. Ashworth, *The relationship between the roles of BRCA genes in DNA repair and cancer predisposition.* 2002.
30. Stinson, B.M. and J.J. Loparo, *Repair of DNA Double-Strand Breaks by the Nonhomologous End Joining Pathway.* Annual Review of Biochemistry, 2021. **90**(1): p. 137-164.
31. Wood, R.D. and S. Doublié, *DNA polymerase θ (POLQ), double-strand break repair, and cancer.* DNA Repair, 2016. **44**: p. 22-32.
32. Yang, W., *An Overview of Y-Family DNA Polymerases and a Case Study of Human DNA Polymerase η.* Biochemistry, 2014. **53**(17): p. 2793-2803.
33. Heinrich, P.C., M. Müller, and L. Graeve, *DNA-Reparatur*, in *Löffler/Petrides Biochemie und Pathobiochemie*. 2014. p. 562-566.
34. Malumbres, M., *Cyclin-dependent kinases.* Genome Biology, 2014.
35. Malumbres, M. and M. Barbacid, *Cell cycle, CDKs and cancer: a changing paradigm.* Nature Reviews Cancer, 2009. **9**(3): p. 153-166.
36. Zhang, T., et al., *Covalent targeting of remote cysteine residues to develop CDK12 and CDK13 inhibitors.* Nature Chemical Biology, 2016. **12**(10): p. 876-884.

37. Blazek, D., et al., *The Cyclin K/Cdk12 complex maintains genomic stability via regulation of expression of DNA damage response genes.* Genes & Development, 2011. **25**(20): p. 2158-2172.
38. Pilarova, K., J. Herudek, and D. Blazek, *CDK12: cellular functions and therapeutic potential of versatile player in cancer.* NAR Cancer, 2020. **2**(1).
39. Liang, S., et al., *CDK12: A Potent Target and Biomarker for Human Cancer Therapy.* Cells, 2020. **9**(6).
40. Paculová, H. and J. Kohoutek, *The emerging roles of CDK12 in tumorigenesis.* Cell Division, 2017. **12**(1).
41. *cBioPortal for Cancer Bladder Cancer*. 26 August 2024]; Available from: https://www.cbioportal.org/results/oncoprint?cancer_study_list=blca_tcga%2Cblca_tcga_pub_2017%2Cblca_msk_tcga_2020%2Cblca_tcga_gdc%2Cblca_tcga_pub%2Cblca_tcga_pan_can_atlas_2018&tab_index=tab_visualize&profileFilter=mutations%2Cgistic%2Ccna%2Cstructural_variants&case_set_id=all&Action=Submit&gene_list=CDK12.
42. *cBioPortal for Cancer Prostate Cancer*. 26 August 2024]; Available from: https://www.cbioportal.org/results?cancer_study_list=prad_cpcg_2017%2Cprad_tcga_pub%2Cprad_tcga%2Cprad_tcga_gdc%2Cprad_tcga_pan_can_atlas_2018&tab_index=tab_visualize&profileFilter=mutations%2Cgistic%2Ccna%2Cstructural_variants&case_set_id=all&Action=Submit&gene_list=CDK12.
43. Szarvas, T. and H. Reis, *Cisplatin Resistance and Subtyping (unpublished work)*. University Medicine Essen.
44. Johnson, S.F., et al., *CDK12 Inhibition Reverses De Novo and Acquired PARP Inhibitor Resistance in BRCA Wild-Type and Mutated Models of Triple-Negative Breast Cancer.* Cell Reports, 2016. **17**(9): p. 2367-2381.
45. Quereda, V., et al., *Therapeutic Targeting of CDK12/CDK13 in Triple-Negative Breast Cancer.* Cancer Cell, 2019. **36**(5): p. 545-558.e7.
46. Turner, N., A. Tutt, and A. Ashworth, *Hallmarks of 'BRCAness' in sporadic cancers.* Nature Reviews Cancer, 2004.
47. Wang, C., et al., *CDK12 inhibition mediates DNA damage and is synergistic with sorafenib treatment in hepatocellular carcinoma.* Gut, 2020. **69**(4): p. 727-736.
48. Sungwan, P., et al., *Anti-Tumor and Chemosensitizing Effects of the CDK Inhibitor Dinaciclib on CholangiocarcinomaIn VitroandIn Vivo.* In Vivo, 2024. **38**(5): p. 2284-2293.
49. Drakaki, A., et al., *"Real-world" outcomes and prognostic indicators among patients with high-risk muscle-invasive urothelial carcinoma.* Urol Oncol, 2021. **39**(1): p. 76 e15-76 e22.
50. Bellmunt, J., et al., *Adjuvant atezolizumab versus observation in muscle-invasive urothelial carcinoma (IMvigor010): a multicentre, open-label, randomised, phase 3 trial.* Lancet Oncol, 2021. **22**(4): p. 525-537.
51. Li, H., et al., *CDK12 inhibition enhances sensitivity of HER2+ breast cancers to HER2-tyrosine kinase inhibitor via suppressing PI3K/AKT.* Eur J Cancer, 2021. **145**: p. 92-108.
52. Hanahan, D., *Hallmarks of Cancer: New Dimensions.* Cancer Discov, 2022. **12**(1): p. 31-46.
53. Emadi, F., et al., *CDK12: a potential therapeutic target in cancer.* Drug Discov Today, 2020. **25**(12): p. 2257-2267.
54. Juan, H.C., et al., *Cdk12 is essential for embryonic development and the maintenance of genomic stability.* Cell Death Differ, 2016. **23**(6): p. 1038-48.
55. Siddik, Z.H., *Cisplatin: mode of cytotoxic action and molecular basis of resistance.* Oncogene, 2003. **22**(47): p. 7265-79.

56. Dai, W., et al., *New insights into the dule roles CDK12 in human cancers: Mechanisms and interventions for cancer therapy.* J Pharm Anal, 2025. **15**(7): p. 101173.
57. Tien, J.F., et al., *CDK12 regulates alternative last exon mRNA splicing and promotes breast cancer cell invasion.* Nucleic Acids Research, 2017. **45**(11): p. 6698-6716.
58. Antonarakis, E.S., et al., *CDK12-Altered Prostate Cancer: Clinical Features and Therapeutic Outcomes to Standard Systemic Therapies, Poly (ADP-Ribose) Polymerase Inhibitors, and PD-1 Inhibitors.* JCO Precis Oncol, 2020. **4**: p. 370-381.
59. Ajit, K. and M. Gullerova, *From silence to symphony: transcriptional repression and recovery in response to DNA damage.* Transcription, 2024. **15**(3-5): p. 161-175.
60. Ivashkevich, A.N., et al., *gammaH2AX foci as a measure of DNA damage: a computational approach to automatic analysis.* Mutat Res, 2011. **711**(1-2): p. 49-60.
61. Fiszer-Kierzkowska, A., et al., *Liposome-based DNA carriers may induce cellular stress response and change gene expression pattern in transfected cells.* BMC Mol Biol, 2011. **12**: p. 27.
62. Chilà, R., et al., *Stable CDK12 Knock-Out Ovarian Cancer Cells Do Not Show Increased Sensitivity to Cisplatin and PARP Inhibitor Treatment.* Frontiers in Oncology, 2022. **12**.
63. Wu, C., et al., *CDK13 phosphorylates the translation machinery and promotes tumorigenic protein synthesis.* Oncogene, 2023. **42**(16): p. 1321-1330.
64. Magnuson, B., et al., *CDK12 regulates co-transcriptional splicing and RNA turnover in human cells.* iScience, 2022. **25**(9): p. 105030.
65. Lui, G.Y.L., C. Grandori, and C.J. Kemp, *CDK12: an emerging therapeutic target for cancer.* J Clin Pathol, 2018. **71**(11): p. 957-962.
66. Houles, T., et al., *CDK12 is hyperactivated and a synthetic-lethal target in BRAF-mutated melanoma.* Nature Communications, 2022. **13**(1).
67. Lu, K.-Q., et al., *CDK12 is a potential biomarker for diagnosis, prognosis and immunomodulation in pan-cancer.* Scientific Reports, 2024. **14**(1).
68. Krajewska, M., et al., *CDK12 loss in cancer cells affects DNA damage response genes through premature cleavage and polyadenylation.* Nat Commun, 2019. **10**(1): p. 1757.
69. Frei, K., et al., *Inhibition of the Cyclin K-CDK12 complex induces DNA damage and increases the effect of androgen deprivation therapy in prostate cancer.* Int J Cancer, 2024. **154**(6): p. 1082-1096.
70. Shyamsunder, P., et al., *THZ531 Induces a State of BRCAness in Multiple Myeloma Cells: Synthetic Lethality with Combination Treatment of THZ 531 with DNA Repair Inhibitors.* Int J Mol Sci, 2022. **23**(3).
71. Wekking, D., et al., *CDK4/6 inhibitors in the treatment of metastatic breast cancer: Focus on toxicity and safety.* Semin Oncol, 2023. **50**(6): p. 131-139.
72. Cesari, E., et al., *Dual inhibition of CDK12 and CDK13 uncovers actionable vulnerabilities in patient-derived ovarian cancer organoids.* J Exp Clin Cancer Res, 2023. **42**(1): p. 126.
73. Pujala, V., et al., *Abemaciclib-Associated Panniculitis With Fibrosis: Expanding the Dermatologic Spectrum of Cyclin-Dependent Kinase 4/6 Inhibitors.* Cureus, 2025. **17**(5): p. e83380.
74. Bahl, A.K., et al., *Abstract 7004: CT7439 an oral first-in class selective CDK12 and 13 inhibitor and cyclin K degrader: Profiling activity and combination efficacy in an ovarian cancer model.* Cancer Research, 2025.
75. Nemunaitis, J.J., et al., *A first-in-human, phase 1, dose-escalation study of dinaciclib, a novel cyclin-dependent kinase inhibitor, administered weekly in subjects with advanced malignancies.* J Transl Med, 2013. **11**: p. 259.

76. Elmorsy, E.A., et al., *Advances in understanding cisplatin-induced toxicity: Molecular mechanisms and protective strategies.* Eur J Pharm Sci, 2024. **203**: p. 106939.
77. Oluwajembola, A.M., et al., *A Review of Novel Cancer Therapeutics and Current Research Trends.* ScientificWorldJournal, 2025. **2025**: p. 5056618.
78. Dasari, A., et al., *Fruquintinib versus placebo in patients with refractory metastatic colorectal cancer (FRESCO-2): an international, multicentre, randomised, double-blind, phase 3 study.* Lancet, 2023. **402**(10395): p. 41-53.
79. Goldman, J.M., *Treatment strategies for CML.* Best Pract Res Clin Haematol, 2009. **22**(3): p. 303-13.
80. Li, Q., et al., *Signaling pathways involved in colorectal cancer: pathogenesis and targeted therapy.* Signal Transduct Target Ther, 2024. **9**(1): p. 266.

Danksagung

Ich danke Frau PD Dr. Michèle Hoffmann für die fachliche Betreuung dieser Arbeit sowie für die wertvollen Anregungen und die konstruktive Unterstützung während der gesamten Promotionszeit.

Mein Dank gilt außerdem den Mitarbeiterinnen und Mitarbeitern des Labors für translationale Uroonkologie des Universitätsklinikums Düsseldorf für die Einführung in die experimentellen Methoden sowie für die hilfreiche Unterstützung bei der praktischen Durchführung der Versuche.

Abschließend danke ich meinen Eltern sowie meinen Freundinnen und Freunden für ihre Unterstützung und ihren Rückhalt während des Studiums und der Promotionszeit.

Unterterzen, den 04. Januar 2026